UNIVERSITY OF PADUA

DEPARTMENT OF CIVIL, ENVIRONMENTAL AND ARCHITECTURAL ENGINEERING

Master degree in Environmental Engineering

Master Thesis

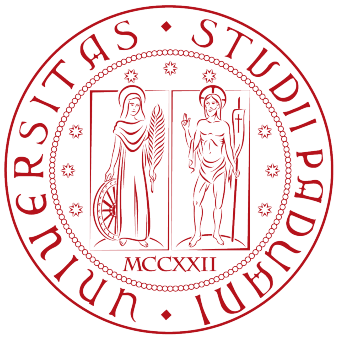

Implementation of a stomatal optimization approach into a light spectrum-aware model of photosynthesis and transpiration

Supervisor:
Matteo Camporese

Student:
Matteo Berton

ACADEMIC YEAR 2023/2024

Abstract

The use of agrivoltaic systems is seen as a trade-off between energy storage and food production, however, although the measure of the power absorbed by solar panels is easily quantifiable, the same cannot be said for agricultural yield. For this reason, it is difficult to determine whether or not the use of this technique is cost-effective. The development of theories that can replicate the behavior of the plant to the variation of climatic forcings allows to evaluate the efficiency and productivity of an agrivoltaic system depending on the type of crop and the boundary conditions of the problem.

In this study, an in-depth look is taken at different models for quantifying stomatal conductance with a focus on the effect that the light spectrum plays in the process of stomatal cavities regulation. The combination of the Fick's law with Farquhar's photosynthetic model and with the optimality theory allows us to obtain analytical expressions for the photosynthetic rate (f_c), the intercellular CO_2 concentration (c_i) and the stomatal conductance (g). The formula of g, thus obtained, depends on a single parameter (λ) and can be differentiated according to the most limiting process between Rubisco carboxylation (light-saturated) and RuBP regeneration (light-limited) rates. The results reveal that optimization models, maximizing g for blue instead of red light, do not provide a correct response to changing light spectrum and they are in contrast to experimental results and empirical model predictions.

Contents

List of Figures

List of Tables

List of Abbreviations and Symbols

APV	Agrophotovoltaics
WUE	Water use efficiency
PV	Photovoltaics
FM_{AVS}	Fresh biomass in the APV field
FM_{CP}	Fresh biomass in the control plot
E_{AVS}	APV electrical productivity
E_{PV}	PV electrical productivity
LSC	Luminescent solar concentrator
WSPV	Wavelength-selective photovoltaic panels
PPMA	Polymethyl methacrylate
FD	Full density
HD	Half density
PAR	Photosynthetically active radiation
C_s	Solar constant
I_L	Light intensity
L	Vertical layer thickness
m	Optical air mass
k	Light extinction coefficient
I_k	Light adaption parameter
NPQ	Non-photochemical quenching
ET	Evapotranspiration
VPD	Vapor pressure deficit
SCAPV	Spectral separated concentrated agricultural photovoltaic
PCE	Power conversion efficiency
CAPEX	Capital expenditures
OPEX	Operational expenditures
GM	Ground mounted
g	Stomatal conductance
g_s	Stomatal conductance

g_0	Intercept fitting parameter
g_1	Slope fitting parameter
c_a	CO_2 concentration at the leaf surface
c_p	CO_2 compensation point
D	Vapor pressure deficit
D_0	Vapor pressure deficit constant
H	Mean air relative humidity
f_c	Photosynthetic rate
A_n	Photosynthetic rate
q_L	Fluorescence parameter
Φ_{PSII}	Efficiency of photosystem II
J	Electron transport rate
PFD_{abs}	Absorbed photon irradiance
NPQ_0	Initial level of NPQ
NPQ_{max}	Maximum level of NPQ
K_{NPQ}	Photon irradiance at half amplitude
$nNPQ$	Hill coefficient
f_{PSII}	Proportion f absorbed light partitioned to PSII
$F_m^{'}$	Maximum fluorescence without dark-adaption
F_m	Dark-adapted maximum fluorescence
$F_0^{'}$	Minimum fluorescence without dark-adaption
F_m	Dark-adapted mininum fluorescence
F_v	Difference between maximum and minimum dark-adapted fluorescence
$F_v^{'}$	Difference between maximum and minimum fluorescence without dark-adaption
m	Empirical parameter fitted on light response curve of chlorophyll fluorescence
n	Empirical parameter fitted on light response curve of chlorophyll fluorescence
f_w	Water vapor flux
a	Relative diffusivity of water vapor compared to carbon dioxide
a_1	Limiting process parameter
a_2	Limiting process parameter
R_d	Non-photorespiratory mitochondrial CO_2 release in the light
RuBP	Ribulose 1,5-bisphosphate
$f_{c,C}$	Rubisco photosynthetic rate
$f_{c,L}$	RuBP regeneration rate

$f_{c,TPU}$	Triose phosphate utilization rate
c_i	Intercellular CO_2 concentration
e_i	Intercellular moisture
e_a	Ambient moisture
$V_{c,max}$	Maximum rate of Rubisco activity
K_c	Michaelis-Menten constant for Rubisco kinetics
K_0	Michaelis-Menten constant for Rubisco kinetics
$C_{o,a}$	Oxygen concentration in the chloroplasts
ATP	Adenosine triphosphate
NADPH	Nicotinamide adenine dinucleotide phosphate
λ	Wavelength
$b_s(\lambda)$	Photon irradiance spectrum
$a(\lambda)$	Absorptance
$\varphi_e(\lambda)$	Quantum yield spectrum
α	Maximum value of quantum yield spectrum
Q	Potential rate of electron transport
J_{max}	Maximum rate of electron transport
θ	Shape factor of the electron transport rate
λ	Marginal water cost of carbon gain
T	Transpiration rate
λ_w	Latent heat of water vaporization
γ_w	Psychrometric constant
c_p	Specific heat of air
p_a	Atmospheric pressure
g_{ba}	Series of atmospheric and leaf boundary layer conductance
Phi	Leaf available energy
ρ	Air density
ρ_w	Water density
S	Slope of the Clausius–Clapeyron relation
h	Plank constant
N_a	Avogadro number
c	Speed of light
mw_{CO_2}	CO_2 molecular weight
mw_{H_2O}	H_2O molecular weight
s	Ratio between intercellular and ambient CO_2 concentrations
k_1	Co-limitation model parameter

k_2	Co-limitation model parameter
k_3	Co-limitation model parameter
M	Target function for the calibration of the models
SCE-UA	Shuffled complex evolution method developed at The University of Arizona
LED	Light-emitting diode
RB	Red to blue ratio
PPFD	Photosynthetic photon flux density
FW	Fresh weight
r_a	Leaf resistance
r_b	Atmospheric boundary layer resistance
λ_{LI}	Linear marginal water use efficiency
R^2	Coefficient of determination
r	Pearson correlation coefficient
NSE	Nash–Sutcliffe efficiency coefficient
KGE	Kling–Gupta efficiency coefficient
RMSE	Root mean square error
rjv	Ratio between maximum electron transport rate and Rubisco rate at reference temperature
λ_0	Initial value of the marginal water use efficiency
$c_{a,0}$	Reference CO_2 concentration
β	Curvature parameter in the smoothing operation
ε	Curvature parameter in the smoothing operation
A_p	Smoothed minimum between Rubisco and RuBP regeneration rates

Chapter 1

Introduction

Energy and food production have been considered separate goals for many years. However, more recently, the growth of the world population has led to an increased demand for both of them. A new approach, called agrophotovoltaic (APV), is proposed as a solution to the problem, since it combines electrical power generation and farming on the same portion of land. The concept of agrophotovoltaics (APV) was introduced by Goetzberger and Zastrow in 1982. Their idea was to increase the solar collectors height up to 2 m above the ground in order to improve the shading effect under the structure and the crop yield. From 1982 to the present, this technology has evolved and differentiated across the world adopting different strategies according to the type of climate, crop and state policies. The synergistic effect of electrical power generation and agricultural productivity may lead to a reduced efficiency in solar energy or crop yields, or both productions. The main problem that arises when combining the two techniques is to find the best compromise between the maximization of both the electrical yield and crop productivity; the first one is obtained by increasing the PV module density which simultaneously reduces the available solar radiation underneath, the second one is obtained by reducing the PV module density and increasing the light availability for plants growth.

The development of this innovative system fits within a rapidly changing historical context from the demographic, economic and agricultural point of view. The recent population growth and economic development result in a reduction of available spaces devoted to agriculture and power generation. An interesting finding is shown by Schindele et al. (2020), who report a 48% decrease in the space allocated to agriculture between 1961 and 2016 due to global population increase. For this reason the use of this new method of farming could bring beneficial effect.

The highest potential of APV is evident in arid regions where crops usually are subjected to the effect of high solar radiation and scarce water availability. In these lands the presence of panels above the cultivated fields can lead to an increase in water use efficiency (WUE) and a decrease in water demand for irrigation (Adeh et al., 2018).

An important parameter for assessing the advantages of a dual-use APV system over a single-crop and PV production is the Land Equivalent Ratio (LER). It measures the efficiency of the combined production of crops and electricity respect to the single use case and it is defined as follows:

$$LER = \frac{FM_{AVS}}{FM_{CP}} + \frac{E_{AVS}}{E_{PV}} \tag{1.1}$$

where FM_{AVS} is the fresh biomass in the APV field, FM_{CP} is the biomass on the control plot field and E_{AVS} and E_{PV} represent the APV and PV electrical productivity.

If LER value is greater than one, it means that the dual use system is more effective than separating the two techniques (Abidin et al., 2021).

The benefits that an agrivoltaic system brings are many, here is a list of the most important:

(1) The profitability of farming can be enhanced by the installation of APV thanks to the production of electrical energy;

(2) APVs contribute to the off-grid electrification of rural areas because usually agricultural lands are not located in densely populated regions where an implemented electrical system is already available and create a decentralized energy system that can be self-sufficient (Malu et al., 2017);

(3) The ambient air temperature is reduced by the crops cultivated beneath the solar structure. If the solar panel temperature decreases the PV efficiency increases (Patel et al., 2018);

(4) The water used to clean the dust accumulated on top of PV panels can be used to irrigate the crops beneath, increasing the water use efficiency (Proctor et al., 2021);

(5) The yield of shade-acclimated species can be enhanced by the shading effect of the solar PV modules and the consequent decrease of light irradiance (Marucci et al., 2018);

(6) Increase in job opportunities (Shybut, 2023);

(7) APV provides shelter in the horticulture sector where some plants could suffer damages due to extreme weather events (Trommsdorff et al., 2022);

(8) APV reduces the fossil fuel dependency for the development of renewable energies, if the produced electricity is directly used on site agriphotovoltaic could also contribute to reduce the carbon footprint (Li and Ma, 2020).

To understand wether the use of the APV system is beneficial or not it is necessary to analyze in detail several aspects, since the advantage of the APV depends on the type of technology used in the PV cells, on the spatial distribution of the PV modules and on the agricultural practice used on site.

In Weselek et al. (2019) it's possible to find a first distinction between groundmounted PV (GM-PV) and APV. In the first case the PV structure is a free-standing solar array mounted on the ground using either a rigid metal frame or a top single pole, in the second case the structure is raised from the ground of a few meters in order to increase the crop productivity underneath.

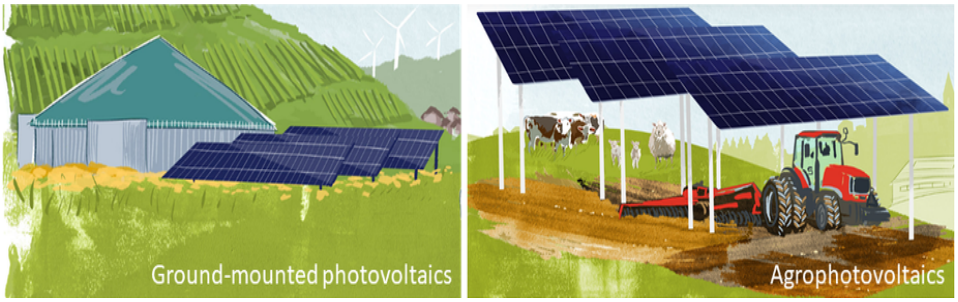

Figure 1.1: Comparison between GM-PV and APV (source: Hilker et al. (2023)).

Different types of strategies can be adopted in the use of an agriphotovoltaic system and three distinct approaches can be used: energy-centric, agricultural-centric and integrated agricultural-energy-centric (Pascaris et al., 2020). The first one is oriented towards maximizing electricity production and at the same time promoting the growth and the development of crops underneath the panels; the second one is optimized for the maximization of biomass production and mitigation of actions that might alter the plant's growth, but still using the advantages of the photovoltaic technology; the third one tries to maximize both practices by improving the disadvantages that would arise by adopting only one of the two strategies.

1.1 The PV module

The understanding of the APV functioning requires the definition of its fundamental parts. It is composed of photovoltaic panels whose performance depends on the type of cell used. A photovoltaic (PV) system is made of one or more solar panels combined with an inverter and other electrical and mechanical hardware that use energy from the sun to generate electricity. The solar PV modules consist of photovoltaic cells that are able to absorb the incident solar radiation and convert only a part of it into electricity. Different types of materials can be used to achieve the optimal conversion, such as crystalline silicon (c-Si), amorphous silicon (a-Si), copper-indium-gallium-diselenide (CIGS) and cadmium telluride (CdTe) modules. As reported by Trommsdorff et al. (2022) there are two configurations: the multicrystalline and the mono-crystalline modules. The distinction between the two is based on the growth and cut characteristics of the starting crystal. Nowadays this technology is widely used and guarantees an efficiency from around 12% to 17%. Depending on the specific case three different types of panels can be used in the APV system: monofacial, bifacial and semitransparent (Figure 1.2). Monofacial modules are characterized by the presence of photovoltaic cells only on the front side, while bifacial ones are able to absorb also the reflected solar radiation coming from the back side. Different factors are responsible for the efficiency of bifacial modules such as the site configuration, albedo and the ratio between the back to front side efficiency.

It is also possible to use semitransparent silicon modules. In this type of panel the cells are interspersed with empty spaces that allow the passage of light. The cells configuration and the ratio between empty and full space can be properly chosen in order to maximize the efficiency. A different technique, instead, consists in the use of luminescent solar concentrators (LSCs), which are made of transparent plastic or glass that has a fluorescent dye or quantum dots embedded or painted on it. The dye absorbs light and then fluoresces, creating a glow that propagates by total internal reflection to the edge of the sheet where the light is absorbed by a narrow solar cell (Currie et al., 2008).

An emerging new technology consists in the use of wavelength-selective photovoltaic (WSPV) panels, which combines the luminescent solar concentrator unit with the standard silicon cells of the PV module. The idea behind its operation is to absorb a certain fraction of the light and to transmit the remaining part below for plants photosynthesis and growth. The WSPV unit is made of polymethyl methacrylate (PMMA) plastic inserted in a luminescent perylene red dye, the energy demand of the entire system (ventilation, microclimate sensors, data loggers) can be sustained by the produced electricity (Loik et al., 2017). The main advantages are: the reduction of the absorbed light energy dissipated into heat (nonphotochemical quenching), the increased efficiency due to the use of a frontal energy reception system instead of a lateral one and the reduced distance

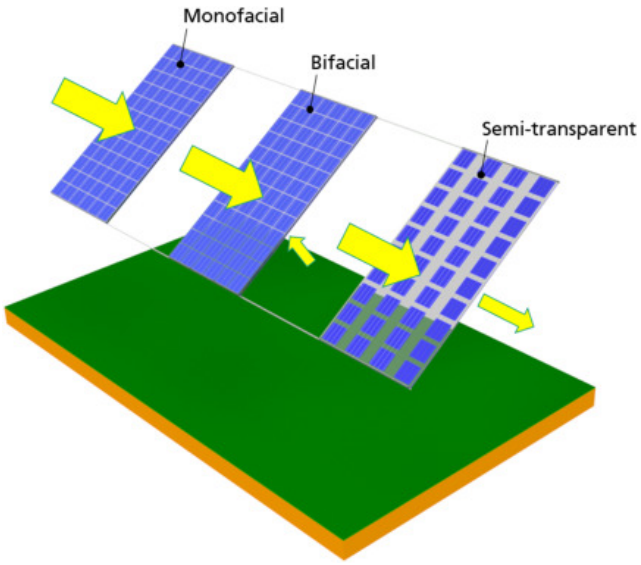

Figure 1.2: Representation of the three types of panels used in APV (source: Trommsdorff et al. (2022)).

the light has to travel to reach the PV cells due to the alternating presence of PV cells and LSCs. The efficiency of the WSPV module is given by the sum of the contributions of all the components that constitute it. Loik et al. (2017) report theoretical efficiencies ranges between 8.8% and 9.4%, the results obtained depend on the relative area of the LSCs and the PV cells, the fraction of the absorbed solar spectrum, the portion of wavelengths delivered to the PV cells and the conversion efficiencies. They show that WSPVs are characterized by higher efficiencies when light conditions are limiting. A WSPV unit can concentrate light more efficiently compared to the classic installation with opaque panels, its performance does not depend on the inclination of the solar panels and it can receive light from both side, increasing the fraction of absorbed reflected light. The color and type of LSC is chosen in order to remove the part of the light spectrum that is not needed for the plant's growth: the blue fraction is diverted to the PV cells to generate electricity, instead, the red one is allowed to pass since it is responsible for the plant's photosynthetic activity (Liu and van Iersel, 2021; Wang et al., 2016).

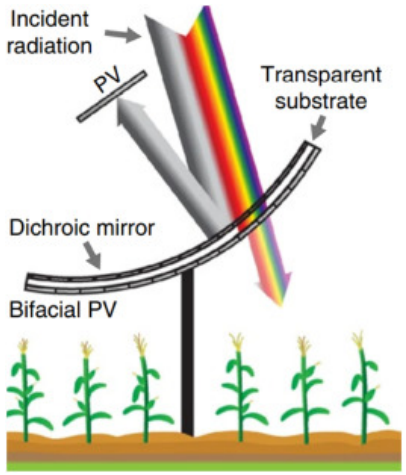

Figure 1.3: Illustration of a WSPV module with a filtering mirror, allowing the visible spectrum to pass and the near-infrared to be reflected towards the PV cell (source: Trommsdorff et al. (2022)).

Organic photovoltaics (OPV) represent a rapidly emerging technology with the potential to revolutionize large-scale power generation. The absorbing layer of OPV cells, composed of organic semiconductors, offers a cost-effective alternative to traditional inorganic semiconductors. Carbon-based nanostructures like fullerenes and graphene contribute to OPV's promising applications, boasting excellent optical and mechanical properties (Pathakoti et al., 2018). This economically practical technology not only offers low production costs but also enables the production of thin and flexible solar cells, making it more suitable for widespread implementation in the solar energy industry (Kumar et al., 2014).

Different spatial configurations and arrangements are possible in the field of agrophotovoltaic. A first technical problem is given by the requirement for a higher vertical clearance of the panels compared to a traditional ground-mounted PV system. In addition, an optimization of the distance between the rows and an appropriate selection of the panels density are necessary. Full-density (FD) panels are used to optimize energy production and allow the 50% of energy to pass below, while half-density (HD) are used to balance energy production and agricultural growth (Abidin et al., 2021).

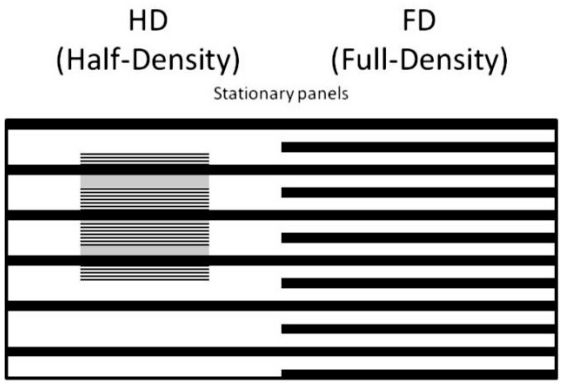

Figure 1.4: Full-density and half-density configurations, top view. Thin black lines are the planting rows within the grey agricultural plot, the thick lines in black represent the PV strips (source: Valle et al. (2017)).

The angle of inclination of the panels, the distance between them, their height and density depend on the type of cultivation underneath, the climatic conditions and therefore the geographical position in which they are installed. A distinction is made between interspace PV and overhead PV systems. In the first case the efficiency and the installation costs are lower, the agricultural fields are interspersed with rows of PV panels. Generally, this system focuses on energy production and is limited by the little space between one field and the next in which agricultural machinery struggle to pass. In the overhead system the panels are placed above the agricultural field at heights that depend on the type of crop and on the size of the agricultural machinery that have to pass below them. This system benefits from being positioned at higher levels, in this way all electrical equipment must not be placed on the ground, thus obtaining an optimization of the available space and an increase in productivity thanks to the greater amount of shaded areas and protection against extreme weather events. The height of this structure (usually 4-5 m) makes it vulnerable to horizontal forces that are transferred directly to the base. Steel frames can be used for small-scale installations and concrete foundations when the wind load is very high (Trommsdorff et al., 2022).

The energy production can be enhanced with the use of a solar tracking system (Figure 1.5). This device is able to automatically correct its inclination thanks to mono or biaxial rotation axes. Three different configurations are possible: in the passive configu-

ration the thermal expansion of the material or the pressure gradient between two points at the end of the tracker are exploited, in this way the system requires minimal maintenance costs but is highly influenced by the climatic conditions and its main drawback is inaccuracy; in the active configuration the presence of sensors and motors is exploited, the result is a more precise and efficient sun tracking system except for cloudy days during which unnecessary consumption of electricity is recorded; and in the chronological configuration the rotation to a constant specific rate is used, minimal tracking errors are obtained with an excess work during cloudy days due to the continuous spinning mechanism (Abidin et al., 2021).

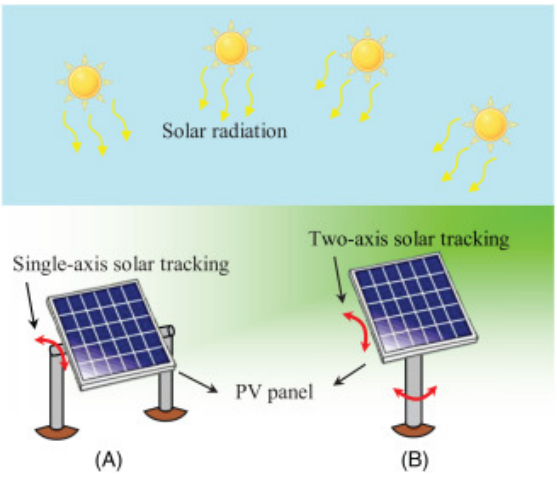

Figure 1.5: Single axis (A) and dual axis (B) solar tracking systems (source: Aktaş and Kirçiçek (2021)).

In order to maximize the light availability for both plant's growth and energy production the position of the PV modules can change. For example, orienting the panels towards east or west can avoid the formation of shade patterns, which are formed using a north or south orientation depending on the hemisphere (Figure 1.6).

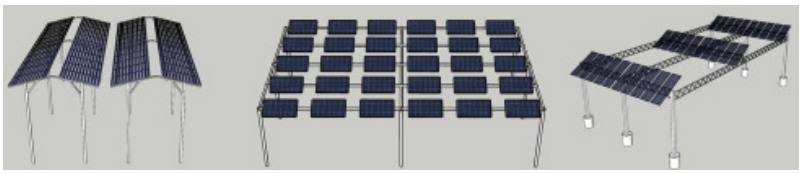

Figure 1.6: Different types of orientation of PV panels (from left to right: east-west, south- and south-east orientations) (source: Trommsdorff et al. (2022)).

1.2 Microclimatic variations

It is important to assess the impact and changes that the APV system induces on the main climatic variables such as: irradiance, temperature, soil moisture and vapor pressure deficit. Any change in quantity and quality of natural light can affect the growth and the development process of a plant. The application of a cover above the crop therefore entails a substantial change not only in the photomorphogenesis of the plant but also in the climatic conditions of the air and soil in which it lies. The main advantage due to the presence of the panels is the reduction of evapotranspiration and excessive solar warmth, resulting in increased soil moisture.

Not all the light spectrum is used by the plant, but only a defined portion of it, which is called "photosynthetically active radiation" (PAR) and includes wavelengths within the visible spectrum that vary between 400 and 700 nm (Figure 1.7). When wavelengths are too short (x rays, gamma rays, ultraviolet radiation) and carry too much energy they can break the molecular bonds and bring potential damages and DNA alterations with loss of genetic material (Rastogi et al., 2010). On the other hand, too long wavelengths with little energy fail to activate the photoreceptors of plants and start the electron transport chain necessary for the plant light dependent phase.

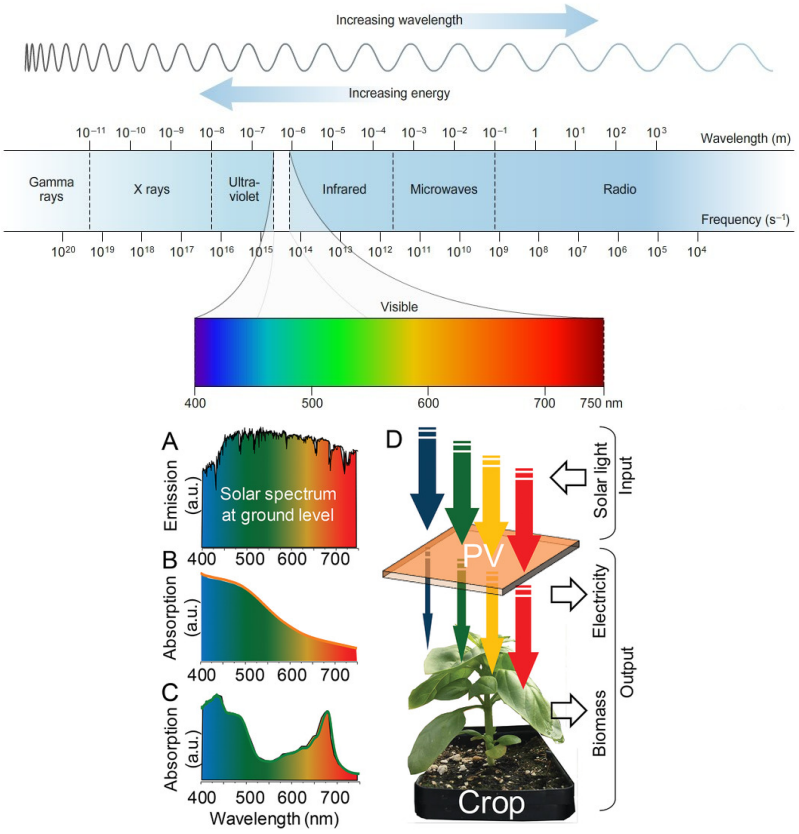

Figure 1.7: Electromagnetic spectrum radiation from the lowest to the highest frequency. (A) Solar spectrum at the ground level. (B) Absorption spectrum of the solar PV panel. (C) Absorption spectrum for a generic crop. (D) Schematization of the input (solar radiation) and the outputs (electricity and biomass). Electromagnetic spectrum (source: Macmillan Learning, The Electromagnetic Spectrum (2023)). The absorption spectrum (source: Thompson et al. (2020)).

1.2.1 Light dependence

Not all the radiation emitted by the sun is able to reach the surface of the PV panels and the plant's leaves, and during its path it encounters different resistances to the motion. The solar radiation intercepted by the Earth above the atmosphere at the average distance of the earth–sun (the astronomical unit) from a unit surface that is perpendicular to the rays per unit time is called "solar constant" (C_s) and its value ranges between 1360 and 1370 Wm^{-2} (Li et al., 2011). This energy is not uniformly distributed on the terrestrial surface but depends on latitude, altitude, time, day of the year, slope, cloud cover, humidity, temperature and climate. The effective radiation that reaches the surface of the planet is approximately equal to 46%, a lot of energy

is absorbed and re-emitted by atmospheric gases or intercepted by clouds. The process by which light intensity is reduced due to the interaction with matter is known as light extinction. The light intensity I_L reaching the soil through an atmospheric vertical layer with thickness L is modeled according to the Lambert-Beer's formula, as in Palmeri et al. (2013):

$$I_L = I_0 e^{-kmL} \tag{1.2}$$

where I_0 is the incident light intensity at the atmosphere, m is the optical air mass which accounts for the solar angle of the zenith - θ - and k is the light extinction coefficient which expresses a measure of the resistance to the motion and depends on the extinction property of the medium.

The design of an APV system must therefore take into account the amount of light that reaches the Earth's surface (C_s, I_L) and its quality (PAR) because photovoltaic panels and plants are not optimized for the same wavelengths of the spectrum (Figure 1.7). While PV panels and irradiance are linked by a linear proportionality, plants absorptance is determined by the nature of the photosynthetic pigments (Thompson et al., 2020) and depends on the light response curve, which illustrates the relationship between irradiance and photosynthetic rate with a Michaelis–Menten trend curve.

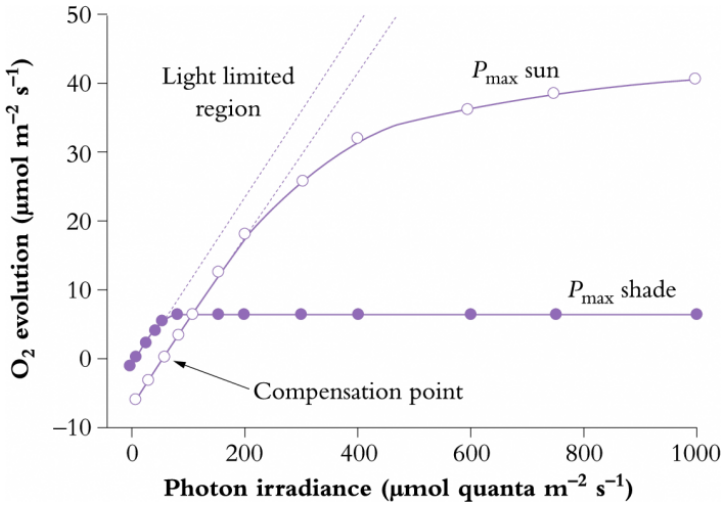

Figure 1.8: Generic saturation curves of shade acclimated and sun loving plants (source: Munns et al. (2018)).

Light acclimated plants reach the saturation point with higher irradiance, while shade acclimated species reach saturation quicker and with lower irradiance. The response depends on the type of plant and on the light adaption parameter - I_k -, which accounts for the type of plant acclimation (Jørgensen and Bendoricchio, 2001). Shade-tolerant species showed a number of adaption strategies including an increased total leaf area, an altered leaf orientation and a modified morphology with longer, wider, thinner but lower number of leaves (Weselek et al., 2019). However, the relation between photosynthesis and light availability is not always positive correlated (too much light can induce photoinhibition effect), but is characterized by an optimum-curve behavior. The excess solar radiation can compromise the plants functioning, for this reason plants have evolved over time looking for ways to prevent potential damages induced by heat and excessive irradiance, such as non-photochemical quenching (NPQ) (Ruban, 2016). Therefore a correct interpretation of the saturation curve of the plant can help us to define the type of coverage to be used knowing that the lower the light saturation point the more shade a crop can experience

without having relevant yield losses.

1.2.2 Water dependence

As reported by Elamri et al. (2018), the main difficulty in the design process of an APV system is to combine short-term fluctuations in the climatic forcings (radiation interception and rain redistribution below the panels) and long-term agronomic management, finding the best match in terms of panel type, tilt angle and irrigation technique.

An uneven distribution of water can be the immediate consequence of the installation of PV panels above the crops, since during intense precipitation events high water runoff can induce localized erosion and the formation of channels and moisture patches. A possible solution consists in changing the inclination angle of the panel which determines a new rainfall spatial distribution. It is necessary to state that the panels inclination can lead to accumulation of dust on the surface with a consequent reduction of electricity production especially in arid regions, as suggested by Ravi et al. (2016). An attempt can be made in the implementation of an irrigation system that also provides for the cleaning of the panels, avoiding additional water losses.

In areas characterized by limited water availability, the action provided by the photovoltaic panels is beneficial in terms of reduced evaporation and water demand of plants, thus also reducing the demand for the irrigation system due to the increase in soil humidity. However, an appropriate sizing for the irrigation system and the adoption of an adequate strategy are necessary to minimize losses caused by too much water availability which can lead to leaching phenomena.

1.2.3 Air temperature and humidity

Air temperature represents another climatic forcing that is affected by the presence of an APV system. The effect on air and soil temperature is quite debated in literature and not all studies lead to the same results. For example, Marrou et al. (2013a) showed that neither the average daily air temperature nor the VPD and the wind have been significantly affected in the shade of solar photovoltaics panels compared to the full-sun case, regardless of the climatic season. They explain how this phenomenon is due to convection air movements that seem to be powerful enough to homogenize air characteristics. However, the results are limited by their prototype which is much smaller in size than large-scale agrivoltaic installations, therefore the impacts of this type of structure on air temperature are not known. On the contrary, they recorded a decrease in crop temperature under the photovoltaic panels due to the reduction in the incoming shortwave radiations compared to the full-sun treatment. Other studies in literature found that temperature tends to decrease under shaded conditions compared to full-sun case (Pang et al., 2019; Williams et al., 2023). Negative aspects due to the heat stress could be: the decrease level of nutrient-uptake and assimilation of proteins in tomato roots (Giri et al., 2017), the decrease of the starch content in C_3 cereals (Ben Mariem et al., 2021) and the reduction of the time needed for late peas to reach maturity with associated reduced seed size (Bisbis et al., 2018).

As a result of the decrease in irradiance below the panels, the evapotranspiration is reduced. Evapotranspiration (ET) is defined as the combination of evaporation, which is responsible for water movement from soil to the air directly and transpiration that occurs through the openings of the leaves called stomata. A correct estimation of the transpiration rate is crucial and plays an important role in estimating the volumes of water to be allocated for plants for irrigation purposes. ET is usually estimated using the FAO Penman–Monteith approach which expresses the flux as a function of the crop

type, the actual water availability and the actual climate. ET is proportional to the net radiation, this means that the greater the irradiance the greater the flux, and to the vapor pressure deficit (VPD). As VPD decreases, due to the growing air humidity, the flux becomes less relevant. The magnitude of the reduction depends on the crop type and is time dependent as the crop coefficient varies in time according to the lifecycle of a plant species (Pereira et al., 2015).

1.3 Crop yield and innovations

The microclimatic conditions change over time, consequently the impacts on agricultural cultivation depends on the sowing period and the growing phase of the plant. For example, vegetative species that well tolerate light (lettuce, cabbage) can better adapt to the reduction of irradiance showing adaption techniques. Marrou et al. (2013b) highlighted the capability of lettuce to produce biomass more efficiently when the light is limiting. Lettuce shows an increased leaf area to overcome shade-related drawbacks and a modified morphology with longer, wider, but lower number of leaves. An important result was found by Elamri et al. (2018), who discovered a delay in the development phase of lettuce in partially darkened conditions, this may lead to an extension of the period of harvesting and consequently to increased profits for farmers.

As a general rule, it can be stated that under unsaturated light conditions and no other limiting factors the presence of PV panels contributes to a decrease in agricultural yield, instead, in conditions of water stress and unfavourable temperatures, the reduction of irradiance can bring benefits. In very arid regions (e.g. Arizona) plants like chiltepin pepper and tomato showed a yield increase of 150% and 90%, with shading rates of $70\% \div 80\%$ (Trommsdorff et al., 2022). In addition, the presence of panels can help eliminate all protective operations that are used in case of extreme adverse meteorological events, also acting as protection.

A different result was obtained by Zhang et al. (2023), who analyzed the variation in yield of certain types of plants below a spectral separated concentrated agricultural photovoltaic (SCAPV) system. This innovative technology exploits the ability of the materials of which it is composed to act as a spectral filter, separating the sunlight so that the red wavelength (responsible for the growth) is transmitted for photosynthesis, while the blue wavelength is reflected and concentrated for energy production. The results are increased soil moisture, crop yield and better management of water resources for irrigation.

The components of the SCAPV plant include a concentrator module (consisting of a curved glass, a layer of multilayer polymer, a high-efficiency PV cell concentrator and a dissipative structure), a dual axis-tracking system capable of adjusting the inclination based on the solar altitude and azimuth angle, and the supporting arms for the entire structure.

Zhang et al. (2023) found higher yields for plants such as ginger, peanut, sweet potato, bok choy and lettuce, with yield growth rates up to 47.9% below SCAPV compared to the open-air cultivation. The increase in yield is due to the microclimatic variation induced by the presence of the filtering structure. They recorded under the SCAPV unit a decrease in irradiance, air temperature and wind speed, resulting in decreased evaporation and increased soil moisture. However, it should be noted that the results obtained from these experiments were carried out on carefully selected plants in order to obtain a perfect agreement between the growth period and the optimal soil conditions. In addition, some plants tested are of the shade acclimated type. It is necessary to conduct further experiments on light acclimated species to compare yields and have more general

results. The value of the average land equivalent ratio ($LER = 1.61$) they obtained is remarkable. It is well known how LER values greater than the unit imply a higher yield compared to the mono production for the same size of cultivated area, or, they imply a smaller crop area for the same agricultural and electric yield compared to the mono production.

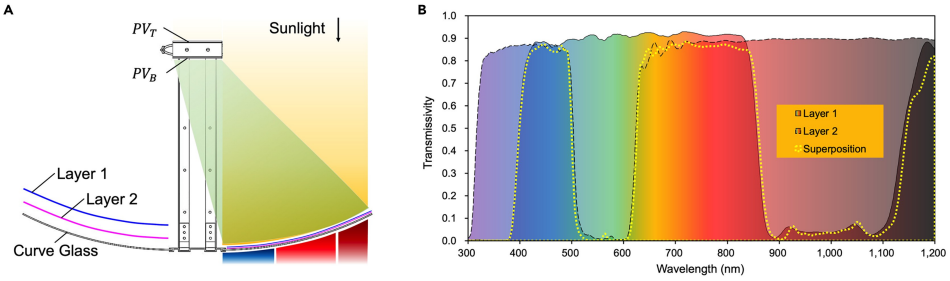

Figure 1.9: (A) Operating principle of the concentrator module with two layers of MPF attached in the SCAPV plant. (B) Transmission spectrum of the 2 layers and superposition (source: Zhang et al. (2023)).

This result is very important in terms of improving land efficiency, especially in densely populated regions where the agricultural space can be optimized through the development of a dual-use system. In China the SCAPV plant measured power conversion efficiency (PCE) value of 11.6% thanks to the modular design of the concentrator module and the optimization of cell components, concentrating curve and dual axis tracking system. As regards energetic aspects, the agrivoltaic system can be implemented in order to use the energy produced on site, for example to power the irrigation and pumping systems through the use of energy storages and to disconnect the farm from the main electricity grid facilitating the electrification of rural areas.

1.4 Economics

The main disadvantages in the implementation of the agrivoltaic system concern the aspect of costs, social acceptance and in particular the issue of farmers themselves. The main factors that determine the final cost of the structure are: the size of the APV system, the management of agricultural practices, the location of the structure and the type of technology used by the panels. Furthermore, installation costs including labour, additional costs due to the raised steel or concrete structure and any modification of machinery and agricultural practices due to the reduced height available in ground-mounted systems should be taken into account (Trommsdorff et al., 2022).

Costs are usually subdivided into capital expenditures (CAPEX) and operational expenditures (OPEX). The former refer to the initial investment required for setting up the agrophotovoltaic system. They include the costs associated with purchasing solar panels, mounting structures, inverters, electrical components and any other equipment, as well as the costs of preparing the land for agricultural use. The latter refer to the ongoing operational expenses incurred in the maintenance and running of the agrophotovoltaic system. This may include costs related to land lease, labor for maintenance, repair and replacement of components, insurance, taxes and other recurring expenses associated with the system's operation.

In general, the CAPEX of an APV system are higher than the traditional ground mounted (GM) system due to the higher vertical clearance and the greater amount of material that must be used to elevate the PV panels. The expenditure increases in the case of double-sided panels usage, even if it is then offset by higher profits due to the

absorption of the reflected light. There is an increase in costs also in the preparation and installation of the site due to the forced passage of agricultural machinery on alternative roads in order to avoid too much soil compaction. On the other hand, the OPEX of agrophotovoltaics are lower compared to the GM-PV case. The cost related to the soil maintenance below the panels (weeding) is eliminated since it is already accomplished by definition in the concept of APV. In addition, the dual use of the soil guarantees lower land cost per year than the GM-PV. The costs coming from agricultural machinery operation can increase due to the greater care with which the equipment must be moved between the structural support pillars. Consequently, permanent crops are preferred, otherwise the costs, due to structural changes and the use of different agricultural vehicles, can increase a lot.

A problem that should not be underestimated is the social acceptance for this type of structure, especially in the case of large-scale installations or facilities located near residential areas, and the concern of farmers themselves, who must be instructed in the new maintenance techniques and procedures associated with the use of the dual land-use technology. However, social acceptance is only part of the problem, it fits into the wider context of conflict in land use between energy and food production, spaces intended for urbanization and protection from extreme weather events, tourism and landscape and ecosystems conservation.

A wide range of innovative techniques and solutions that can be used in agrophotovoltaic installations for maximizing electricity can be found in the literature. However, a broader perspective must be adopted in order to maximize agricultural yield as well and ensure that the investment for the installation itself is not worthless. For this reason, a detailed study of plant functioning and, in particular, of the regulatory action of stomata as a function of the light spectrum should be included in agrophotovoltaic plant construction projects.

1.5 Thesis objectives

To assess the impact of agrivoltaic systems it is necessary to analyze in detail what happens at the leaf scale, because the processes that determine the gas echanges of the plant take place at the microscopic level. The importance of plants and photosynthesis is often underestimated or taken for granted, not considering the great contribution they make to the reduction of CO_2 emissions in the planet; therefore, the analytical control of their development and growth could bring benefits not only in terms of food production but also in terms of improving air quality. The regulation of the gas exchanges, in particular that of CO_2, allows us to quantify the amount of carbon assimilated by the plant and converted into sugars and to determine the agricultural yield in the agrivoltaic plants. Since the light dependent phase of the photosynthetic process, responsible for the synthesis of ATP and NADPH necessary for carbon fixation, is determined by the quantity and quality of light, a more careful assessment of the impact of light spectrum on the functioning of plants has been evaluated in this study, analyzing the effect of different wavelengths on CO_2 and H_2O exchange processes.

What follows is therefore intended to give a general theoretical overview of some of the models that exist in the literature and are applied to the leaf scale with the aim of predicting the plant behavior as external climatic conditions change, including temperature, relative humidity, CO_2 concentration, quantity and quality of incident light.

The objective of this discussion is to verify the correct response of the optimization models in terms of stomatal conductance, photosynthetic rate, water use efficiency, transpiration and intercellular CO_2 concentration against measured data in the literature.

The models were tested on two different types of C_3 plants (basil and strawberry) and the response to different light treatments was compared with the results obtained by Camporese and Abou Najm (2022).

The optimization models analyzed are those of Katul and Medlyn. They differ in a fundamental hypothesis that is made about the regulatory action of stomata. Katul assumes that plants are always in light saturated conditions and includes only the limitation induced by the ability of the Rubisco enzyme to catalyze the carboxylation reaction, Medlyn, on the other hand, assumes that plants are always in limiting light conditions, including the dependence of light spectra in the expression of the assimilation rate.

The analytical models that have been implemented are based entirely on the equations obtained by Katul et al. (2010), which, being completely general, can be differentiated within the iterative scheme distinguishing between the hypothesis of Medlyn and that of Katul. The models are the result of the optimization scheme including the regulatory action of the plant in limiting water losses and maximizing carbon fixation, complemented by the transport equation for CO_2, a non-linear (or linear) photosynthesis and transpiration models. The ability to capture light-induced variability is included within the photosynthetic model, and the dependence of stomatal conductance on light is considered implicitly in the expression of the assimilation rate. The result is therefore a new mathematical framework that can be used to describe the stomatal conductance as not only the external climatic conditions but also incident radiation change, while still taking into account the regulatory optimization process carried out by stomata. The importance of the models lies not only in their predictive capabilities of the plant's response to given climatic conditions, but also in the possibility to determine the most appropriate choices to be made in terms of crop and panels type, in order to maximize agricultural yields and profits from electricity production.

1.6 Thesis structure

The following paragraph provides an overview of the thesis structure, outlining the chapters and the topics addressed in each.

In Chapter 2, the different models of stomatal conductance are analyzed and the mathematical steps necessary to derive the equations are reported. Chapter 3 shows the calibration of the models on the experimental data (basil and strawberry) and explains how the calibration algorithm operates. Chapter 4 analyzes the sensitivity of the models to the variation of the main climatic variables. Chapter 5 provides conclusions on the functioning and limitations of the models and offers a perspective for improvement.

Chapter 2

Stomatal conductance models

The role that stomata play in regulating gas exchanges between leaf and atmosphere affects not only the plant's economy, but also the entire ecosystem in terms of energy and water balance. The parameter that allows us to quantify the action of stomata is called stomatal conductance. It is determined by the action of guard cells, which, in response to energy gradients, are able to regulate the opening and closure of stomatal pores adapting the physiological condition of the plant to external changes.

Several models have been used in the literature to predict stomata movement in response to changes in external climatic conditions, many of these are empirical models and the expression they use for stomatal conductance relies on experimental observations and does not include a physical basis in it. Among the most used empirical models we can find that of Ball et al. (1987) and that of Leuning (1995). Both use an expression for stomatal conductance that depends on relative air humidity, CO_2 concentration in the surrounding of the leaf, photosynthetic rate and slope (g_1) and intercept (g_0) fitting parameters.

The formulations, respectively, are:

$$g = g_0 + \frac{g_1}{c_a - c_p} f_c \left(1 + \frac{D}{D_0}\right)^{-1} \tag{2.1}$$

and

$$g = g_0 + \frac{g_1}{c_a - c_p} f_c H \tag{2.2}$$

where H is the mean air relative humidity, f_c is the photosynthetic rate, c_a is the concentration at the leaf surface, c_p is the CO_2 compensation point, D is the vapor pressure deficit, D_0 is a vapor pressure deficit constant and g_0 is the conductance as f_c and the leaf irradiance approach to 0.

Both models take into account the response of stomatal conductance to changes in assimilation rate and ambient CO2 concentration. However, they do not consider at all the role of light in the process of stomatal regulation. This omission, as will be seen later, leads to the formulation of models that are unable to correctly interpret the stomatal conductance trends as the climatic variables change.

A step forward was made by Camporese and Abou Najm (2022), who consider the effect of different light spectra on the gas exchange between leaf and atmosphere. They analyzed the plant's response to the variation of the incident light spectra trying to understand which portion of light was more efficient in terms of productivity and water consumption. In their model they use the formulation proposed by Kromdijk et al. (2019) to estimate the stomatal conductance:

$$g = g_0 + 1.64\left(1 + \frac{g_1}{\sqrt{D}}\right)\frac{1 - q_L}{c_a} \tag{2.3}$$

where D is the atmospheric water vapor pressure deficit computed from the air relative humidity and $1 - q_L$ is a proxy for fluorescence and estimates the light-induced changes in the redox state of quinone A. They applied a correction to the original formula by replacing $1 - q_L$ instead of f_c based on the experiments of Głowacka et al. (2018), who observed a direct dependence between light-induced stomatal movement and PQ redox signal that can be approximated by the term $1 - q_L$. The fluorescence term is computed starting from the definition of the operating efficiency of the photosystem II, as:

$$\Phi_{PSII} = \frac{J}{PFD_{abs} \times f_{PSII}} \tag{2.4}$$

where J represents the rate of electron transport, PFD_{abs} the absorbed photon irradiance and f_{PSII} the proportion of absorbed light partitioned to the photosystem II. The next step is the computation of NPQ, a mechanism that plants adopt to protect themselves by dissipating the excess light intensity as heat. It is modeled using a sigmoidal Hill function with basal level NPQ_0, photon irradiance at half amplitude K_{NPQ}, Hill coefficient and asymptote $nNPQ$ and NPQ_{max}, respectively.

$$\begin{cases} NPQ = NPQ_0 + \frac{NPQ_{max} - NPQ_0}{\left[\left(\frac{K_{NPQ}}{PFD_{abs}}\right)^{nNPQ} + 1\right]} & \text{if } PFD_{abs} > 0 \\ \\ NPQ = 0 & \text{if } PFD_{abs} = 0 \end{cases} \tag{2.5}$$

After determining NPQ and the dark-adapted maximal fluorescence (F_m) the next step is the computation of the maximum fluorescence without dark-adaption at a fixed light level ($F_m^{'}$) as:

$$F_m^{'} = \frac{F_m}{NPQ + 1} \tag{2.6}$$

The corresponding level of $F^{'}$ is computed using Φ_{PSII} from equation (2.4) as:

$$F^{'} = F_m \times (1 - \Phi_{PSII}) \tag{2.7}$$

The minimal fluorescence without dark-adaptation ($F_0^{'}$) as a function of light intensity is computed considering a first contribution due to fluorescence suppression via NPQ:

$$F_{0NPQ}^{'} = \frac{F_0}{\frac{F_v}{F_m} + \frac{F_0}{F_m^{'}}} \tag{2.8}$$

where $F_{0NPQ}^{'}$ represents the decrease in minimal fluorescence relative to F_0 due to NPQ and is computed according to Oxborough and Baker (1997). From $F_{0NPQ}^{'}$ computed according to equation (2.8), it is possible to predict the variation of the maximum $PSII$ quantum efficiency in the light due to NPQ as:

$$\left(\frac{F_v^{'}}{F_m^{'}}\right) = 1 - \frac{F_{0NPQ}^{'}}{F_m^{'}} \tag{2.9}$$

The second contribution is the increase in fluorescence due to photo-inactivation of the reaction centers, it is modeled using the empirical relationship developed by Hendrickson et al. (2005) as:

$$1 - \frac{\left(\frac{F_v'}{F_m'}\right)}{\left(\frac{F_v'}{F_m'}\right)_{NPQ}} = m \times \left(0.5 \times PFD_{abs} \times \frac{F'}{F_m'}\right) + n \tag{2.10}$$

where $F_v = F_m - F_0$, $F_v' = F_m' - F_0'$, m and n are empirical parameters fitted on light response curves of chlorophyll fluorescence.

From the combination of equations (2.10), (2.6) and (2.7) it is possible to compute the fluorescence as:

$$q_L = \frac{F_m' - F'}{F_m - F_0} \times \frac{F_0'}{F'} \tag{2.11}$$

The model developed by Camporese and Abou Najm (2022) combines the empirical expression of stomatal conductance with Fick's law and with Farquhar's photosynthetic model to obtain a closed-form solution for g. It does not consider the regulatory action that stomata have in minimizing water losses and maximizing carbon fixation according to a specific optimization function.

A different approach to the study of stomatal movement has been developed by the so-called optimization models. They arise in response to a lack of theoretical physical knowledge underlying stomatal functioning and the uncertainty regarding the predictive capabilities of empirical models, since they depend on parameters that have no physical basis and may vary according to the type of vegetative species. Within this category we find the models developed by Katul et al. (2010) and Medlyn et al. (2011). They coupled the optimization scheme with the Farquhar's photosynthetic model and the Fick's law to obtain an expression of stomatal conductance that no longer depends directly on the light spectrum (as in Kromdijk et al. (2019)), but is a function of the assimilation rate and a new model parameter derived from the optimization (λ). Light dependence is included in the definition of the assimilation rate which may vary according to the most limiting process between regeneration of the Rubisco enzyme and availability of the RuBP substrate, which changes with the light spectrum.

2.1 The non-linear optimality model

The mathematical framework needed to get a closed-form solution is the following: the first equation is the Fick's law, which describes how the diffusion of water and carbon dioxide is proportional to the concentration gradient between the external environment and the internal part of the plant:

$$\begin{aligned} f_c &= g(c_a - c_i) \\ f_w &= ag(e_i - e_a) \approx agD \end{aligned} \tag{2.12}$$

where f_c and f_w are the carbon dioxide and water vapor fluxes, g is the stomatal conductance, c_a and c_i are ambient and intercellular CO_2 concentrations, a is the relative diffusivity of water vapor compared to carbon dioxide and D represents the water vapor pressure deficit expressed as the difference between e_i and e_a (intercellular and ambient moisture).

The second equation is the biochemical model of leaf photosynthesis developed by Farquhar et al. (1980), which describes the relationship between the photosynthetic rate and the intercellular concentration of CO_2 when the non-photorespiratory mitochondrial CO_2 release in the light (R_d) is negligible:

$$f_c = \frac{a_1(c_i - c_p)}{a_2 + c_i} \tag{2.13}$$

where c_p is called compensation point and represents the CO_2 concentration at which the rate of photosynthesis exactly matches the respiration rate, and the parameters a_1, a_2 are selected on the basis of the most limiting process between the Rubisco photosynthetic rate ($f_{c,C}$) and the RuBP regeneration (light-limited) rate ($f_{c,L}$). A third limiting factor called "triose phosphate utilization limited rate" has been neglected here ($f_{c,TPU}$) since it is not as relevant as the other two processes. It occurs when carbon is not exported from the Calvin-Benson cycle as quickly as it is fixed (Lombardozzi et al., 2018).

The photosynthetic rate therefore depends both on the concentration gradient according to Fick and on the CO_2 demand of the plant according to Farquhar. The combination of the two equations returns the assimilation rate and the concentration ratio in terms of conductance:

$$f_c = \frac{1}{2}\left(a_1 + (a_2 + c_a)g - \sqrt{[a_1 + g(a_2 - c_a)]^2 + 4g(a_1 c_p + a_2 c_a g)}\right) \tag{2.14}$$

$$\frac{c_i}{c_a} = \frac{1}{2} + \frac{-a_1 - a_2 g + \sqrt{[a_1 + g(a_2 - c_a)]^2 + 4g(a_1 c_p + a_2 c_a g)}}{2gc_a} \tag{2.15}$$

The Rubisco-limited (light-saturated) process is related to the rate of carbon fixation and the availability of the Rubisco enzyme itself, which catalyzes the carboxylation reaction. It is defined as follows:

$$f_{c,C} = \frac{V_{c,mac}(c_i - c_p)}{K_c(1 + \frac{C_{o,a}}{K_o}) + c_i} \tag{2.16}$$

In this case $a_1 = V_{c,max}$ (maximum rate of Rubisco activity) and $a_2 = K_c(1 + \frac{C_{o,a}}{K_o})$, where K_c and K_o are the Michaelis-Menten constants for Rubisco kinetics and $C_{o,a}$ is the oxygen concentration in the chloroplasts, which is assumed equal to the oxygen concentration in air.

The RuBP regeneration-limited process depends on the capability of the plant to regenerate RuBP using ATP and NADPH, and is controlled by the light availability according to the following formula:

$$f_{c,L} = \frac{J}{4}\frac{c_i - c_p}{2c_p + c_i} \tag{2.17}$$

where J represents the rate of the electron transport chain, which depends on the incident light according to the incident photon irradiance spectrum - $b_s(\lambda)$ -, the response of the plant in terms of absorptance - $a(\lambda)$ - and quantum yield spectrum - $\varphi_e(\lambda)$ -, normalized with respect to its maximum value - α -. These three quantities are functions of the wavelength λ . In this case $a_1 = J/4$ and $a_2 = 2c_p$.

To calculate J it is necessary first to define the absorbed photon irradiance (PFD_{abs}), which expresses the amount of active photons reaching the leaf surface per unit time available for the photosynthetic activity. It is defined as:

$$PFD_{abs} = \int b_s(\lambda)a(\lambda)d\lambda \tag{2.18}$$

and the potential rate of electron transport:

$$Q = \alpha \int b_s(\lambda) a(\lambda) \varphi_e(\lambda) d\lambda \tag{2.19}$$

Now, the actual rate of electron transport (J) is computed using the expression of the non-rectangular hyperbola:

$$J = \frac{Q \times f_{PSII} + J_{max} - \sqrt{(Q+J_{max})^2 - 4 \times \theta \times Q \times f_{PSII} \times J_{max}}}{2 \times \theta} \tag{2.20}$$

where f_{PSII} represents the light fraction used by the photosystem II, which is a multi-subunit pigment-protein complex found in thylakoid membranes of oxygenic photosynthetic organisms and has the ability to capture photons and use the energy to extract electrons from water molecules (Lu, 2016). J_{max} is the maximum rate of the electron transport chain and θ is a shape factor (Ögren and Evans, 1993).

The novelty of this approach lies in the fact of including the dependence of the photosynthetic rate on J, and consequently on the incident spectrum, within the optimization scheme described by Konrad et al. (2008). They postulate that stomata should act to maximize carbon gain ($f_{c,C}$ or $f_{c,L}$) while at the same time minimizing water losses through transpiration (λf_w). λ is the marginal water cost of carbon gain and represents the amount of water lost to fix a certain quantity of carbon, it can vary according to different environmental (temperature, humidity, water availability) and biological (plant's photosynthetic apparatus efficiency) factors. In this optimization problem the dynamic component is neglected and the stomatal conductance is assumed to adapt instantaneously to changing environmental conditions. The target function to be maximized is as follows:

$$\begin{aligned} f(g) = f_c - \lambda f_w = \frac{1}{2} \Bigg[& a_1 + (a_2 + c_a) g \\ & - \sqrt{[a_1 + g(a_2 - c_a)]^2 + 4g(a_1 c_p + a_2 c_a g)} \Bigg] - \lambda (agD) \end{aligned} \tag{2.21}$$

The search for the optimum point is obtained by imposing $\delta f(g)/\delta g = 0$ and assuming that λ does not depend on g, the solution of the optimization problem expressed in terms of conductance is the following:

$$\begin{aligned} g = & \frac{-a_1(a_2 - c_a + 2c_p)}{(a_2 + c_a)^2} \\ & + \frac{\sqrt{aD\lambda a_1^2 (c_a - c_p)(a_2 + c_p)(a_2 + c_a - 2aD\lambda)^2 (a_2 + c_a - aD\lambda)}}{aD\lambda (a_2 + c_a)^2 (a_2 + c_a - aD\lambda)} \end{aligned} \tag{2.22}$$

In equation (2.22) λ is provided as an input parameter to the model and is assumed constant, a_1 and a_2 are selected depending on the most limiting process between $f_{c,C}$ and $f_{c,L}$. The selection criterion used in the code is as follows:

$$\begin{cases} a_1 = V_{c,max} & \text{if } f_{c,C} < f_{c,L} \\ a_2 = K_c(1 + \frac{C_{o,a}}{K_o}) & \\ & \\ a_1 = \frac{J}{4} & \text{if } f_{c,C} > f_{c,L} \\ a_2 = 2c_p & \end{cases} \tag{2.23}$$

The obtained value of stomatal conductance is also necessary to compute the transpiration rate (T), which is responsible for the decrease in soil moisture together with the evaporation rate induced by the heat of the solar radiation.

Under the assumption of negligible water storage changes in the plant and steady state conditions, it can be stated that root water uptake is equal to transpiration, which is modeled according to Daly et al. (2004):

$$T = \frac{(\lambda_w \gamma_w g_{ba} \rho D + S\phi)g}{\rho_w \lambda_w \left[\lambda_w(\gamma_w(g_{ba} + g) + gS\right]} \tag{2.24}$$

where λ_w is the latent heat of water vaporization, $\gamma_w = (p_a c_p)/(0.622\gamma_w)$ is the psychrometric constant, p_a is the atmospheric pressure, c_p the specific heat of air, D is the difference between the air relative humidity at saturation and at ambient temperature T_a, S is the slope of the curve relating saturation vapor pressure to temperature, ϕ is the leaf available energy, and $g_{ba} = (r_a + r_b)^{-1}$ is the series of conductances of the leaf boundary layer (per unit leaf area) and of the atmospheric boundary layer (per unit ground area). For simplicity it is assumed that $g_b = g_a$ and that they are constant.

The leaf available energy (ϕ) depends on the photon irradiance spectrum and the plant absorptance. It can be modeled as follows:

$$\phi = \int b_s(\lambda) a(\lambda) \frac{h \times c}{\lambda} N_A d\lambda \tag{2.25}$$

where h is the Plank constant, c the speed of light and N_A the Avogadro number.

The water use efficiency (WUE) is a parameter that allow us to estimate the efficiency of the plants in terms of mass of CO_2 assimilated per mass of water used. It is defined as follows:

$$WUE = \frac{mw_{CO_2} \times f_c}{mw_{H_2O \times T}} \tag{2.26}$$

where mw_{CO_2} and mw_{H_2O} are the molecular weights of carbon dioxide and water, respectively.

The value of g is computed according to equation (2.22) once the values of a_1, a_2 and c_p (calculated according to Leuning (1995)) are known. Since the intercellular CO_2 concentration is not known a priori an initial guess is assigned to c_i and f_c is computed by solving iteratively equations (2.14) and (2.15).

2.2 The linear optimality model

A further simplification of the model can be achieved by linearizing the expression of the carbon biochemical demand in equation (2.13) as suggested by Katul et al. (2010). The main assumption here is that $c_p \ll c_i$, as a result equation (2.13) becomes:

$$f_c = \frac{a_1 c_i}{a_2 + \left(\frac{c_i}{c_a}\right) c_a} = \frac{a_1 c_i}{a_2 + s c_a} \tag{2.27}$$

The combination of the Fick's law with equation (2.27) returns a new expression for the photosynthetic rate given by:

$$f_c = \frac{g a_1 c_a}{a_1 + g(a_2 + s c_a)} \tag{2.28}$$

where s is not treated as a constant and equal to the long-term mean of c_i/c_a but has been computed using equation (2.32), allowing s to vary as a function of temperature, vapor pressure deficit and ambient CO_2 concentration.

The objective function in equation (2.21) now becomes:

$$f(g) = f_c - \lambda f_w = \frac{g a_1 c_a}{a_1 + g(a_2 + s c_a)} - \lambda(agD) \tag{2.29}$$

and the result of the differentiation in the maximum point search returns the following expression for the stomatal conductance:

$$g = \left(\frac{a_1}{a_2 + s c_a}\right)\left[-1 + \left(\frac{c_a}{a\lambda D}\right)^{\frac{1}{2}}\right] \tag{2.30}$$

By replacing equation (2.30) into equation (2.28) it is possible to get a new expression for the photosynthetic rate:

$$f_c = \frac{a_1}{a_2 + s c_a}\left(c_a - \sqrt{a\lambda D c_a}\right) \tag{2.31}$$

and to determine the value of s:

$$s = \frac{c_i}{c_a} = 1 - \sqrt{\frac{a\lambda D}{c_a}} \tag{2.32}$$

Again, the parameters a_1 and a_2 are selected based on the smaller rate determining the limitation of carbon fixation according to the schematization shown in equation (2.23).

Compared to the non-linear case, the model is simpler but limited by the assumptions behind it. The solution in terms of stomatal conductance is obtained by the resolution of a system with 3 equations (2.30, 2.31, 2.32) and 3 unknowns (c_i, f_c, g). In this case an initial estimate of c_i is not required as c_i/c_a no longer depend on g and can be calculated directly once λ, D and c_a are known.

The model was evaluated on the basis of its ability to correctly reproduce the response of plants to different types of light treatments. The parameters used in the model were calibrated on the experimental data obtained by Pennisi et al. (2019) for basil and Mochizuki et al. (2019) for strawberry.

2.2.1 Optimitazion approaches

The response of the plant has been analyzed comparing the linear and the non-linear model, but adopting two different approaches. The first is that of Katul et al. (2010), which assumes that both the regulatory action of stomata (opening and closure) and the carbon fixation process are determined by the minimum between Rubisco and RuBP regeneration rates. The second is that of Medlyn et al. (2011), which assumes that the stomata guard cells are regulated by the rate of electron transport only, and not by the balance between the two processes.

Consequently, four case studies were analyzed. The term "linear" refers to the the linearized model and the group of simplified equations, the term "non-linear" refers to the more general case with the complete set of equations. The addition of "Katul" or "Medlyn" subscriptions refers to the different hypothesis made on the regulatory action of stomata described above. Since the process of carbon assimilation takes place inside the thylakoid membrane and not on the surface of the leaf, f_c is always assumed equal to the minimum rate between $f_{c,C}$ and $f_{c,L}$. Instead, the opening of the stomata (and therefore the estimate of g) may follow respectively the behavior of f_c, with a_1, a_2 given

by the scheme in equation (2.23), according to Katul, or is controlled only by the incident radiation ($f_{c,L}$) with a_1, a_2 always equal to the values corresponding to the light limited case, according to Medlyn. For simplicity we decided to call the different cases as follows: "linear Katul", "non-linear Katul", "linear Medlyn", "non-linear Medlyn", each of them was applied to both basil and strawberry data.

2.3 The co-limitation model

Empirical and optimality models based on Farhuhar's minimum function, where the photosynthetic rate (f_c) is chosen as the minimum between $f_{c,C}$ and $f_{c,L}$, present the problem of an abrupt transition at the switch point between the two limitations. For this reason they need a smoothing parameter to ensure the curve to be continuous.

The development of a model able to take into account at the same time of both limitations without having to specify a priori the limiting process or having to choose the minimum between the limiting rates is proposed as a valid solution and simplification of the problem.

The optimal stomatal conductance formulation developed by Vico et al. (2013) contains parameters that can be selected in order to refer to individual limitations (i.e., Rubisco or RuBP-regeneration) or to consider both. The mathematical framework approximates the Farquhar's photosynthetic equation with a hyperbolic function:

$$f_c = \frac{k_1(c_i - c_p)}{k_2 + c_i} \tag{2.33}$$

where the parameters k_1 and k_2 are determined by imposing the behavior of the hyperbolic curve on the asymptotes. If the intercellular CO_2 concentration is very high ($c_i \gg c_p$), the process is light limited and k_1 is found by equating equation (2.33) with equation (2.17). Instead, if the intercellular CO_2 concentration is very low ($c_i \approx c_p$) the process is Rubisco limited and k_2 is found by equating equation (2.33) and equation (2.16). The values of the two photosynthetic parameters are as follows:

$$\begin{cases} k_1 = \frac{J}{4} \\ \\ k_2 = \frac{J}{4}\frac{a_2}{V_{c,max}} \end{cases} \tag{2.34}$$

where a_2 is always equal to the value assumed in the Rubisco limited case according to equation (2.23). Differentiating equation (2.21) using the new expression for f_c and the Fick's law to derive c_i gives us the optimal stomatal conductance including the two limitations:

$$\begin{aligned} g = & \frac{-V_{c,max}[a_2 - k_3(c_a - 2c_p)]}{(a_2 + k_3 c_a)^2} \\ & + \frac{\sqrt{aD\lambda V_{c,max}^2 (c_a - c_p)(a_2 + k_3 c_p)[a_2 + k_3(c_a - 2aD\lambda)]^2 [a_2 + k_3(c_a - aD\lambda)]}}{aD\lambda(a_2 + k_3 c_a)^2 [a_2 + k_3(c_a - aD\lambda)]} \end{aligned} \tag{2.35}$$

where $k_3 = a_2/k_2 = 4V_{c,max}/J$. In the case of permanent Rubisco limitation, the optimal formulation assumes an expression identical to that in equation (2.35), but with k_3 set to unity. In the case of permanent light limitation the expression of g is analogous to that in equation (2.22), but with a_1 and a_2 always equal to $J/4$ and $2c_p$. A further simplification can be obtained by linearizing the expression of the carbon biochemical

demand in equation (2.33) similarly to (2.27) by imposing that s is constant and equal to 0.7 for C_3 plants. Here, the complete formulation without the linearization hypothesis has been analyzed.

Substituting the values of k_1 and k_2 in equation (2.33) gives an expression for the photosynthetic rate that depends on both limitations:

$$f_c = \frac{V_{c,max}(c_i - c_p)}{a_2 + \left(\frac{4V_{c,max}}{J}\right) c_i} \tag{2.36}$$

Equation (2.36) converges to the Rubisco limited rate case when

$$V_{c,max} \approx J/4 \tag{2.37}$$

and to the light limited rate when

$$\frac{J/4}{V_{c,max}} \approx \frac{2c_p}{K_c\left(1 + \frac{O_a}{K_0}\right)} \tag{2.38}$$

The mathematical steps necessary to derive equations (2.37) and (2.38) are given in the Appendix A.

The model equations can be used to predict gas exchanges at the leaf level with time scales varying from hours to days. Effects due to high-frequency fluctuations in light, vapor pressure deficit and the presence of nutrients (i.e., nitrogen) that may alter the magnitude of the photosynthetic rate and the stomatal conductance were neglected.

Table 2.1 summarizes all the parameters used in the models and their units of measurement. The boxes represented with a bar indicate that the corresponding parameters have been calibrated and vary according to the case under consideration.

Parameter	Description	Value or temperature dependence	Units
$V_{c,\max,25}$	Maximum Rubisco capacity at reference temperature	/	μmol m^{-2}s^{-1}
α	Maximum value of quantum yield spectrum	/	mol electrons mol^{-1}photons
λ	Marginal water cost of carbon gain	/	μmol mol^{-1}kPa^{-1}
r_a	Air resistance	/	sm^{-1}
$J_{\max,25}$	Electron transport rate at reference temperature	/	μmol m^{-2}s^{-1}
rjv	Ratio between $J_{\max,25}$ and $V_{c,\max,25}$	/	dimensionless
θ	Shape parameter for hyperbola	/	dimensionless
$K_{c,25}$	Michaelis constant for CO_2 at reference temperature	302	μmol mol^{-1}
$K_{o,25}$	Michaelis constant for O_2 at reference temperature	256	μmol mol^{-1}
$C_{o,a}$	O_2 concentration in air	0.209×10^6	μmol mol^{-1}
γ_0	CO_2 compensation point at $T_{\text{ref},1}$	34.6	μmol mol^{-1}
γ_1	Coefficient in c_p	0.0451	dimensionless
γ_2	Coefficient in c_p	0.000347	dimensionless
$T_{\text{ref},1}$	Reference temperature for c_p	293.2	K
T_s	Ambient temperature	297.15(basil) - 298.15(strawberry)	K
$T_{\text{ref},2}$	Reference temperature for k_T	298.15	K
c_p	Compensation point	$\gamma_0 \left[1 + \gamma_1(T_s - T_{\text{ref},1}) + \gamma_2(T_s - T_{\text{ref},1})\right]^2$	$\mu\text{mol}_{\text{CO}_2}/\text{mol}_{\text{air}}$
$H_{d,V_{c,\max}}$	Deactivation energy for $V_{c,\max}$	200	$kJ\text{mol}^{-1}$
$H_{a,V_{c,\max}}$	Activation energy for $V_{c,\max}$	72	$kJ\text{mol}^{-1}$
$H_{d,J_{\max}}$	Deactivation energy for $J_{\max}$	200	$kJ\text{mol}^{-1}$
$H_{a,J_{\max}}$	Activation energy for $J_{\max}$	50	$kJ\text{mol}^{-1}$
H_{a,K_c}	Activation energy for K_c	59.43	$kJ\text{mol}^{-1}$
H_{a,K_o}	Activation energy for K_o	36.00	$kJ\text{mol}^{-1}$
ΔS	Entropy factor	0.650	$kJ\text{mol}^{-1}\text{K}^{-1}$
k_T	Arrhenius function for temperature dependence	$\exp\left[\frac{H_{a,i}(T_s - T_{\text{ref},2})}{T_{\text{ref},2} R T_s}\right] \frac{1+\exp\left(\frac{T_{\text{ref},2}\Delta S - H_d}{T_{\text{ref},2} R}\right)}{1+\exp\left(\frac{T_s \Delta S - H_d}{T_s R}\right)}$	dimensionless
$V_{c,\max}$	Maximum Rubisco capacity	$V_{c,\max,25} \times k_T$	μmol m^{-2}s^{-1}
$J_{\max}$	Electron transport rate	$J_{\max,25} \times k_T \times r_{J,V}$	μmol m^{-2}s^{-1}
K_c	Michaelis constant for CO_2	$K_{c,25} \times \exp\left(H_{a,K_c} \frac{T_s - T_{\text{ref},1}}{T_{\text{ref},1} R T_s}\right)$	dimensionless
K_o	Michaelis constant for O_2	$K_{o,25} \times \exp\left(H_{a,K_o} \frac{T_s - T_{\text{ref},1}}{T_{\text{ref},1} R T_s}\right)$	dimensionless

Table 2.1: Model parameters, c_p is computed as in Leuning (1995) and temperature dependence is taken into account as in Kattge and Knorr (2007).

Chapter 3

Models calibration

The algorithm used for the model calibration is called Shuffled Complex Evolution (SCE-UA) method and was developed at the University of Arizona by Duan et al. (1993). It is a global optimization algorithm used in hydrology to refine and calibrate hydrological models with greater accuracy and it uses an evolutionary approach to optimize model parameters.

The SCE-UA algorithm begins by initializing a population of individuals randomly or using other initialization methods. Each individual represents a potential solution to the optimization problem. The fitness of each individual is evaluated using an objective function, which quantifies how well the individual performs in solving the problem. Based on the evaluation results, new sets of parameters are generated, which represent improvements compared to the previous generation. The parameter combinations are mixed and rearranged through an exchange process (shuffle) to generate new combinations that must be evaluated by running the model and calculating the specific target function. This iterative process involves the mixing of the new parameter combinations and their evaluation until a solution that has a good match between the observed data and the model results is found. Throughout the iterations, the individuals in the population undergo evolutionary processes, gradually improving the overall fitness of the population.

In this case the target function to be minimized is as follows:

$$M = n - \sum_{i=1}^{n} KGE_i \tag{3.1}$$

where n represents the number of variables to be calibrated and KGE_i the individual Kling–Gupta efficiency. The method evaluates the average percentage change in the target function in the number of previously specified loops, if it is less than 1% the code stops and reaches convergence.

The calibration procedure was carried out for all models described in the previous chapter. Each model was calibrated on the experimental data set obtained for basil and strawberry.

3.1 Basil

The calibration carried out on the basil test case refers to the results obtained by Pennisi et al. (2019). They have grown basil plants within growth chambers with 5 different types of LED light treatments featuring different R:B ratio (respectively, $RB_{0.5}$, RB_1, RB_2, RB_3 and RB_4) and using fluorescent lamps as control (Figure 3.1). Within the

growth chambers they kept a constant photosynthetic photon flux density (PPFD) of $215 \pm 5.5\ \mu molm^{-2}s^{-1}$, a photoperiod of 16/8 hours of light/dark, air temperature of 24 ± 2 °C, relative humidity of $55 - 70\%$ and ambient CO_2 concentration of 450 ppm.

Water use efficiency (WUE), stomatal conductance (g) and chlorophyll content were measured and compared with the results provided by the different models. WUE is computed as the ratio between the leaf fresh yield or edible fresh weight (FW) and the volume of water consumed by the plant and the unit is $g\ FW\ L^{-1}\ H_2O$. The stomatal conductance is measured using a leaf porometer and expressed as $mmol\ H_20\ m^{-2}s^{-1}$. The chlorophyll content is computed using a hand-held leaf chlorophyll meter and is considered as an approximation of the assimilation rate. The unit is the N-Tester value (Orsini et al., 2018).

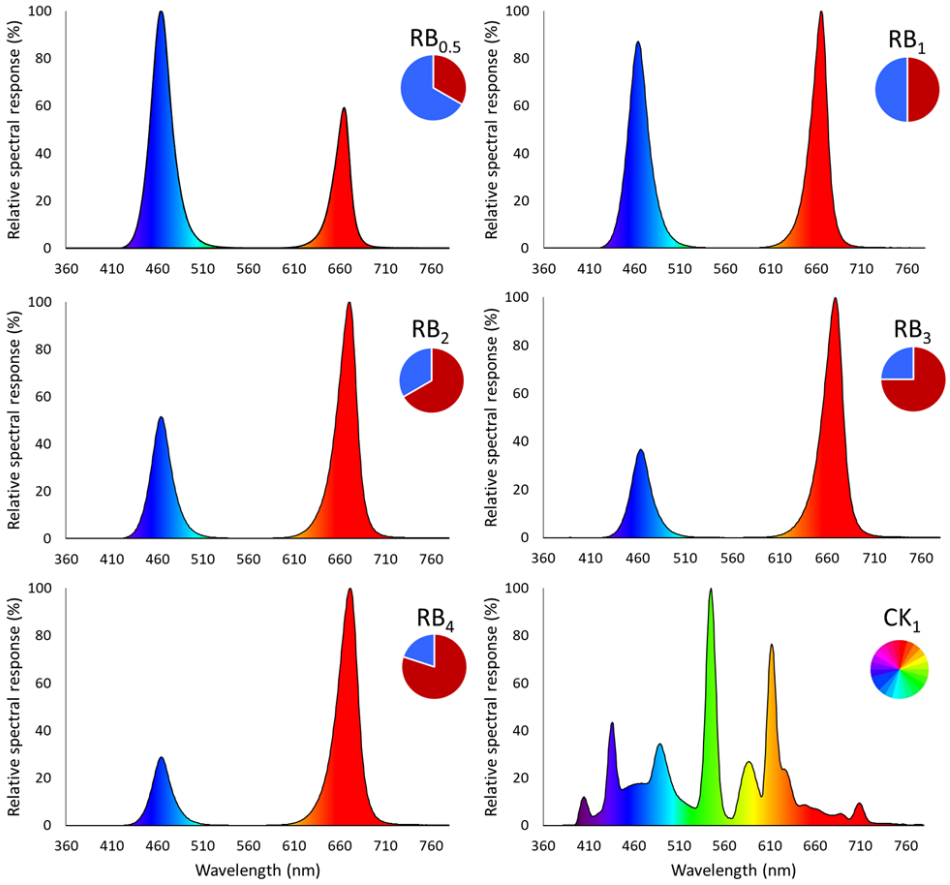

Figure 3.1: Relative spectral response as a function of the wavelength for different R:B ratios in the Pennisi et al. (2019) experimental setup.

The results obtained by Pennisi et al. (2019) suggest that an increase in the portion of blue light is responsible for an increase in stomatal conductance and is associated to higher water consumption. A more efficient yield is achieved through the increase in the fraction of red light, which brings greater benefits in terms of WUE and edible fresh weight, despite the partial stomatal closure.

As concerns basil, the parameters that have been calibrated within the algorithm are shown in Table 3.1. The correct functioning of the iterative scheme requires the definition of the upper (ub) and lower (lb) boundaries and the initial guess (x_0) of the parameters. The upper and lower limits were selected on the basis of the physiological characteristics of the plants. Due to limited knowledge of ventilation conditions, the leaf and atmospheric boundary layer resistances were calibrated assuming that $r_a = r_b$.

Parameter	$J_{max,0}$	rjv	r_a	θ	α	λ
Unit	μmol $m^{-2}s^{-1}$	*dimensionless*	sm^{-1}	*dimensionless*	*dimensionless*	μmol $mol^{-1}kPa^{-1}$
lb	75	1.50	1	0.70	0.20	0
ub	300	2.50	600	0.90	0.80	100
x_0	150	2.00	50	0.74	0.79	20

Table 3.1: Upper limits (ub), lower limits (lb) and initial starting point (x_0) in the SCE-UA calibration algorithm.

The extremes of the λ parameter have been selected taking into account the frequency distribution curve (Figure 3.2) obtained from the gas exchange measurements collected in a maturing pine forest under ambient and enriched atmospheric CO_2 concentration (Katul et al., 2010). The λ parameter is obtained from the definition of equation (2.21) as:

$$\lambda = \frac{\delta f_c / \delta g}{\delta f_w / \delta g} \tag{3.2}$$

From the measured data of stomatal conductance, compensation point and vapor pressure deficit, λ can be computed using the linear and non-linear equations derived from the differentiation of the optimal functions. The equations are, respectively:

$$\lambda_{LI} = \frac{c_a}{aD}\left(1 - \frac{c_i}{c_a}\right)^2 \tag{3.3}$$

and

$$\lambda = \frac{a_1(c_a - a_2 - 2c_p) + (c_a + a_2)[y - g(c_a + a_2)]}{2aDy} \tag{3.4}$$

where

$$y = \sqrt{a_1^2 + 2a_1(a_2 - c_a + 2c_p)g + (a_2 + c_a)^2 g^2} \tag{3.5}$$

It is necessary to emphasize the fact that the values of λ used in the simulation are always set to constant and assumed equal to the output of the calibration algorithm. This hypothesis seems to contradict the simplified linear expression of λ in equation (3.3), where, for $c_a \gg c_i$, λ grows linearly with c_a.

The assumption on the dependence of λ determines the behavior of stomatal conductance as the external CO_2 concentration changes. According to Vico et al. (2013), the hypothesis of $\lambda = const.$ is valid for simulating the plant's response to c_a fluctuations in the short term and for sub-daily variations, such that g grows for sub-ambient CO_2 concentrations and decreases for high c_a. A linear dependence of λ on c_a seems more suitable to capture changes in growth conditions (and thus in the availability of resources) in the long term, such that a decrease of λ is observed even for sub-ambient CO_2 concentrations.

Table 3.2 shows the calibrated parameters on all types of model in the case of basil.

It is important to note that in all cases the values of θ, α and λ are very close to the extreme values set in the algorithm. Moreover, the leaf and atmospheric boundary layer conductances are quite low, suggesting a strong resistance to water vapor flux. In order to test the predictive capabilities of all the models different metrics were evaluated to assess

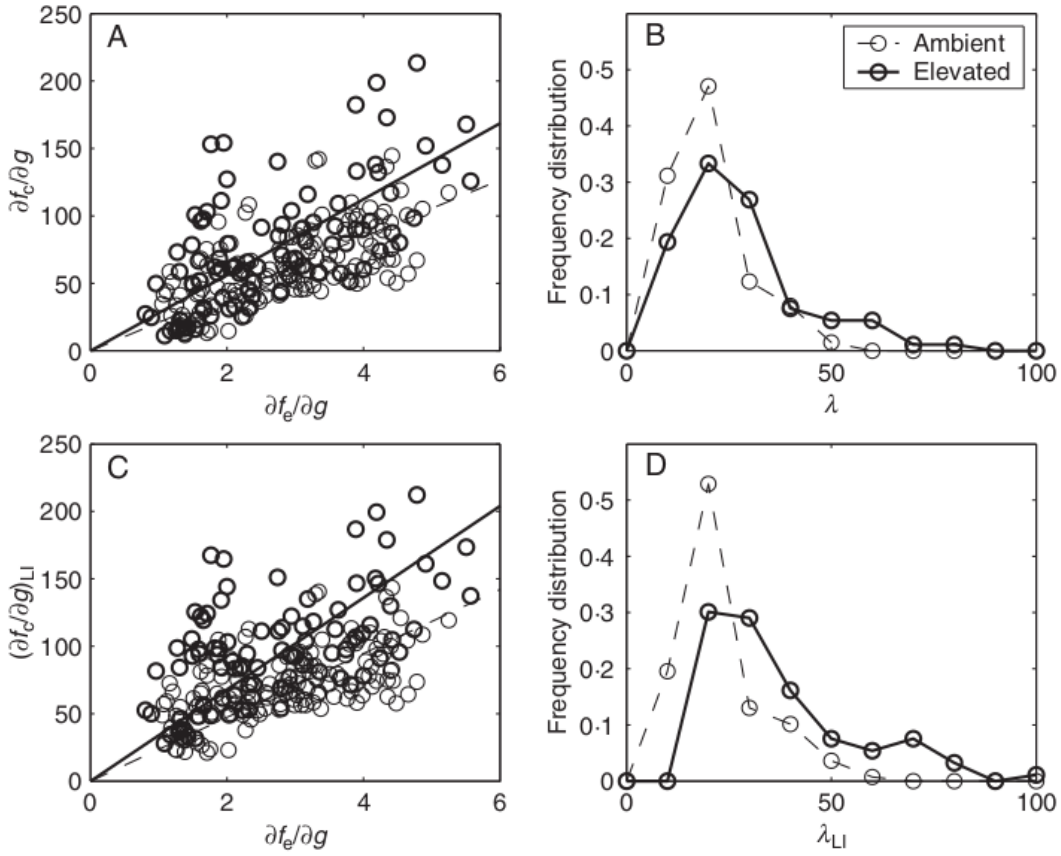

Figure 3.2: Left panels: linear regression-based estimates of the parameter λ from equation (3.2) for the non-linear (A) and the linear optimization models (C), using gas exchange measurements collected under ambient (light circles) and elevated (heavy circles) CO_2 concentration. Right panels: frequency distribution of λ (B) and λ_{LI} (D) for needles exposed to ambient and elevated CO_2 concentration.

the goodness of fit between the data measured by Pennisi et al. (2019) and the models output. The coefficient of determination (R^2) was evaluated for the comparison between assimilation rate (A_n) and chlorophyll content (N-tester value), and between measured and modeled WUE, since they report different units of measurement. Root mean square error (RMSE) and Kling-Gupta efficiency (KGE) were used for the comparison between stomatal conductances.

Figures 3.3 and 3.4 show the differences between the calibrated model results and the measured data.

The coefficient of determination (R^2) is a measure that assesses the ability of a model to predict or explain an outcome in the linear regression setting. It determines the proportion of variance of the modeled data that can be explained by the measured data. The coefficient of determination is the square of the Pearson correlation coefficient, also known as "r" in statistics. The value of "r" can result in a negative number, but because r-squared is the result of "r" multiplied by itself, R^2 can not be a negative number.

Regarding the behavior of A_n all models are very similar and are characterized by a coefficient of determination of about 69%, producing a better fit on experimental data than the Camporese and Abou Najm's model. The assimilation rate and the chlorophyll content are positively correlated ($r \simeq 0.83$) and the magnitude of the correlation suggests a high strength of association between the two variables.

The same can be said for the WUE because all the results are very similar. In this

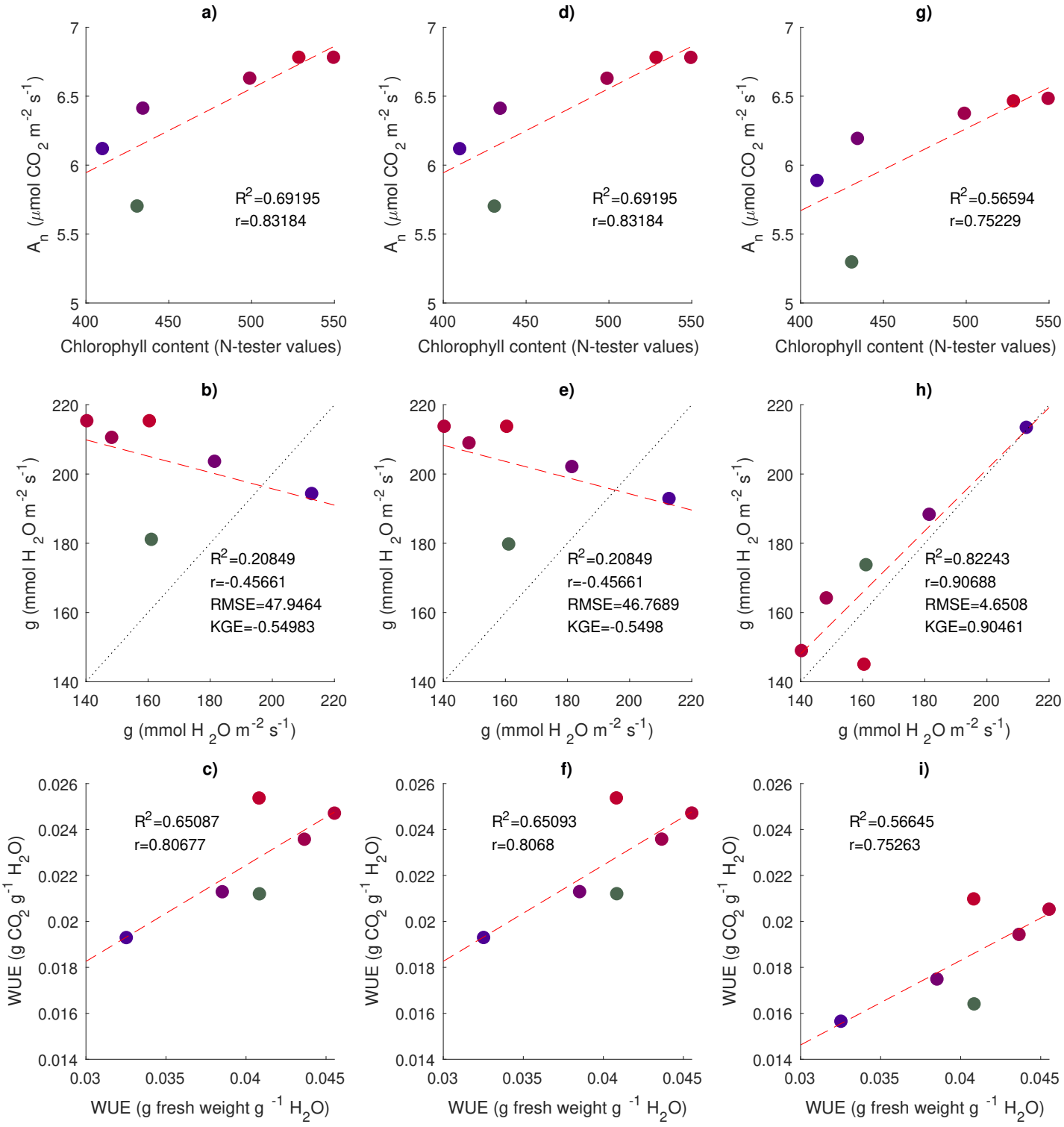

Figure 3.3: Simulated photosynthetic rate (A_n), stomatal conductance (g), water use efficiency (WUE) and related observations from the experimental study of Pennisi et al. (2019). The first, second and third panel rows report photosynthetic rate, stomatal conductance and water use efficiency for the linear Katul (a-b-c), linear Medlyn (d-e-f) and Camporese and Abou Najm (2022) (g-h-i) cases, respectively. The chlorophyll content (a-d) can be considered as proxy for photosynthetic rate. The dot colors denote light treatment, while dashed and dotted lines indicate the correlation and 1:1 lines.

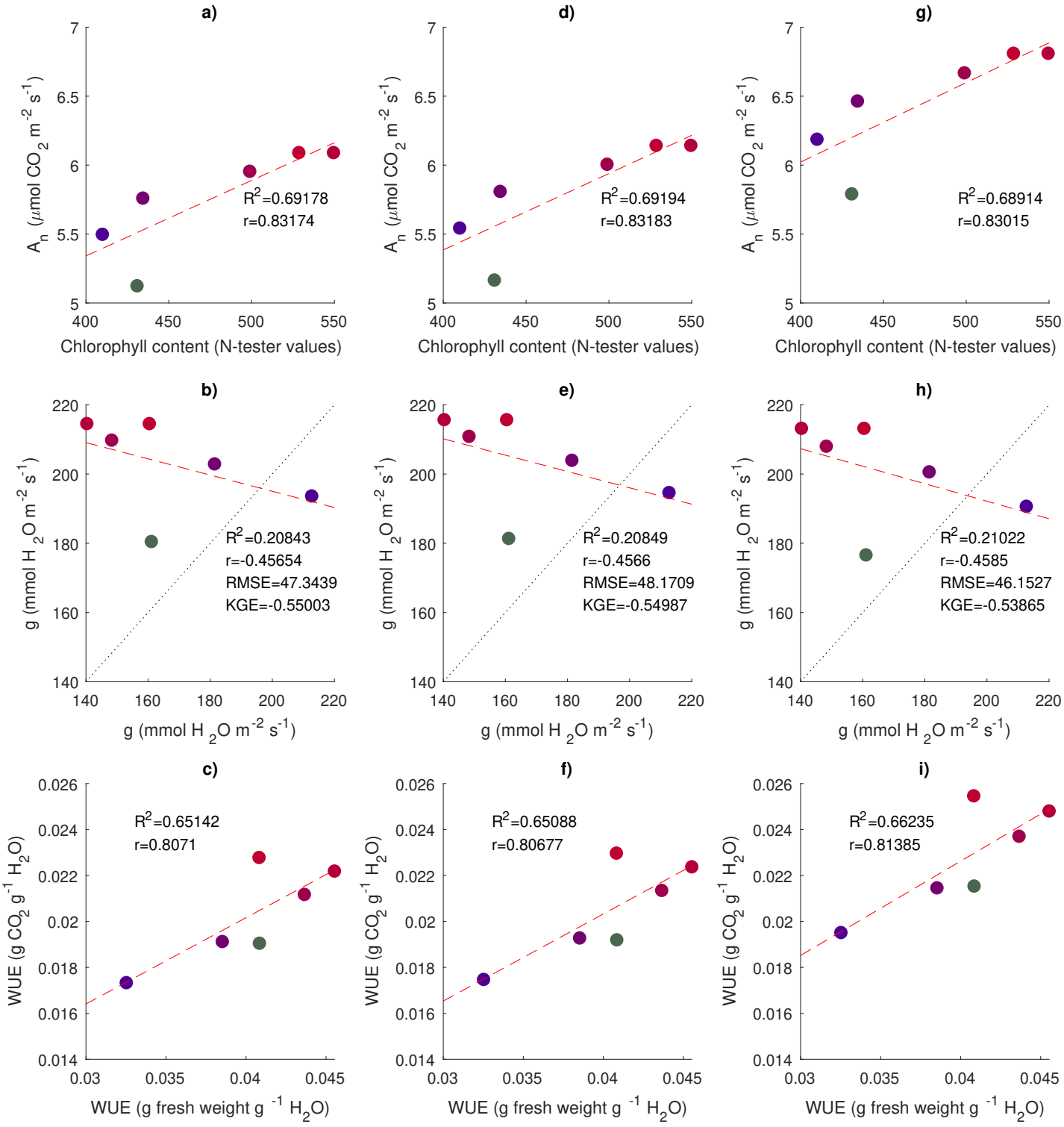

Figure 3.4: Simulated photosynthetic rate (A_n), stomatal conductance (g), water use efficiency (WUE) and related observations from the experimental study of Pennisi et al. (2019). The first, second and third panel rows report photosynthetic rate, stomatal conductance and water use efficiency for the non-linear Katul (a-b-c), non-linear Medlyn (d-e-f) and co-limitation (g-h-i) cases, respectively. The chlorophyll content (a-d) can be considered as proxy for photosynthetic rate. The dot colors denote light treatment, while dashed and dotted lines indicate the correlation and 1:1 lines.

Parameter	$J_{max,0}$	rjv	r_a	θ	α	λ
Unit	μmol $m^{-2}s^{-1}$	*dimensionless*	sm^{-1}	*dimensionless*	*dimensionless*	μmol $mol^{-1}kPa^{-1}$
Linear Katul	299.78	1.53	599.96	0.89	0.20	4.14
Linear Medlyn	298.41	2.20	599.90	0.89	0.20	4.20
Non-linear Katul	299.71	2.02	598.45	0.89	0.20	1.04
Non-linear Medlyn	299.33	2.30	599.21	0.89	0.20	1.04
Co-limitation	299.92	1.50	599.97	0.89	0.20	0.87

Table 3.2: Calibrated model parameters using the SCE-UA algorithm relative to the basil case.

case a coefficient of determination of about 65% tells us that the majority of the data fit the model. The correlation is strongly positive ($r \simeq 0.81$). Again, a higher correlation of the optimization theories respect to the Camporese and Abou Najm's model suggests an improvement in the fit of the data.

Quite different is the case of the correlation between measured and modeled stomatal conductances. The negative correlation given by the opposite slope of the linear regression line ($r \simeq -0.46$) suggests an opposite trend of stomatal conductance with respect to the measured values. In general, we can see that in all cases the conductance values are higher for the red light and decrease as the blue light fraction increases. This result not only differs a lot from the experimental measurements ($\simeq 20\%$ of the data fit the regression line), but also does not allow to correctly interpret the response that stomata have as a function of variation in the light spectrum.

This result is a consequence of the equations underlying the optimization models. By comparing the empirical equation proposed by Kromdijk et al. (2019) (eqn (2.3)) and the equations of the linear and non-linear models (eqns (2.30) and (2.22)), we can see that the parameters on which g depends are reduced from two (g_0,g_1) to one (λ), decreasing the degrees of freedom of the models by one unit. From the standpoint of linear regression between measured and modeled data, reducing one degree of freedom means removing one independent variable from the regression model. This means that one predictor variable is no longer considered in the model, affecting the accuracy and precision of the regression results. With reduced degrees of freedom, the regression model becomes simpler and has lower complexity. It results in a loss of information and bias phenomena in the estimated relationships between the variables. Therefore, reducing one degree of freedom in a regression analysis is a trade-off between simplicity and potential loss of information. The regression line is defined by the angular coefficients and the intercept. Reducing by one degree of freedom means fixing one of these coefficients rather than estimating it from the data. As a result, the regression line is constrained to pass through a specific point or have a specific slope. In summary, reducing by one degree of freedom in a linear regression model limits the choice of parameters of the regression line and may result in a greater reduction in its ability to fit the data.

3.2 Strawberry

Regarding strawberry, a more complete experimental data set is provided by Mochizuki et al. (2019). They evaluated the plant's response in terms of photosynthetic rate (f_c), stomatal conductance (g), transpiration (T) and leaf intercellular CO_2 concentration (c_i) to varying irradiance on the adaxial and abaxial side of strawberry leaves using blue, red and green light. The variables were measured every 100 μmol m^{-2}s^{-1}, increasing $PPFD$ gradually from 0 to 600 μmol m^{-2}s^{-1}, for a total of 7 measurements. The CO_2 concentration within the greenhouse where strawberry plants were cultivated is kept constant at 350 μmol mol^{-1} and temperature is assumed equal to 25 °C. The model results were compared with the variables measured for the adaxial side, since it is the side directly affected by light and characterized by greater variability in measurements than the abaxial one.

The same upper and lower limits shown in Table 3.1 were used in the strawberry SCE-UA algorithm, with the addition of the parameter corresponding to relative humidity (RH) since it was not measured directly and is necessary for the computation of vapor pressure deficit (D), f_c and g.

Table 3.3 shows the parameters calibrated on all models in the case of strawberry.

Parameter	$J_{max,0}$	rjv	r_a	θ	α	λ	RH
Unit	μmol m^{-2}s^{-1}	*dimensionless*	sm^{-1}	*dimensionless*	*dimensionless*	μmol mol^{-1}kPa^{-1}	%
Linear Katul	81.15	2.21	377.64	0.76	0.21	14.14	64.92
Linear Medlyn	101.39	2.26	491.64	0.84	0.27	34.79	77.97
Non-linear Katul	131.00	1.87	159.00	0.75	0.20	11.14	71.34
Non-linear Medlyn	152.21	2.19	215.23	0.84	0.20	29.29	86.20
Co-limitation	205.53	2.50	324.66	0.83	0.20	5.20	42.84

Table 3.3: Calibrated model parameters using the SCE-UA algorithm relative to the strawberry case.

From the comparison between the calibrated parameters for basil and strawberry we can conclude that the former is characterized by $V_{c,max,0}$ values twice as large as those of strawberry, being $V_{c,max,0} = J_{max,0}/rjv$ and $J_{max,0}$ of basil about twice that of strawberry.

This result is in agreement with the data already present in the literature (Rho et al. (2011), Park et al. (2016), Kattge and Knorr (2007)). Although both plants are part of the category of perennial herbaceous plants, basil belongs to the Lamiaceae family and strawberry to the Rosaceae family. Strawberry is characterized by absorptance and quantum yield spectra similar to fruit trees of the same family (e.g., cherry, peach, apricot and almond) than those used for lettuce and basil which are more typical of the herbaceous species (Figure 4.2). Plants similar to strawberry are less productive in terms of photosynthetic activity compared to basil, since they are characterized by lower quantum efficiency, lower electron transport rate and lower carboxylation capacity. In addition, except for the linear Medlyn case, there is a significant decrease in air resistance ($r_a = r_b$) respect to the parameters calibrated on Pennisi et al. (2019). A decrease in r_a corresponds to an increase in the conductance of the leaf and atmospheric boundary

layer, affecting the magnitude of the transpiration process (eqn (2.24)).

As we can see in Figure 3.5 for all cases the model produces a greater photosynthetic rate for red light and lower for blue light. This result is in agreement with the experimental data, however, there is a difference in the behavior of non-linear models, since they never go to saturation. Although the general behavior of A_n is correct, as concerns linear models we can say that the Medlyn one produces an overestimation of A_n and saturates for lower $PPFD$ levels respect to the Katul case. Non-linear models never go to saturation because they do not experience the transition into Rubisco limitation for high values of $PPFD$. This phenomenon can be attributed to the estimation of the Rubisco limited rate ($f_{c,C}$), which, for $PPFD = 600$ μmol m^{-2}s^{-1}, does not intersect the light limited rate ($f_{c,L}$) and does not cause the transition. Using the conversion formula weighed according to the wavelength (eqn (2.25)) a $PPFD$ of 600 μmol m^{-2}s^{-1} corresponds to an irradiance of 135 W m^{-2}. This value is not sufficient to ensure the transition to the Rubisco limitation in non-linear models (see Figures A.10 and A.14).

A higher photosynthetic rate for red light is in agreement with the experimental results, it is responsible for activating the carbon fixation process and promoting the photochemical reactions. The growth of A_n for blue light corresponding to high $PPFD$ seems to be related not only to the increase of the photosynthetic photon flux, but also to the result of stomata opening that assimilate the available carbon more easily. Negative values of A_n can be attributed to the phenomenon of cellular respiration occurring in the nocturnal phases when $PPFD$ is very low. The dark respiration term (R_d) was neglected in Farquhar's photosynthetic model and therefore only positive values are observed. Regarding the fit of the models to the experimental results, the $RMSE$ is not close to 0 because of the large deviation of the modeled red light curve from the measured one. Instead, the efficiency metrics suggest a good fit of the data except for the linear Medlyn case.

While experimental data show that blue light is responsible for the opening of stomata, optimization models produce opposite results, returning a greater stomatal conductance for red light and lower for blue light (Figure 3.6). This limitation can be traced back to the lack of a direct dependence on light in the equations (2.30) and (2.22) for linear and non-linear models, respectively. Because of the misleading results, no assessment can be made on the goodness of fit. A correct interpretation of the trend of g is obtained in the model of Camporese and Abou Najm (2022), where stomatal conductance is higher for blue light and lower for red light as $PPFD$ varies. Although the fit of the data is worse than the optimization models, it is clear that the empirical formula of Kromdijk used for estimating g turns out to be a better predictor of stomatal opening as a function of changing light spectrum.

The transpiration trend (Figure 3.7) is consistent with the experimental results. All cases show $RMSE$ values below 0.41 and efficiency metrics between 0.6 and 1.

Very different is the trend of the intercellular CO_2 concentration (Figure 3.8) that remains constant with the variation of the $PPFD$, showing no change to the different light treatments. Regarding the results of linear models, this behavior is in agreement with equation (2.32) used for the computation of c_i, since no light-dependent terms are present.

As concerns non-linear models, substituting equation (2.22) into equation (2.15) yields a c_i/c_a ratio that no longer depends on the only light-dependent term, i.e., a_1:

$$\frac{c_i}{c_a} = \frac{1}{2} + \frac{(-1 - a_2 z) + \sqrt{1 + (a_2 - c_a)^2 z^2 + 2(a_2 - c_a)z + 4z(c_p + a_2 c_a z)}}{2c_a z} \tag{3.6}$$

where z is a defined as:

$$z = \frac{(c_a - a_2 - 2c_p)}{(a_2 + c_a)^2} + \frac{\sqrt{(c_a - c_p)(a_2 + c_p)(a_2 + c_a - 2aD\lambda)^2}}{(a_2 + c_a)^2\sqrt{(aD\lambda)(a_2 + c_a - aD\lambda)}} \tag{3.7}$$

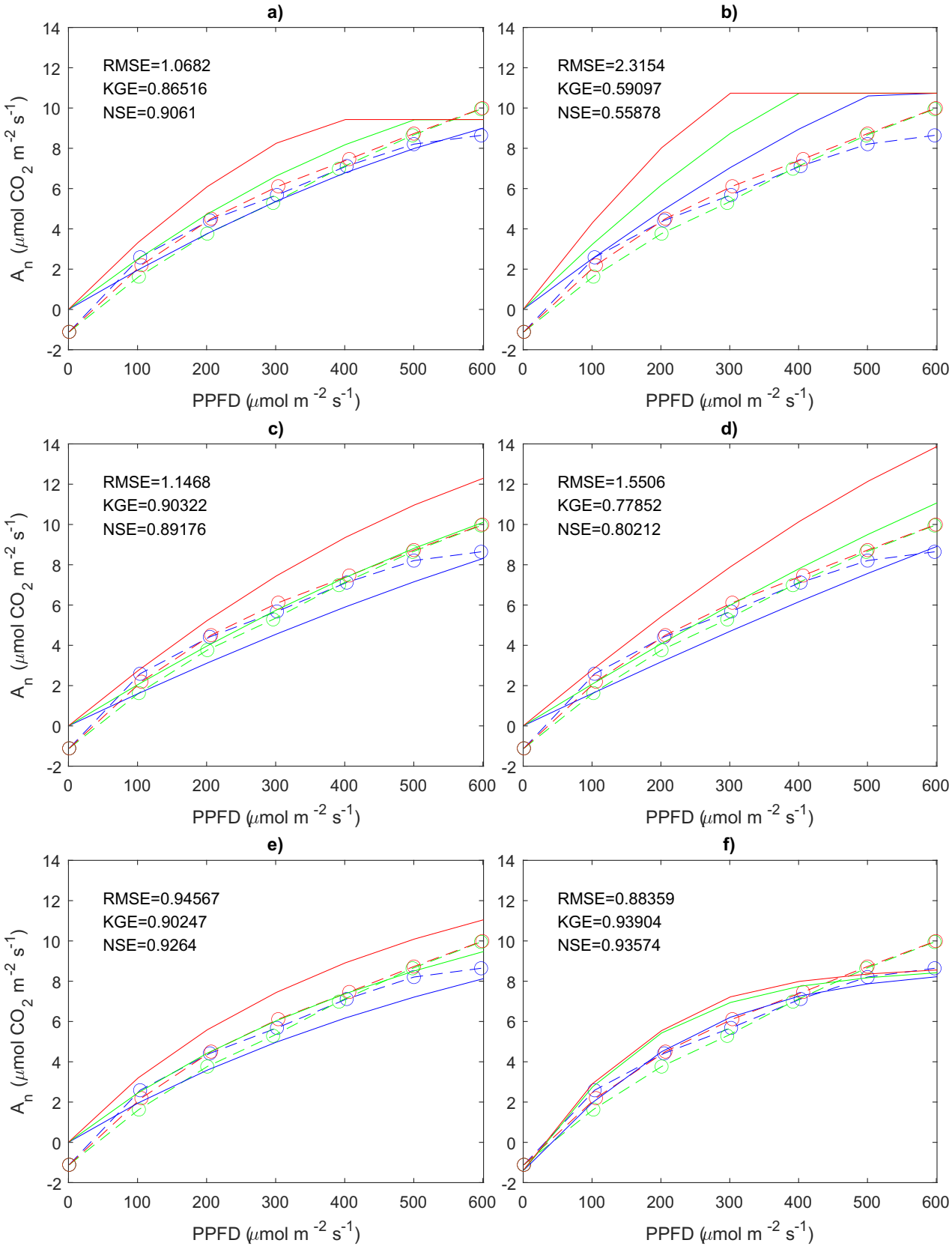

Figure 3.5: Simulated (solid lines) photosynthetic rate (A_n) for the linear Katul (a), linear Medlyn (b), non-linear Katul (c), non-linear Medlyn (d), co-limitation (e) and Camporese and Abou Najm (f) models, compared with observations (symbols with dashed lines) in the experiments by Mochizuki et al. (2019) with strawberry subjected to different light treatments and photon flux densities. The blue and red colors indicate treatments with blue, green, and red LEDs, respectively.

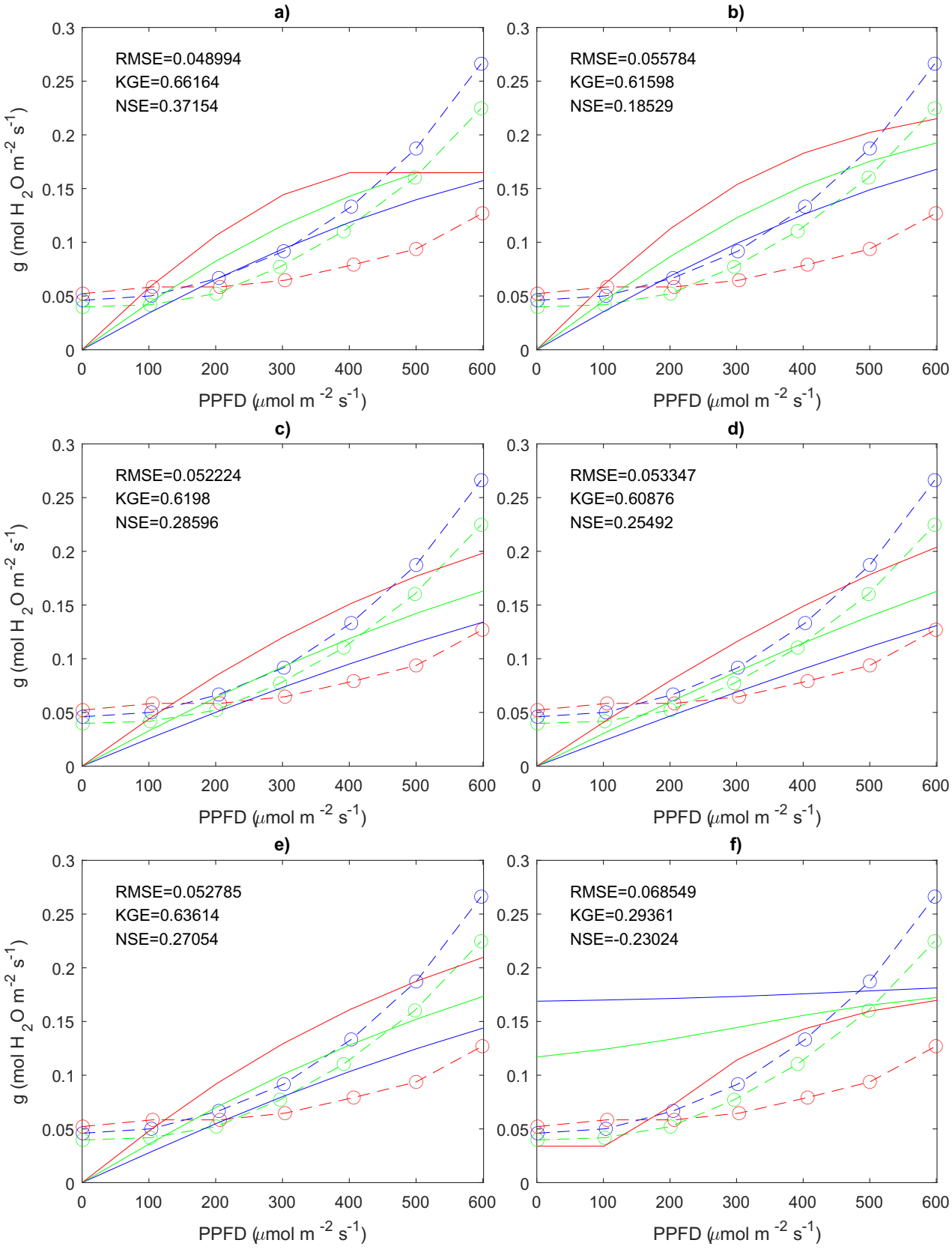

Figure 3.6: Simulated (solid lines) stomatal conductance (g) for the linear Katul (a), linear Medlyn (b), non-linear Katul (c), non-linear Medlyn (d), co-limitation (e) and Camporese and Abou Najm (f) models, compared with observations (symbols with dashed lines) in the experiments by Mochizuki et al. (2019) with strawberry subjected to different light treatments and photon flux densities. The blue, green and red colors indicate treatments with blue, green, and red LEDs, respectively.

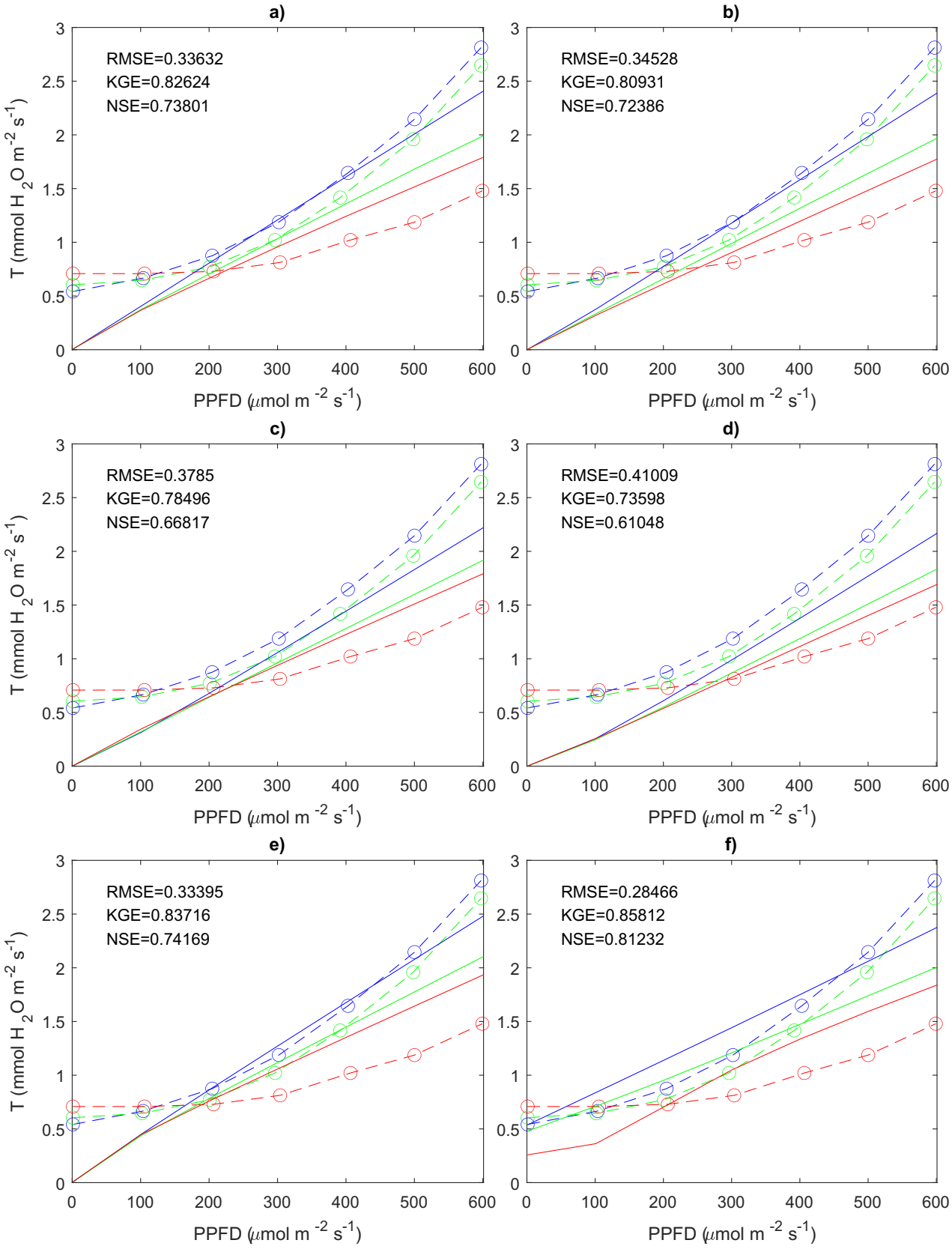

Figure 3.7: Simulated (solid lines) transpiration rate (T) for the linear Katul (a), linear Medlyn (b), non-linear Katul (c), non-linear Medlyn (d), co-limitation (e) and Camporese and Abou Najm (f) models, compared with observations (symbols with dashed lines) in the experiments by Mochizuki et al. (2019) with strawberry subjected to different light treatments and photon flux densities. The blue, green and red colors indicate treatments with blue, green, and red LEDs, respectively.

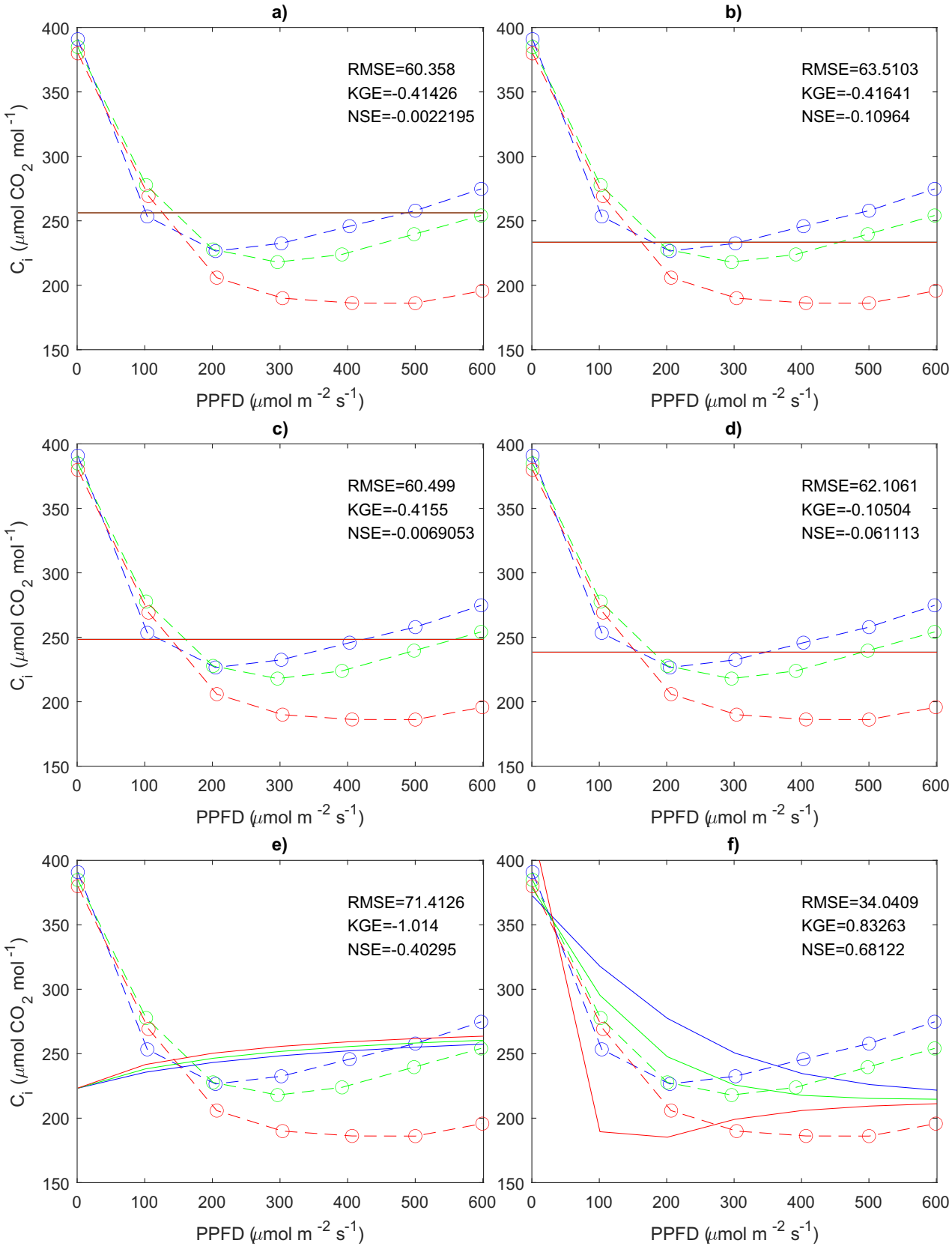

Figure 3.8: Simulated (solid lines) intercellular CO_2 concentration (c_i) for the linear Katul (a), linear Medlyn (b), non-linear Katul (c), non-linear Medlyn (d), co-limitation (e) and Camporese and Abou Najm (f) models, compared with observations (symbols with dashed lines) in the experiments by Mochizuki et al. (2019) with strawberry subjected to different light treatments and photon flux densities. The blue, green and red colors indicate treatments with blue, green, and red LEDs, respectively.

Chapter 4

Sensitivity analyses

The light source is characterized by the definition of spectral irradiance, which provides the power (energy per unit time) received by a surface for a particular wavelength of light. Figure 4.1 allows us to understand how certain wavelengths are more prominent than others. This implies that there are photons with specific energy that the Earth receives in greater quantities. Understanding the mechanism by which the spectrum of light is captured by the plants is immensely valuable as it allows to determine the total energy received from a large number of photons.

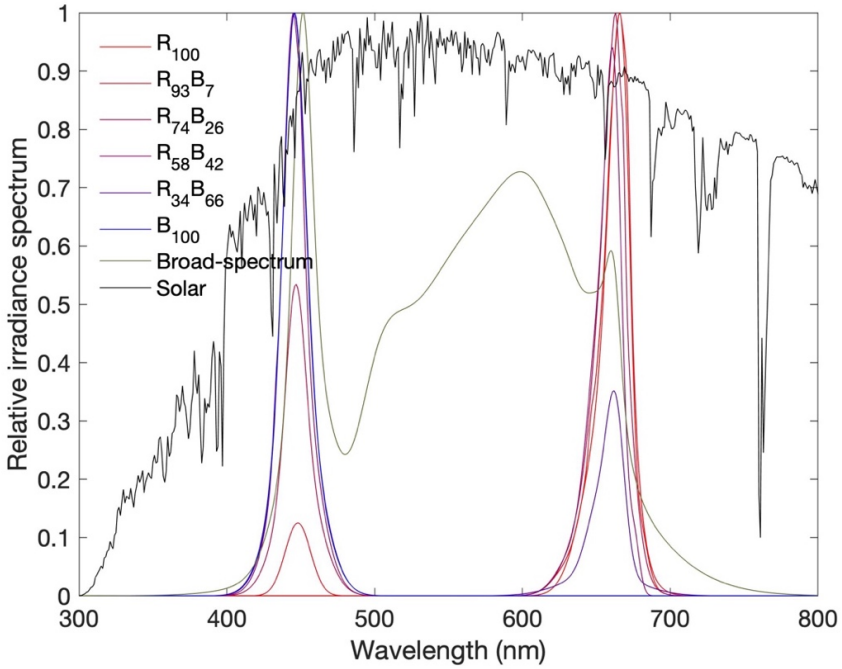

Figure 4.1: Relative (with respect to the maximum value) spectra of irradiance used in the sensitivity analysis. The solar spectrum is the reference irradiance as in Gueymard et al. (2002).

The plant's behavior modifies as light quality changes. The two main parameters determining the plant's response are called "quantum yield" - $\varphi_e(\lambda)$ - and "absorptance" - $a(\lambda)$ -, and they are provided as input parameters in the model (Figure 4.2). The quantum yield represents the number of photons required by a plant to release one molecule of oxygen during photosynthesis and expresses the efficiency with which absorbed photons can be utilized for CO_2 assimilation. The absorptance represents the ratio of the absorbed

to the incident radiant flux and is a proxy for the efficiency with which the plant is able to absorb radiant energy.

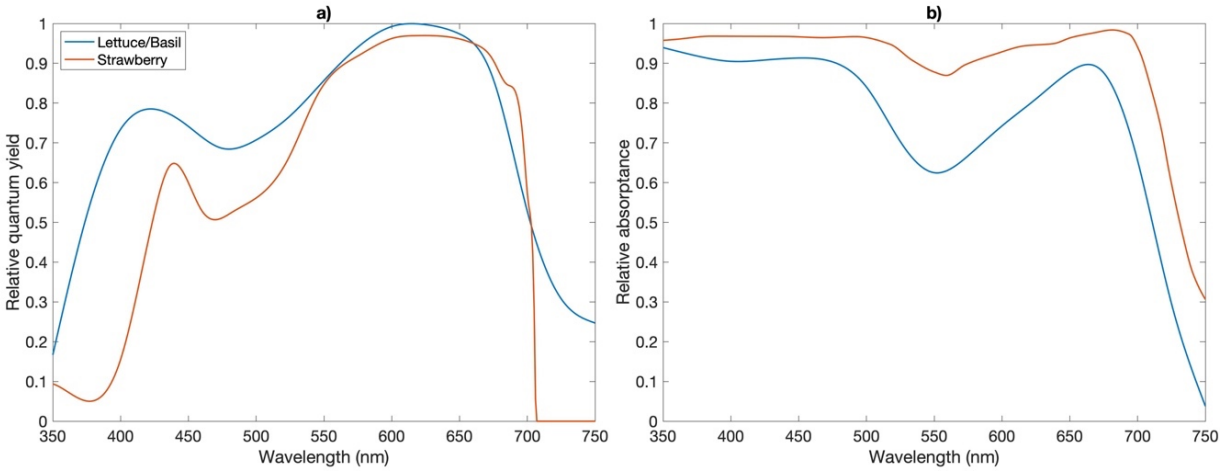

Figure 4.2: Relative (with respect to the maximum value) spectra of a) quantum yield and b) absorptance for the crops used in this study. The lettuce/basil and strawberry spectra were taken from McCree (1971) and Inada (1976), respectively.

The plant's response to different types of light treatments was tested by conducting a sensitivity analysis, changing one parameter at a time and keeping the others fixed. Photosynthetic rate, transpiration, stomatal conductance, water use efficiency, and intercellular-atmospheric CO_2 concentration were modeled as a function of irradiance, temperature, vapor pressure deficit and ambient CO_2 concentration.

As concerns basil, the climatic variables are representative of growth chambers conditions, with irradiance, temperature, relative humidity and CO_2 concentration equal to 80 Wm^{-2}, 24°C, 70% and 450 ppm. As concerns strawberry, the climatic variables are representative of the central California average climate in the growth season, with irradiance, temperature, relative humidity and CO_2 concentration equal to 80 Wm^{-2}, 25°C, 41.2%, and 410 ppm. The obtained figures show the trends of the variables of interest as the light spectrum changes. The color of the lines refers to the percentage of red-blue and green (for the broad-spectrum artificial light), and the black represents the reference solar spectrum as in Gueymard et al. (2002).

A smoothing operation was performed in the sensitivity analysis in order to allow a smooth transition between the Rubisco and the light limited processes and to account for some co-limitation. The non-rectangular hyperbolic (quadratic) smoothing formulation proposed by Cox (2001) was used. The actual rate of photosynthesis (A_n) is computed as the smoothed minimum between three potentially limiting rates ($f_{c,C}$, $f_{c,L}$, $f_{c,TPU}$):

$$\beta A_p^2 - A_p(f_{c,C} + f_{c,L}) + f_{c,C} f_{c,L} = 0 \tag{4.1}$$

$$\varepsilon A_n^2 - A_n(A_p + f_{c,TPU}) + A_p f_{c,TPU} = 0 \tag{4.2}$$

where A_p is the smoothed minimum between $f_{c,C}$ and $f_{c,L}$, β and ε are curvature parameters that vary between 0 and 1 with lower values leading to greater smoothing and $f_{c,TPU}$ is the limiting rate associated to the mitochondrial respiration term (R_d). Since the dark respiration phenomenon was neglected, only the equation (4.1) was used to compute the smoothed rate, assuming ε equal to 0 and β equal to 0.98 and trying to stay as close as possible to the representation of the real curves with transition.

The efficiency metrics in the case of basil are very similar between the different models and sometimes it is necessary to observe the fourth or fifth decimal digits to distinguish them. For this reason, it was decided to report the linear Medlyn as a representative model.

Regarding strawberry, the linear Katul and the co-limitation models are shown because the first minimizes $RMSE$ and maximizes NSE (or KGE) in the calibration of c_i and g, and the second in the calibrations of A_n and T. However, it is necessary to emphasize that the differences between the efficiency metrics are not so important to define a model better than another, therefore all model sensitivities not shown in this chapter are reported in the Appendix A.

4.1 The linear Katul model

The results in Figure 4.3 show that the photosynthetic rate (Figure 4.3a) and the stomatal conductance (Figure 4.3c) are higher for red than for blue light. The transpiration rate (Figure 4.3b) grows monotonically for all light treatments and in the case of red and blue light it is almost identical. The trend of water use efficiency (Figure 4.3d) shows a maximum point for irradiances below 100 Wm^{-2} in all light treatments, in particular, the red one is the most efficient for the plant's growth. For irradiance values above 200 Wm^{-2}, basil is not affected by the different types of light because the Rubisco limitation prevails and all $WUEs$ are equal except for the reference solar spectrum, resulting in larger WUE values starting from around 120 Wm^{-2}. The plots of c_i/c_a (Figures 4.3e, 4.3j, 4.3o, 4.3t) show no variation as the light spectrum changes since the concentration ratio does not include any light dependent term (eqn (2.32)).

The temperature sensitivity shows a bell-shaped trend for the photosynthetic rate (Figure 4.3f), with its maximum between $23 - 28$ °C depending on the type of light. Transpiration growths almost monotonically until 35 °C for all types of light and then shows a maximum before decreasing. This phenomenon, unlike the constantly growing trend of the Camporese and Abou Najm's model, seems to be due to a particular mechanism called "feed-forward". It explains how for high VPD the plant starts to close the stomata to avoid large losses of water. The way plants can perceive change in VPD is quite debated in literature. A first theory (feed-back mechanism) explains how a decrease in g_s as VPD increases is caused by a direct increase in the transpiration process, which causes a reduction in leaf water potential and the stomatal closure. The other hypothesis is a feed-forward response, which explains how the closure of stomata is due to changes in the regulation processes of ABA (abscisic acid) due to local changes of transpiration in the area surrounding stomata (Streck, 2003). Although the two mechanisms differ in the assumptions underlying them, both assume a decrease in g_s as VPD increases. The first due to variations in the energy configuration of the leaf water potential, the second due to the predictive capabilities of the plant.

Stomatal conductance (Figure 4.3h) follows the trend of the photosynthetic rate with its maximum value reached for red light. Water use efficiency (Figure 4.3i) is maximum for red light if the temperature range is between $20-35$ °C and for sunlight if temperature values are below 20 °C. Again, it is important to note that red light is more efficient than blue light due to higher carbon fixation and lower water consumption at the same temperature value.

The trend in vapor pressure deficit sensitivity is consistent with the operation of the plant. If VPD increases the air becomes drier, the transpiration rate increases (since T is proportional to VPD) and the plant responds by decreasing the stomatal conductance and the carbon fixation rate. The transpiration follows the pattern of stomatal conduc-

tance showing larger values for red light. The trend of WUE confirms once again the increased efficiency in the case of red light treatment.

The sensitivity to ambient CO_2 concentration highlights the differences between the different light treatments oppositely to irradiance sensitivity, since the plant transitions from Rubisco to light limited conditions as CO_2 concentration grows (Figure 4.3p).

In addition, the initial increase in stomatal conductance (Figure 4.3r) is due to the permanence, for small CO_2 concentrations, in the Rubisco limited phase (Figure 4.4a). According to Medlyn et al. (2011), the response of stomatal conductance to the variation of CO_2 differs depending on which limitation is considered. If the process is Rubisco limited g_s grows as c_a increases, contrary to experimental observations found in the literature (Morison, 1998). If the RuBP regeneration limitation is considered, stomatal conductance is predicted to decrease non-linearly with c_a. Depending on the type of light the transition occurs for CO_2 concentrations between 280 and 400 ppm. The trend of T follows that of g_s showing an initial increase in transpiration rate followed by a monotonic decline due to the passage in light-limiting conditions. The growth of c_i/c_a as c_a increases is consistent with the increased carbon assimilation rate due to the growth of the concentration gradient between the outside and inside part of the plant.

In Figure 4.4a we can see that, for CO_2 concentrations below 400 ppm, carbon assimilation is determined by the availability of the Rubisco enzyme and, for higher values, the process is always light limited. The opposite case occurs for irradiance sensitivity. In Figure 4.4b it is important to note that $f_{c,C}$ is constant as irradiance changes because its formula contains no light-dependent terms and c_i does not vary with the light spectrum.

Temperature sensitivity (Figure 4.4c) reveals how, for values between 12 and 38 °C the process is always light limited and, for values above or below this range, the bell-shaped curve is always Rubisco limited.

The Rubisco rate ($f_{c,C}$) in the VPD sensitivity (Figure 4.4d) intersects the light limited rate ($f_{c,L}$) only for the two reddest light treatments and the abrupt transition is not visible in Figure 4.3k because of the smoothing operation.

The general trend of the sensitivity curves is consistent with the results of the Camporese and Abou Najm's model applied to the strawberry case (Appendix A). There are differences in the slope of the transpiration rate in the sensitivity to VPD and c_a. Moreover, although for c_a values less than 400 ppm $f_{c,C}$ is the limiting rate, the Camporese and Abou Najm's model does not show an initial growth of g_s for sub-ambient CO_2 concentrations and responds with a continuous decrease of g_s as c_a increases. Finally, the c_i/c_a ratio increases in both models as c_a grows but showing an opposite concavity.

4.2 The linear Medlyn model

The Medlyn approach differs from that of Katul in the expression of the stomatal conductance, which is always determined by the limitation induced by the availability of light ($f_{c,L}$). The results are similar to those obtained in the linear Katul model applied to basil (Figure A.3). By comparing the limiting rates of the linear Katul model applied to strawberry and the linear Medlyn model applied to basil we can notice that, for all sensitivities, $f_{c,L}$ is the most limiting rate except for temperature lower than 5°C and irradiance greater than 300 Wm^{-2} (Figure 4.4 and Figure 4.6).

This type of plant is characterized by a greater photosynthetic rate than that of strawberry in all sensitivities. The bell-shaped curve of A_n (Figure 4.5f) is less pronounced. The maximum of stomatal conductance (Figure 4.5h) and WUE (Figure 4.5i) are shifted towards lower temperature values. In addition, basil is not affected by the feed-forward mechanism and transpiration grows almost monotonically up to 40°C. Interestingly, the

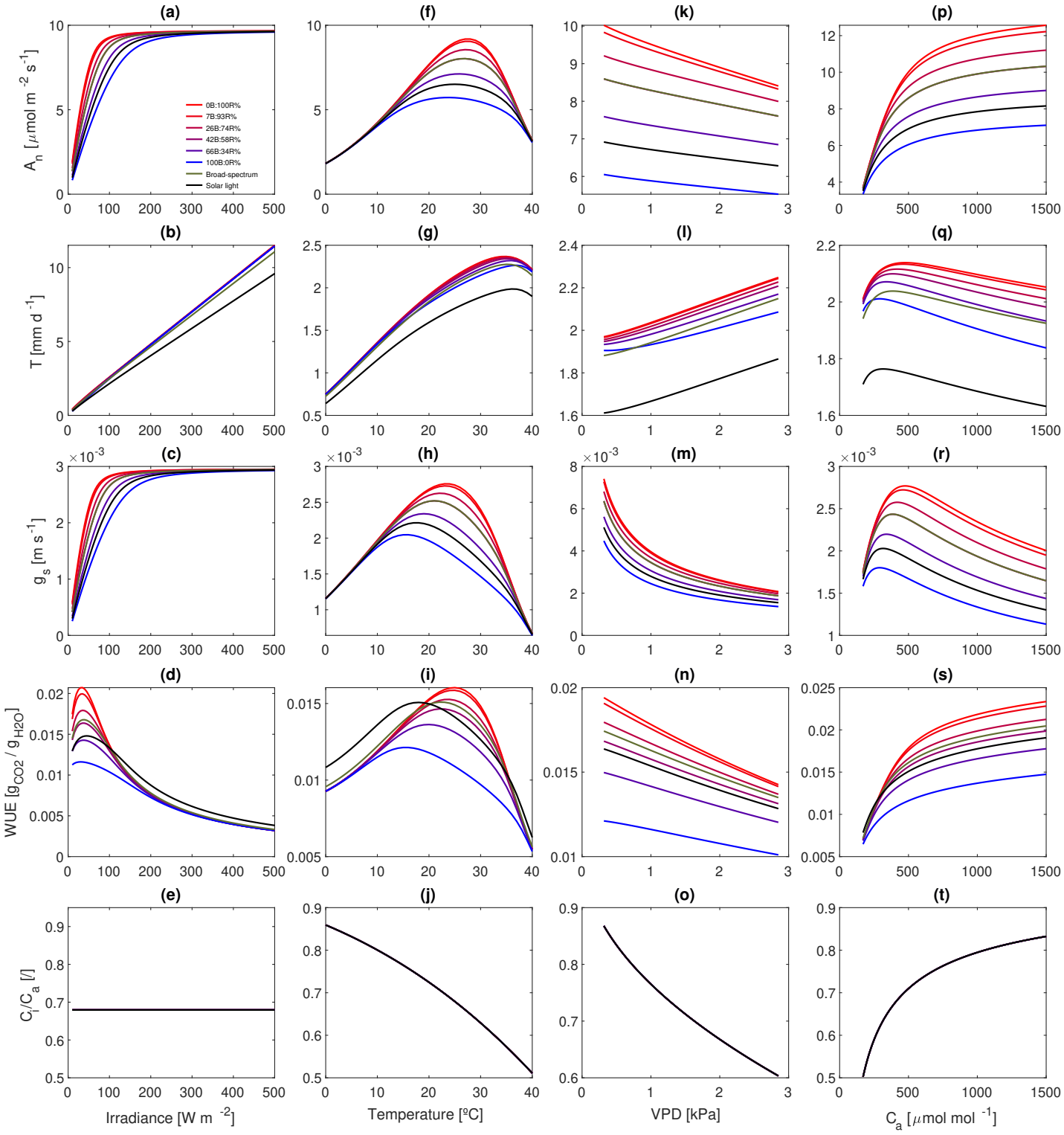

Figure 4.3: Linear Katul model. (a-f-k-p) photosynthetic rate, (b-g-l-q) transpiration rate, (c-h-m-r) stomatal conductance, (d-i-n-s) water use efficiency, and (e-j-o-t) concentration ratio as a function or (a-e) irradiance, (f-j) temperature, (k-o) vapor pressure deficit and (p-t) external CO_2 concentration for strawberry exposed to different light treatments. The reference climatic variables are representative of growth chambers conditions, with irradiance, temperature, relative humidity and CO_2 concentration equal to 80 Wm^{-2}, 25°C, 41.2%, and 410 *ppm*.

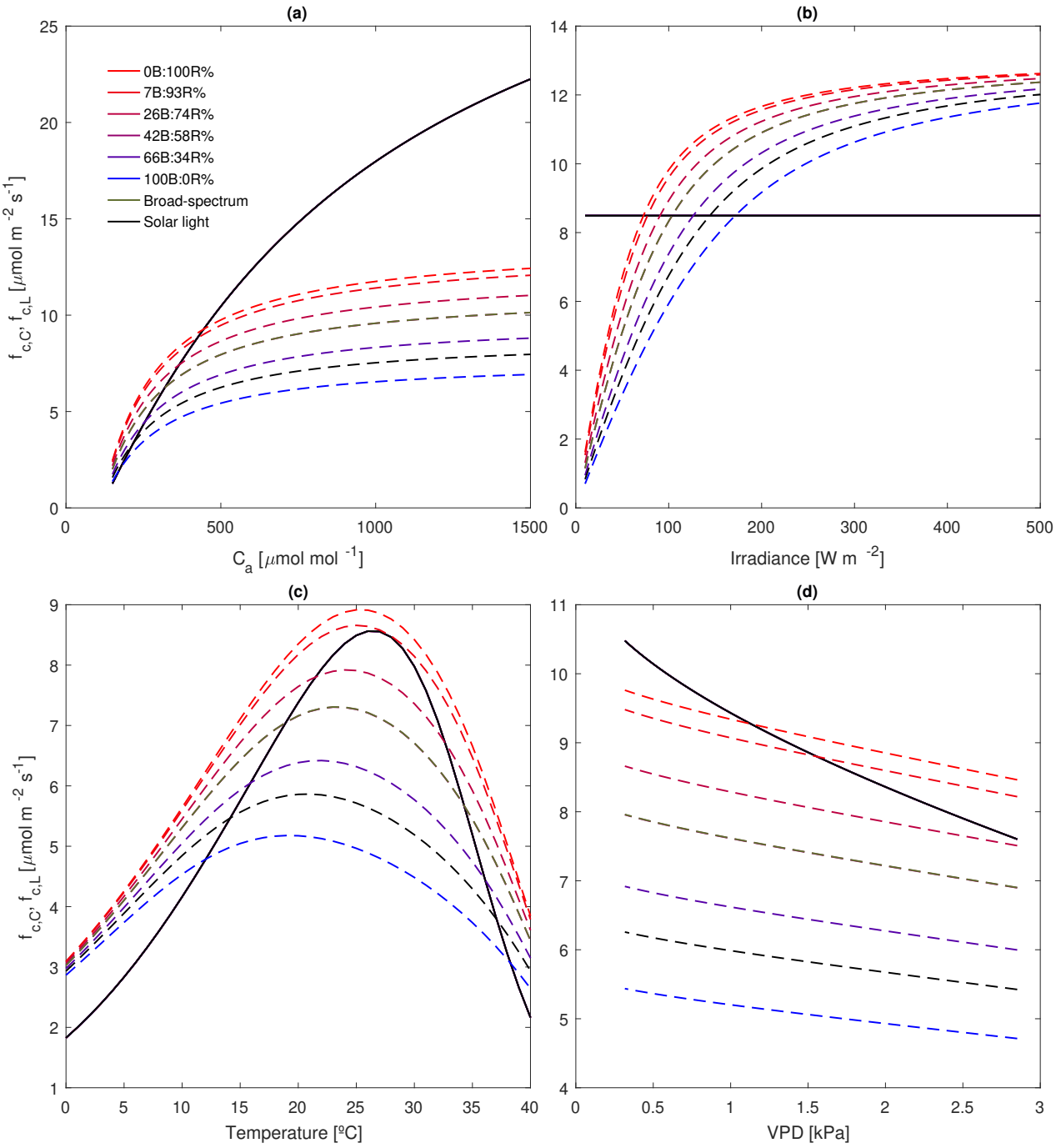

Figure 4.4: Linear Katul model. Rubisco-limited ($f_{c,C}$, solid lines) and RuBP-regeneration limited ($f_{c,L}$, dashed lines) as a function of (a) air CO_2 concentration, (b) irradiance, (c) temperature, (d) vapor pressure deficit for strawberry subjected to different light treatments. The reference values for the climatic variables are as in Figure 4.3.

transpiration rate is greater for blue light (Figure 4.5l) and the photosynthetic rate (Figure 4.5k) is less sensitive to VPD variation than strawberry.

The sensitivity to CO_2 concentration does not show the initial transition phase because the process is always light limited (Figure 4.6a) and stomatal conductance decreases with increasing c_a even for sub-ambient CO_2 concentrations.

It is important to note that basil is more productive than strawberry because it is characterized by higher photosynthetic rate and WUE values. This happens because of the higher quantum yield. The comparison between the linear models applied to strawberry and basil shows that they are equally sensitive to the variation of the light spectrum and that limiting light conditions are more emphasized in the case of basil, which almost never experiences the limitation induced by Rubisco.

The irradiance sensitivity shows a photosynthetic rate twice as large as that obtained by the Camporese and Abou Najm's model calibrated on basil. This is due to the transition into Rubisco limited conditions at higher irradiances and to the different slope with which the electron transport rate goes to saturation. The phenomenon can be attributed to a possible wrong estimation of the α parameter (eqn (2.19)) in the calibration phase of the model. It is known that its value determines the steepness with which the curve reaches saturation.

The stomatal conductance differs by an order of magnitude respect to the Camporese and Abou Najm's model (compare Figure 4.5c and Figure A.1c). The erroneous overestimation of g_s may be due to the presence in the joint calibration phase of A_n and WUE. They have different units of measurement compared to the variables used in the models and this affects the search for the minimum of the objective function, which leads to an incorrect estimation of the parameters. The limited availability of data with comparable units of measurement and the use of a model with only one parameter does not allow the algorithm to provide plausible values. Note that this occurs in all irradiance sensitivities calibrated on the Pennisi data set (Figures A.3, A.7, A.11, A.15) and not on calibrations made on Mochizuki, where a greater number of measurements are provided as the $PPFD$ changes.

In order to solve the problem, attempts were made by minimizing in the objective function only the KGE of stomatal conductance ($M = 1 - KGE_{g_s}$), the KGE of the pair $A_n - WUE$ ($M = 2 - (KGE_{A_n} + KGE_{wue})$) and by changing the objective function with the minimization of $RMSE$ ($M = RMSE_{g_s} + RMSE_{A_n} + RMSE_{wue}$).

The results showed no significant difference from the KGE joint calibration performed on all three variables. The results of the calibrations performed on the different objective functions and the sensitivities to irradiance are given in the Appendix A. No set of parameters (Table A.1) can provide a correct estimate of g_s as the irradiance changes.

4.3 The co-limitation model

The co-limitation model emphasizes the differences between the different light treatments compared to linear models. The photosynthetic rate and the stomatal conductance are greater in all sensitivities compared to the linear Katul case (Figure 4.7). Moreover, the WUE with varying irradiance presents a less steep recession phase after the peak showing higher $WUEs$ at the same level of irradiance (compare Figure 4.3d and Figure 4.7d). In Figure 4.8 we can see that the Rubisco rate ($f_{c,C}$) is no longer light independent because now c_i varies with the light spectrum. Since the model estimates c_i using the Fick's law, the c_i/c_a ratio is light dependent because both A_n and g_s changes with the spectrum. The concentration ratio grows with increasing irradiance for all types of light (Figure 4.7e) without showing the initial recession followed by a minimum and a subsequent growth

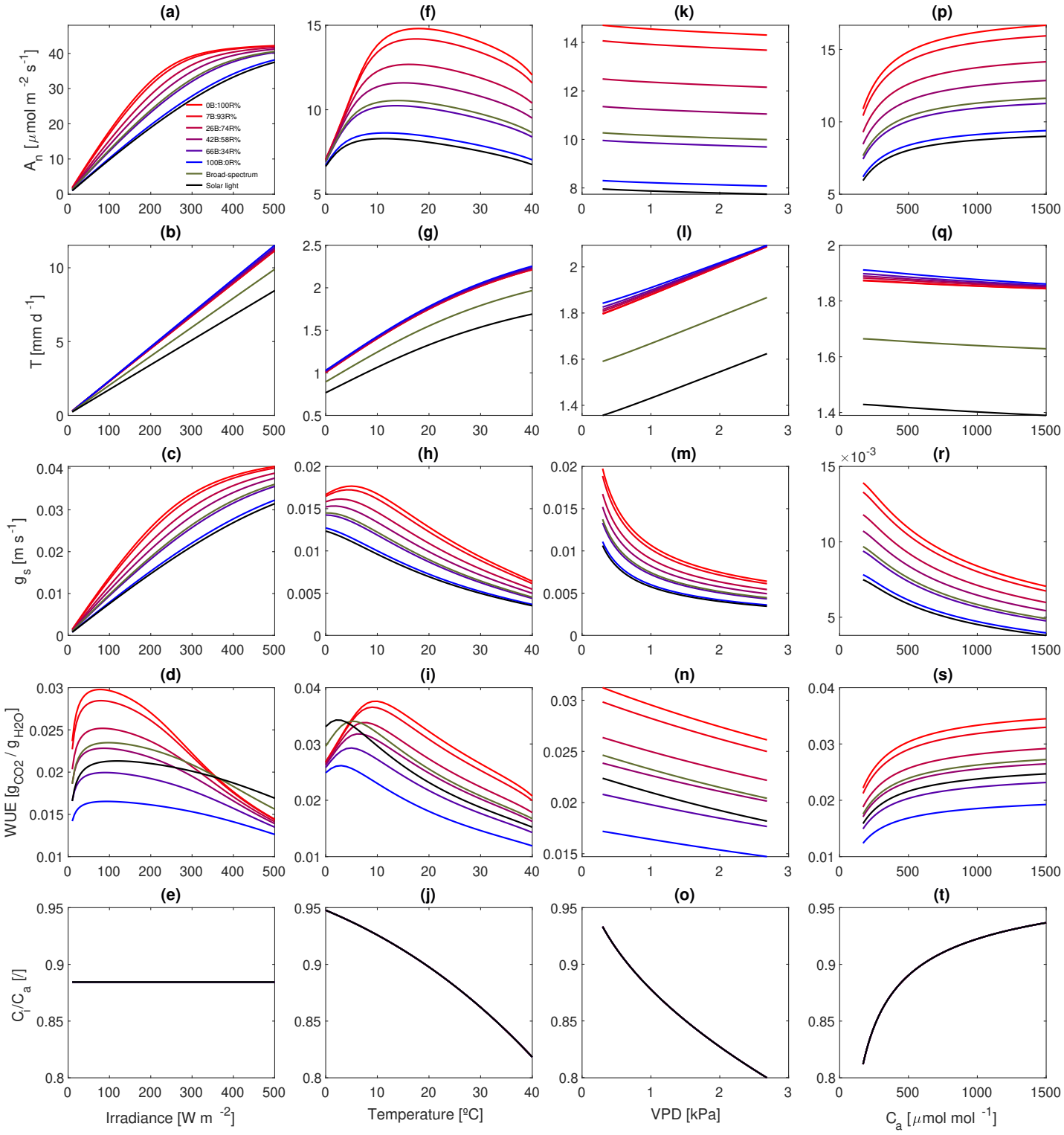

Figure 4.5: Linear Medlyn model. (a-f-k-p) photosynthetic rate, (b-g-l-q) transpiration rate, (c-h-m-r) stomatal conductance, (d-i-n-s) water use efficiency, and (e-j-o-t) concentration ratio as a function or (a-e) irradiance, (f-j) temperature, (k-o) vapor pressure deficit and (p-t) external CO_2 concentration for basil exposed to different light treatments. The reference climatic variables are representative of growth chambers conditions, with irradiance, temperature, relative humidity and CO_2 concentration equal to 80 Wm^{-2}, 24°C, 70%, and 450 *ppm*.

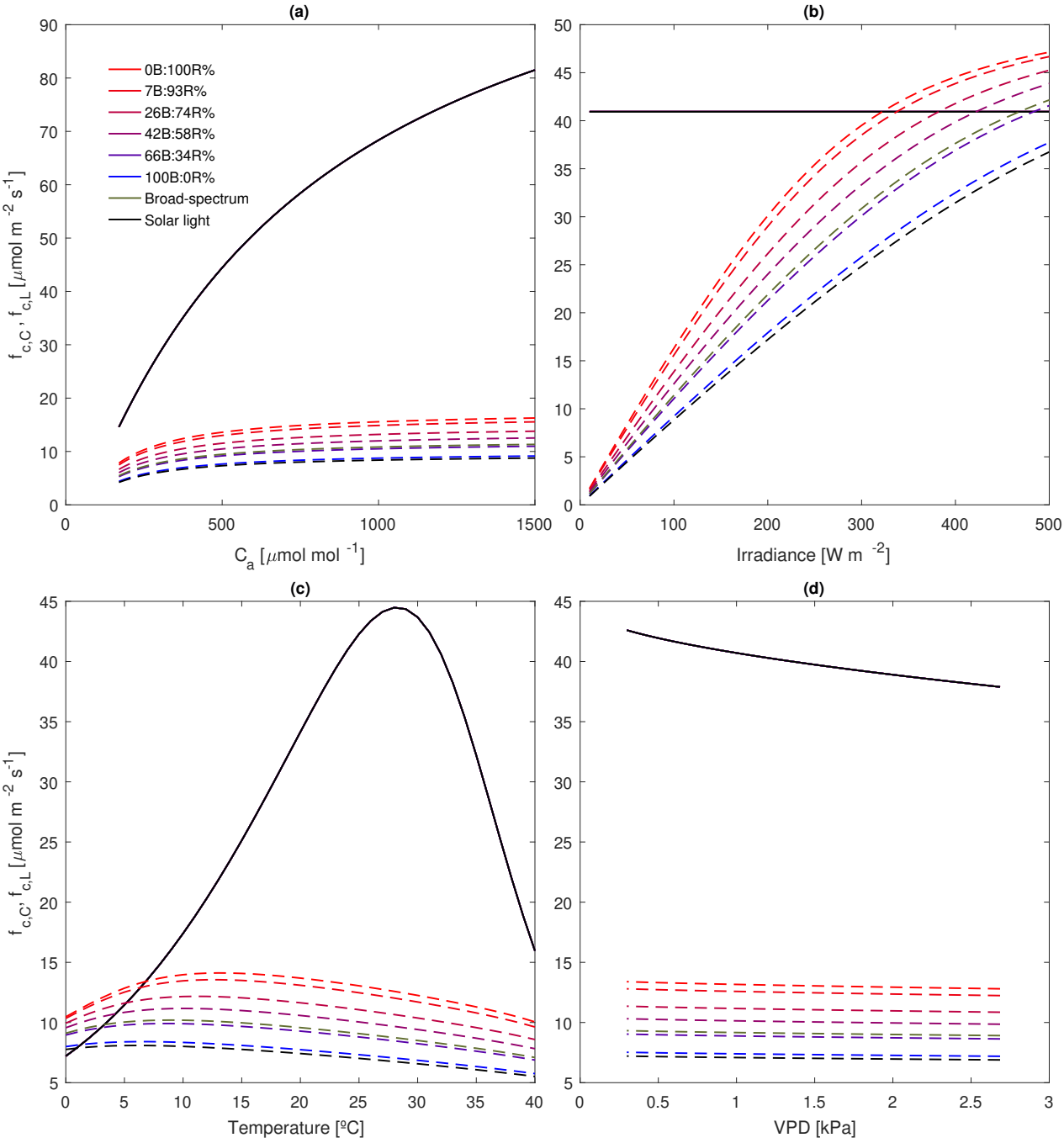

Figure 4.6: Linear Medlyn model. Rubisco-limited ($f_{c,C}$, solid lines) and RuBP-regeneration limited ($f_{c,L}$, dashed lines) as a function of (a) air CO_2 concentration, (b) irradiance, (c) temperature, (d) vapor pressure deficit for basil subjected to different light treatments. The reference values for the climatic variables are as in Figure 4.5.

for the two reddest treatments (Figure A.2e). However, the variation is minimal and the ratio can be considered almost constant. Note how c_i/c_a is greater for red light than blue light in all sensitivities, contrary to the Camporese and Abou Najm's predictions. The phenomenon is due to the incorrect estimate of g_s, which shows the same limitation as linear models.

All the curves converge more slowly to individual limitations. This happens due to the hypothesis of co-limitation that takes into account the electron transport rate (through the term a_2) even when the process is Rubisco limited. The feed-forward mechanism occurs for higher temperatures that have not been analyzed here. The WUE peak (Figure 4.7i) occurs for lower temperature values but showing greater variability than the linear Katul case.

There are no differences in VPD and CO_2 concentration sensitivities and the results are very similar to the linear Katul model.

Interestingly, the co-limitation model applied to basil shows a minimum of c_i/c_a with varying temperature (Figure A.15j), similarly to the Camporese and Abou Najm model. In the sensitivity to CO_2 concentration it exhibits a continuous decrease of c_i/c_a for blue light and a minimum followed by growth for red light (Figure A.15t). However, the variation is very small and c_i/c_a can be considered constant.

4.3.1 The sensitivity to the marginal water use efficiency

A further analysis has been carried out to investigate the influence that the marginal water use efficiency has on the processes of gas exchange of plants. The study was conducted on strawberry and was applied to the co-limitation model only. The response of g_s to constant λ was compared to increasing λ with the external CO_2 concentration.

The results obtained by Katul et al. (2010) suggest that the c_i/c_a ratio is invariant with elevated c_a. Consequently, they state that λ grows linearly with c_a according to equation (3.3). However, they assume D constant and equal to 1 kPa without analyzing the variation of the marginal water use efficiency with temperature and relative humidity and using a dependence of λ on c_a that justifies the observed values for elevated CO_2 concentrations ($\lambda = 0.089 c_a/D$).

Here the response of A_n, T, g_s, WUE and c_i/c_a to varying c_a, VPD, temperature and irradiance was compared in the cases of constant λ and variable λ according to the formulation proposed in Vico et al. (2013), such that:

$$\lambda = \lambda_0 \frac{c_a}{c_{a,0}} \tag{4.3}$$

where λ_0 and $c_{a,0}$ have been calibrated on the Mochizuki data set and are equal to 9.7 μmol mol^{-1}kPa^{-1} and 615 ppm. The calibration of the co-limitation model with linear dependence of λ on c_a is given in the Appendix A (Figure A.17).

Since A_n, T, g_s, WUE and c_i/c_a do not show significant differences in the sensitivities to irradiance, temperature and vapor pressure deficit between the model with constant λ and the one with variable λ, here only the case of CO_2 concentration sensitivity is shown and the others are reported in the Appendix A.

The differences between the two hypotheses on the dependence of λ on c_a are found in the trends of g_s and c_i/c_a (Figures 4.10e-f and 4.10i-l). The stomatal conductance estimated using equation (4.3) predicts a higher peak that occurs at lower CO_2 concentrations (between 90 and 110 ppm) than the constant λ model (between 170 and 250 ppm). Both models show a growth of g_s as c_a increases, however, the hypothesis of linearly dependent marginal water use efficiency predicts a decrease in stomatal con-

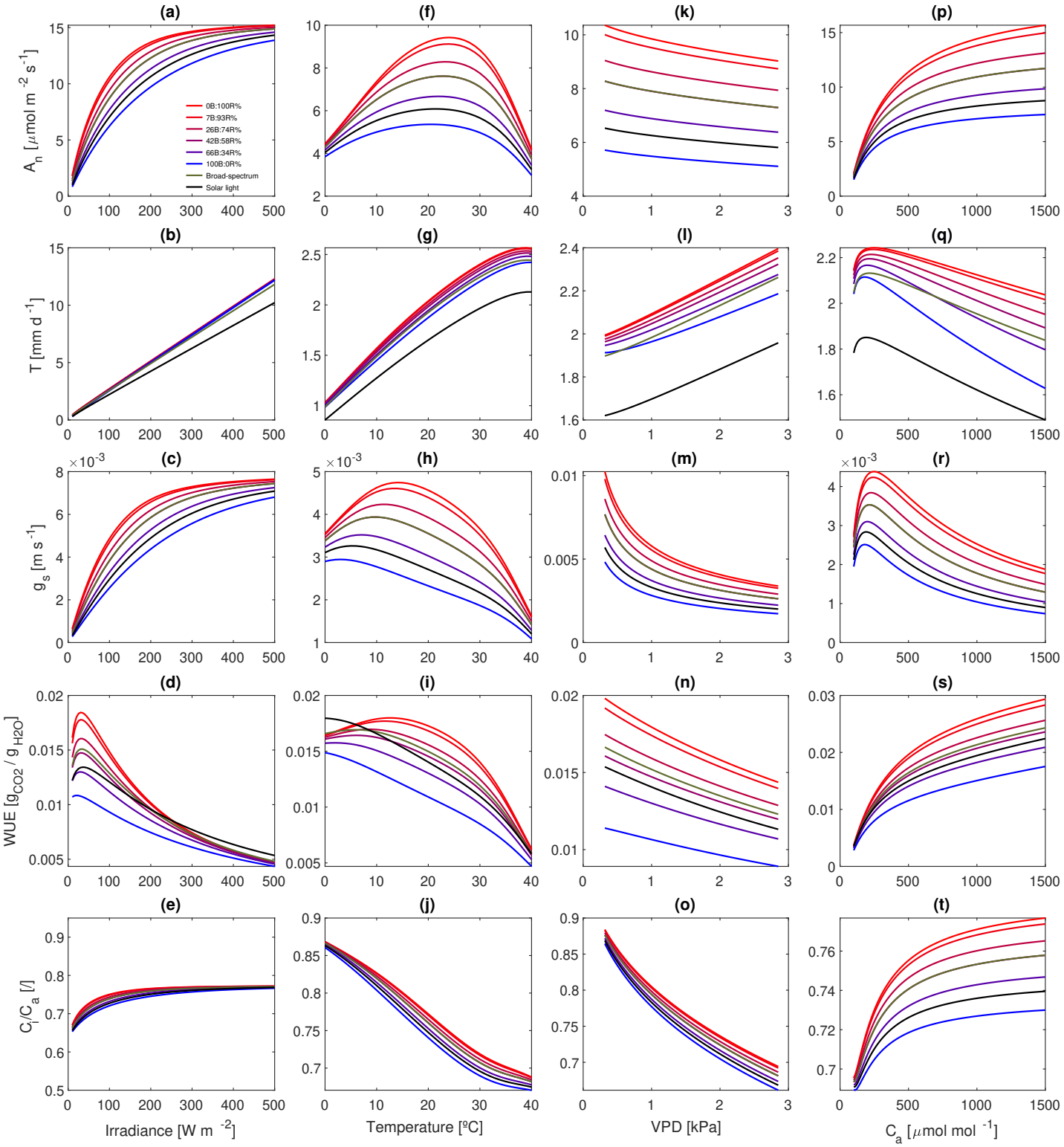

Figure 4.7: Co-limitation model. (a-f-k-p) photosynthetic rate, (b-g-l-q) transpiration rate, (c-h-m-r) stomatal conductance, (d-i-n-s) water use efficiency, and (e-j-o-t) concentration ratio as a function or (a-e) irradiance, (f-j) temperature, (k-o) vapor pressure deficit and (p-t) external CO_2 concentration for strawberry exposed to different light treatments. The reference climatic variables are representative of growth chambers conditions, with irradiance, temperature, relative humidity and CO_2 concentration equal to 80 Wm^{-2}, 25°C, 41.2%, and 410 *ppm*.

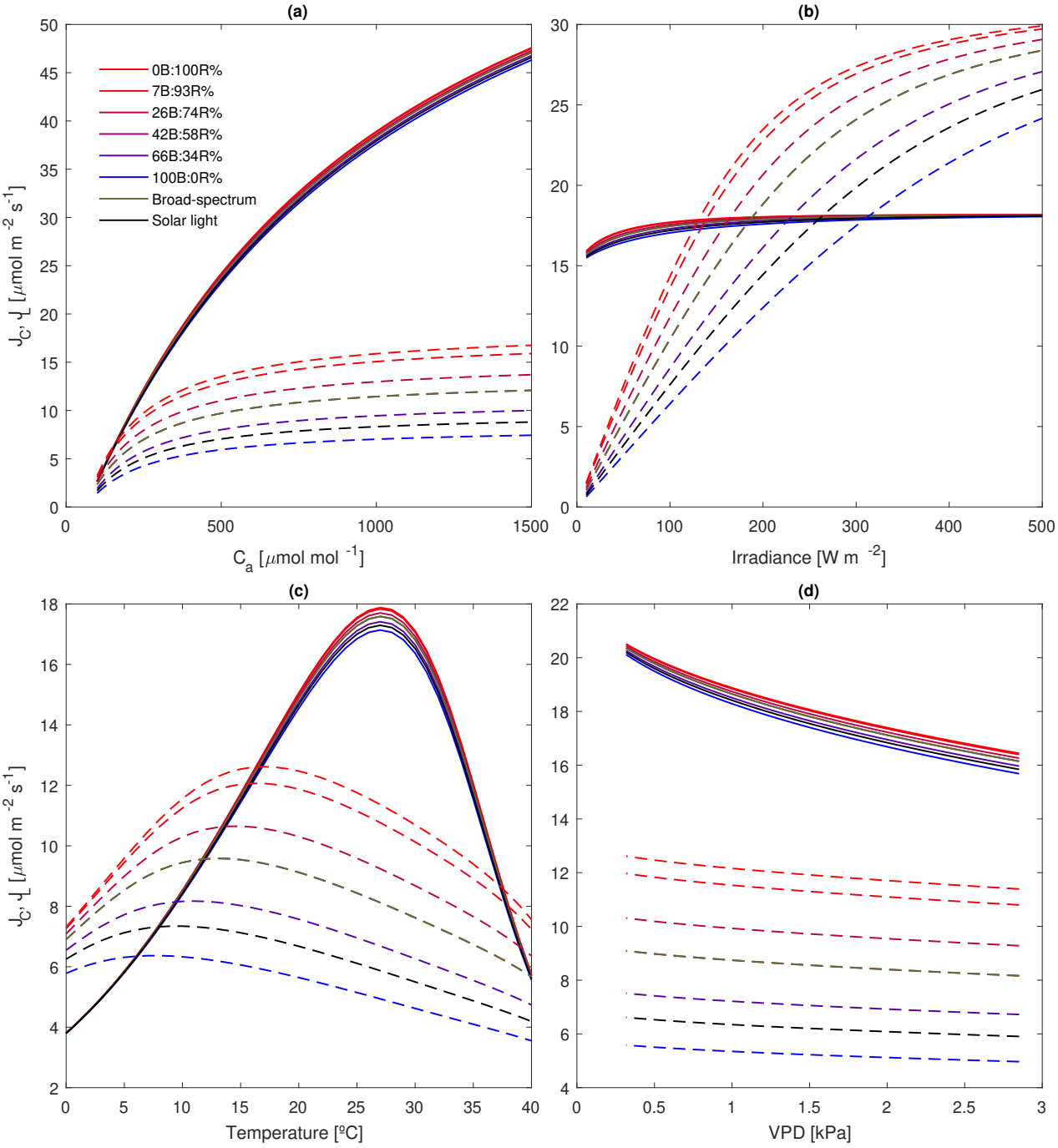

Figure 4.8: Co-limitation model. Rubisco-limited ($f_{c,C}$, solid lines) and RuBP-regeneration limited ($f_{c,L}$, dashed lines) as a function of (a) air CO_2 concentration, (b) irradiance, (c) temperature, (d) vapor pressure deficit for strawberry subjected to different light treatments. The reference values for the climatic variables are as in Figure 4.3.

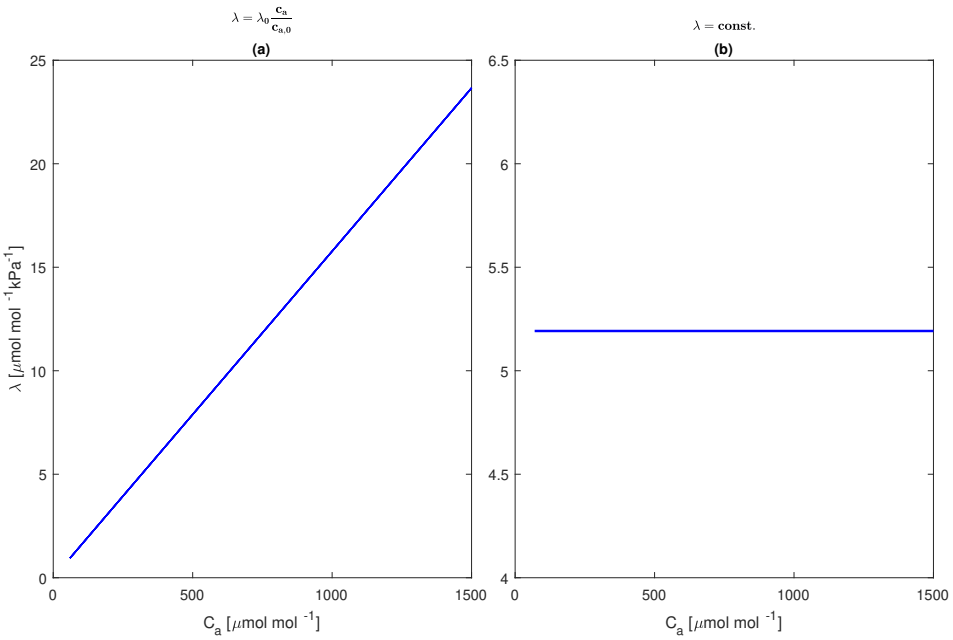

Figure 4.9: Marginal water use efficiency as a function of changing (a-b) air CO_2 concentration. The first column estimates λ using equation (4.3), the second column considers λ as constant and equal to the value calibrated with the SCE-UA algorithm (Table 3.3). The calibrated photosynthetic parameters related to the model with linear dependence of λ on c_a are $J_{max,0} = 196$ μmol m^{-2}s^{-1}, $rjv = 2.50$, $r_a = r_b = 286$ sm^{-1}, $\theta = 0.89$, $\alpha = 0.20$. The reference values for the climatic variables are as in Figure 4.3.

ductance that occurs from lower sub-ambient CO_2 concentrations than the model with constant λ.

There is a significant difference in the trend of c_i/c_a depending on the assumption about the dependence of λ. If it is kept constant, c_i/c_a grows with the increase of c_a; if it is assumed to increase linearly with c_a, c_i/c_a decreases with the growth of c_a.

In the literature we can find both evidences that confirm the growth of c_i/c_a with increasing c_a (Whiteman and Koller (1967), Düring (2003)) and the decrease or almost constancy of c_i/c_a with increasing c_a (Ehleringer and Cerling (1995), Anderson et al. (2001)). Which of the two hypotheses on the dependence of λ is correct for the estimate of c_i/c_a is not clear and needs more study in order to understand if the concentration ratio is species-specific or if there is a fixed response for all plants.

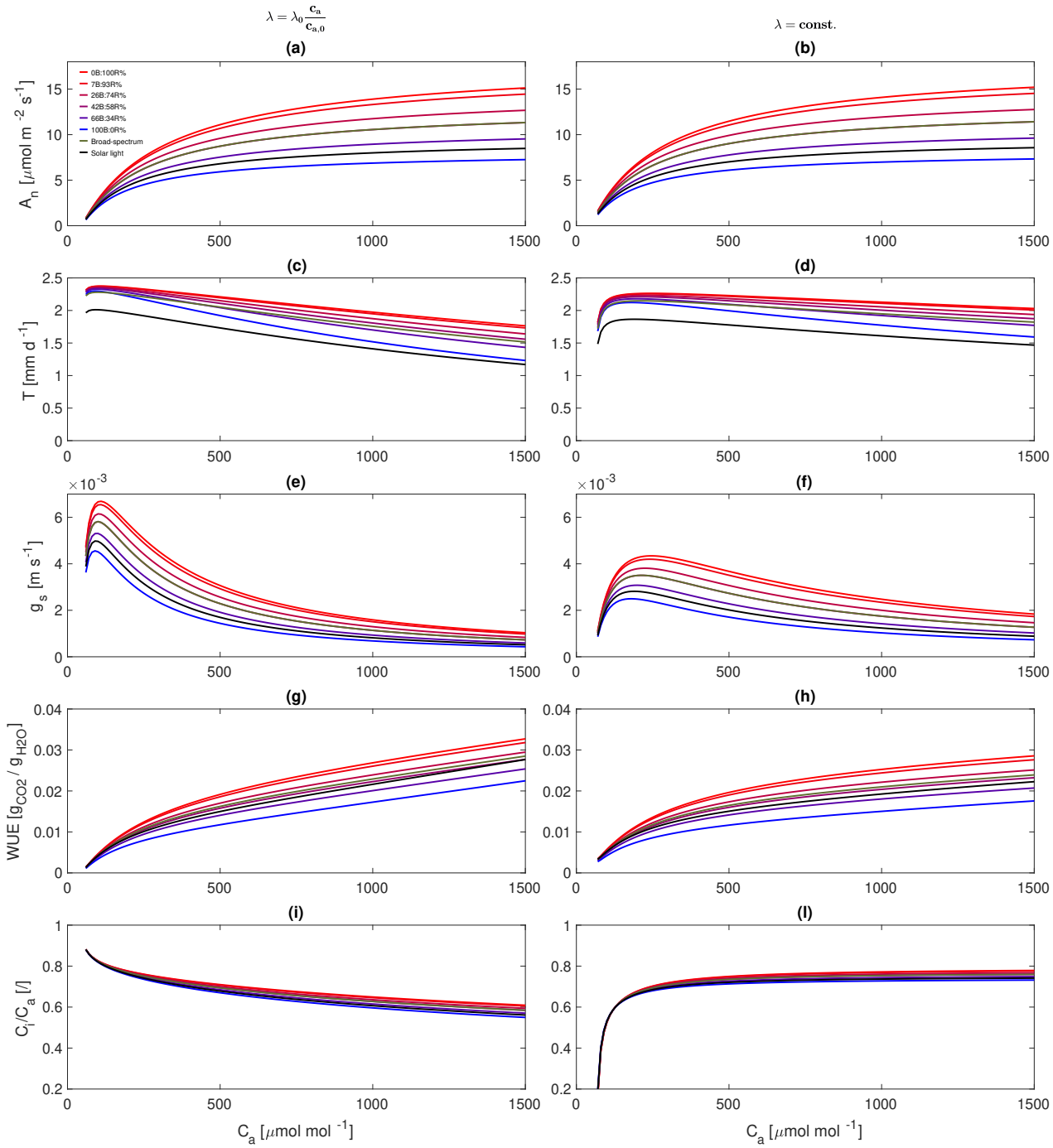

Figure 4.10: Sensitivity to changing air CO_2 concentration for the co-limitation model with different hypothesis on the dependence of λ on c_a. The reference values for the climatic variables are as in Figure 4.3.

Chapter 5

Perspective and concluding remarks

The use of models that can predict the behaviour of plants as a function of climatic forcings can be used as a preliminary step to assess the effectiveness of different species in adapting to limiting light conditions. The reduction of irradiance, due to the presence of the panels above the crop and the increase in the trend of global CO_2 concentration are factors that place plants in limiting light conditions and emphasize the differences between the light treatments. In this perspective, wavelength-selective photovoltaic systems can be used to maximize crop yield as the climate changes and to control the behavior of the plant as a function of wavelength. The knowledge of the absorptance and quantum yield curves and the other input parameters of the models allows to evaluate not only the adaptability of crops to unfavourable light conditions, but also to provide a quantitative estimate of the efficiency of the APV system through the evaluation of the water use efficiency.

An advantage of optimization theories over the use of empirical models based on the Kromdjik's formula is the correct interpretation of the response of g_s as temperature varies. Studies in the literature suggest that g_s increases with increasing temperature and reports a maximum for a certain range (Slot et al. (2019), Urban et al. (2017), Hernández et al. (2020)).

The comparison between Figure 4.3h, Figure 4.5h, Figure A.1h and Figure A.2h in the Appendix A shows that the optimization models are characterized by a maximum of g_s as temperature changes compared to the model of Camporese and Abou Najm (2022), where g_s exhibits a minimum.

This phenomenon can be traced back to the proportionality between g_s and $1 - q_L$ in equation (2.3). The fluorescence term (q_L) shows a maximum as temperature changes and it is therefore immediate how $1-q_L$ exhibits a minimum (see Georgieva and Yordanov (1994)).

Although optimization models can correctly reproduce the trend of the curves in temperature sensitivity, they are severely limited by not being able to evaluate g_s with the variation of the light spectrum. As already pointed out in the models calibration chapter, the sensitivity to irradiance, temperature, vapor pressure deficit and CO_2 concentration always show a higher stomatal conductance for red light, contrary to the experimental observations and the results of the Camporese and Abou Najm's model.

The inclusion of a cascade mechanism involving the dependence of g_s on Φ_{PSII}, NPQ, PFD_{abs} and J allows for higher stomatal conductance values for blue light, being the term $1 - q_L$ of blue light greater than the equivalent of red light. An expression of g_s that includes only the dependence on the photosynthetic rate and therefore on $V_{c,max}$ or $J/4$ produces the opposite effect, since J, with the same plant species, is greater for red light.

In addition, the use of optimization models seems to capture the effect of high VPD on the transpiration rate through the feed-forward mechanism, contrary to the Kromdjik's model, which seems to be insensitive to the variation of VPD with monotonic growth of T up to 40°C.

It is necessary to highlight the fact that all the models analyzed here are based on assumptions valid at the leaf level that may limit their applicability on a larger scale. Factors such as the reduced wind speed below the panels, the impact of nutrient uptake on the photosynthetic processes and the possible conditions of water stress were not considered.

More studies are needed to develop a model that is able to reconcile optimization theories with the Kromdjik's formula by filling the gaps of both models. One attempt might be to include the fluorescence term within the search for the optimum point of the objective function (eqn (2.21)) by replacing the term f_c with $1 - q_L$ and minimizing the function $f(g) = (1 - q_L) - \lambda f_w$. This could be the starting point for an approach that directly includes the light dependent terms in the expression of g_s. This hypothesis has not been tested and further verifications are needed to confirm its validity.

Appendix A

Appendix

The asymptotes of the co-limitation model

The convergence to the Rubisco limitation is obtained equating equations (2.36) and (2.16), the rates are equal when

$$\frac{4V_{c,max}}{J} \approx 1 \tag{A.1}$$

and thus for

$$V_{c,max} \approx \frac{J}{4} \tag{A.2}$$

The convergence to the light limited rate is obtained equating equation (2.36) and (2.17). The terms in equation(2.36) can be rearranged to obtain an expression equivalent to that in equation (2.17) in the following way:

$$\begin{aligned} f_c &= \frac{V_{c,max}(c_i - c_p)}{K_c\left(1 + \frac{O_a}{K_0}\right) + \left(\frac{4V_{c,max}}{J}\right)c_i} = \frac{J \cdot V_{c,max}(c_i - c_p)}{J \cdot K_c\left(1 + \frac{O_a}{K_0}\right) + 4V_{c,max}c_i} \\ &= \frac{\frac{J}{4} \cdot V_{c,max}(c_i - c_p)}{\frac{J}{4} \cdot K_c\left(1 + \frac{O_a}{K_0}\right) + V_{c,max}c_i} = \frac{\frac{J}{4}(c_i - c_p)}{\frac{J}{4V_{c,max}} \cdot K_c\left(1 + \frac{O_a}{K_0}\right) + c_i} \end{aligned} \tag{A.3}$$

The equality is obtained by imposing

$$\frac{J}{4V_{c,max}} \cdot K_c\left(1 + \frac{O_a}{K_0}\right) \approx 2c_p \tag{A.4}$$

It follows that

$$\frac{J/4}{V_{c,max}} \approx \frac{2c_p}{K_c\left(1 + \frac{O_a}{K_0}\right)} \tag{A.5}$$

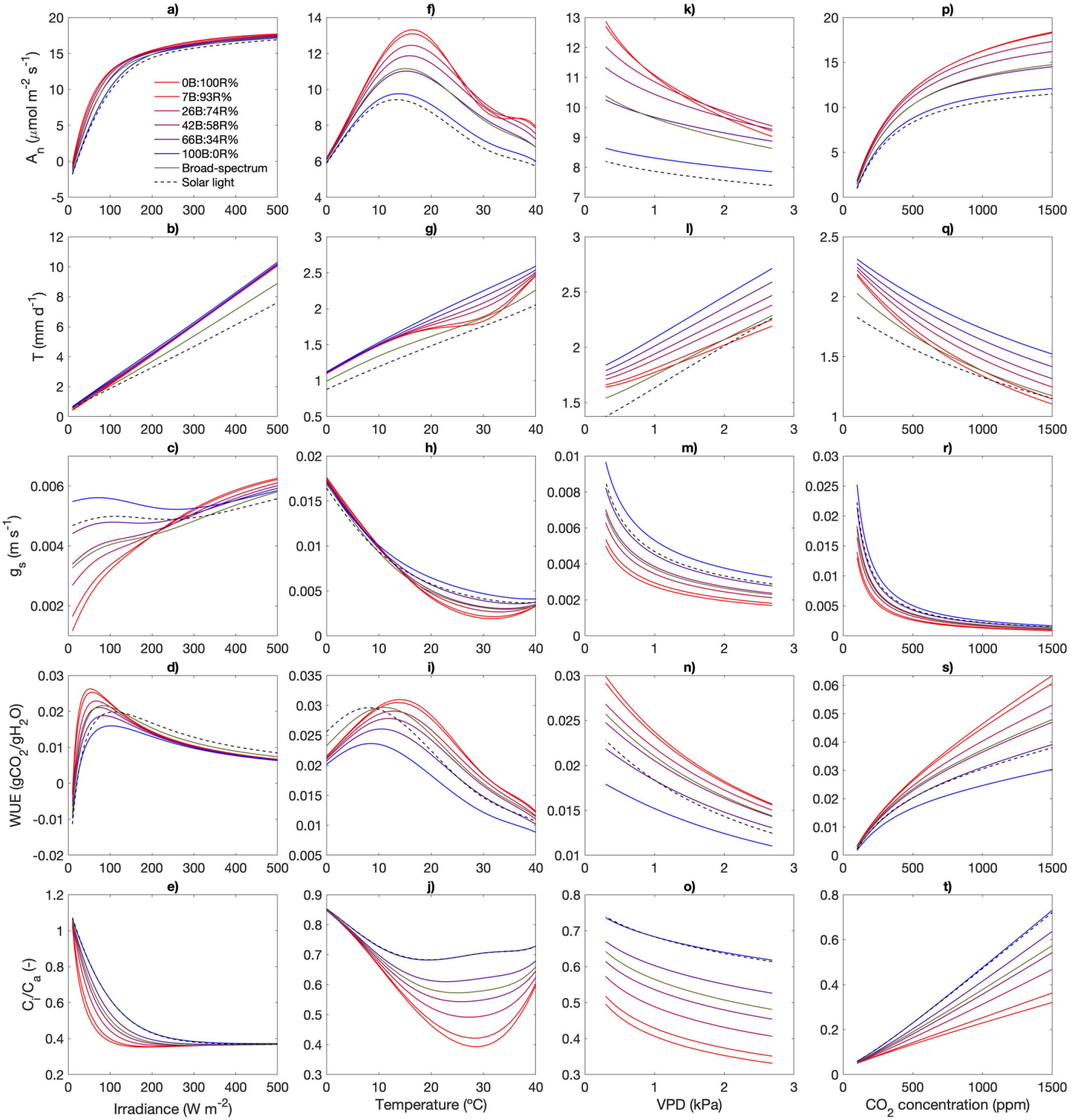

Figure A.1: Camporese and Abou Najm (2022) model. (a-f-k-p) photosynthetic rate, (b-g-l-q) transpiration rate, (c-h-m-r) stomatal conductance, (d-i-n-s) water use efficiency, and (e-j-o-t) concentration ratio as a function or (a-e) irradiance, (f-j) temperature, (k-o) vapor pressure deficit and (p-t) external CO_2 concentration for basil exposed to different light treatments. The reference climatic variables are representative of growth chambers conditions, with irradiance, temperature, relative humidity and CO_2 concentration equal to 80 Wm^{-2}, 24°C, 70%, and 450 *ppm*.

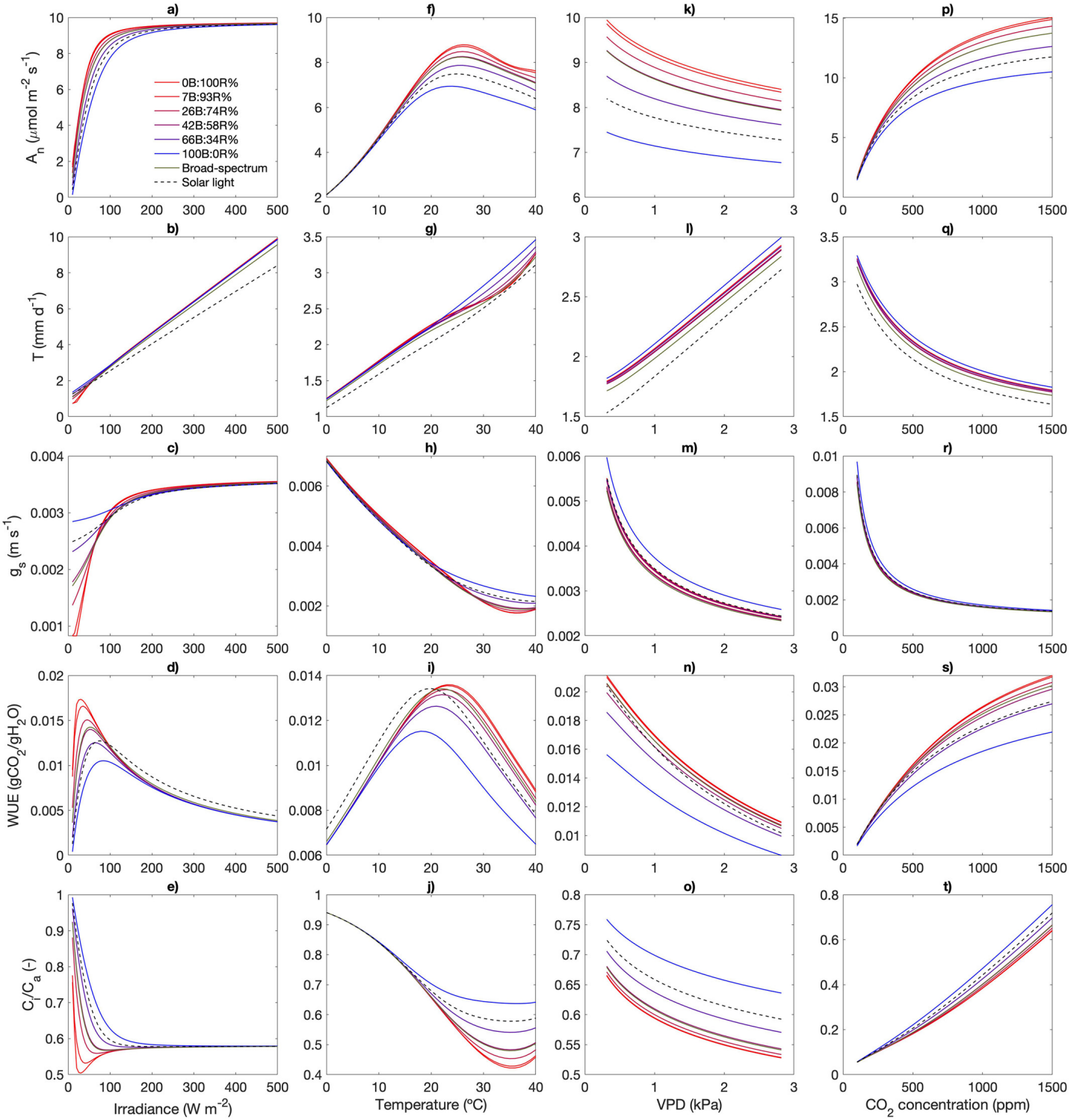

Figure A.2: Camporese and Abou Najm (2022) model. (a-f-k-p) photosynthetic rate, (b-g-l-q) transpiration rate, (c-h-m-r) stomatal conductance, (d-i-n-s) water use efficiency, and (e-j-o-t) concentration ratio as a function or (a-e) irradiance, (f-j) temperature, (k-o) vapor pressure deficit and (p-t) external CO_2 concentration for strawberry exposed to different light treatments. The reference climatic variables are representative of growth chambers conditions, with irradiance, temperature, relative humidity and CO_2 concentration equal to 80 Wm^{-2}, 25°C, 41.2%, and 410 *ppm*.

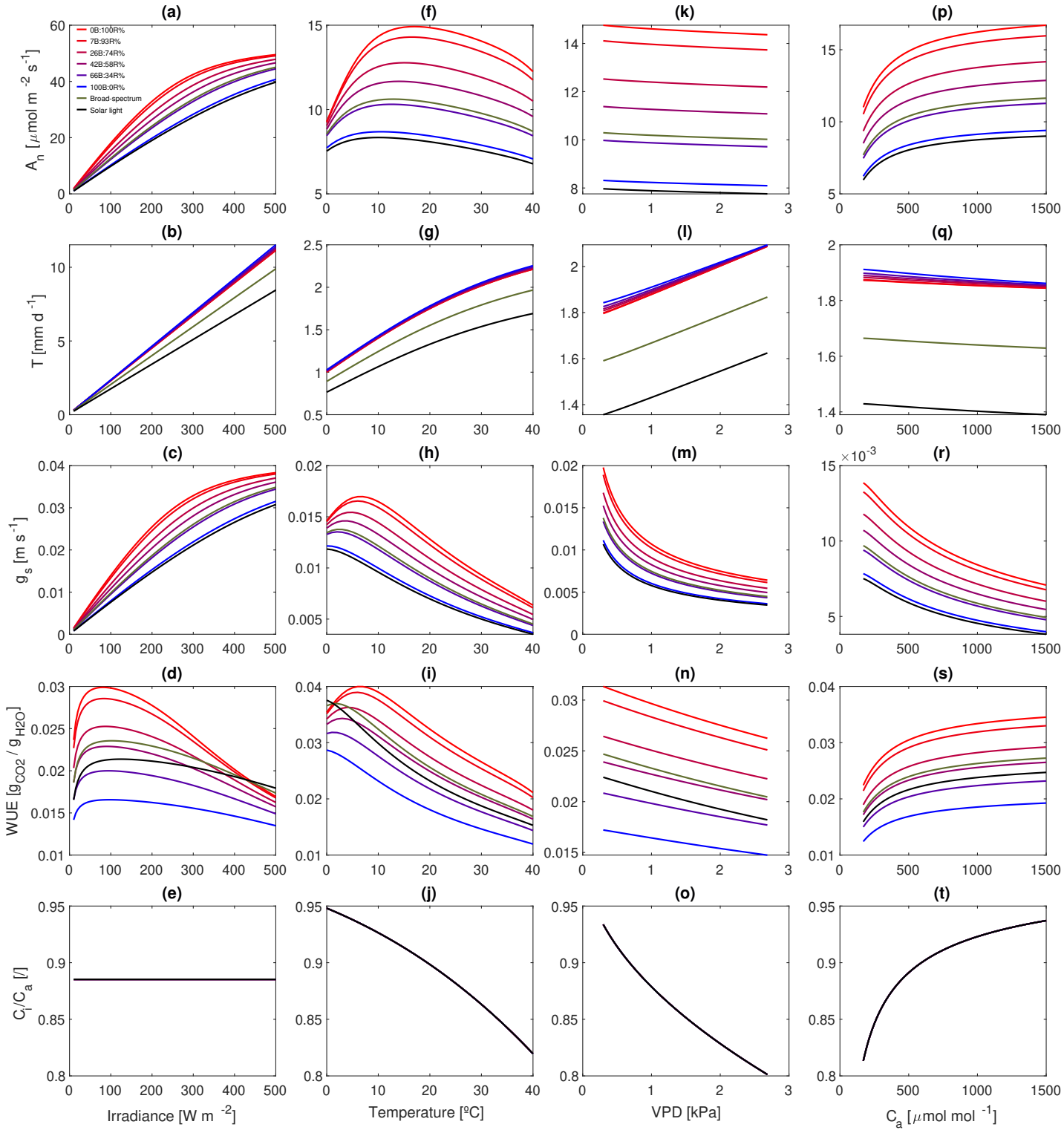

Figure A.3: Linear Katul model. (a-f-k-p) photosynthetic rate, (b-g-l-q) transpiration rate, (c-h-m-r) stomatal conductance, (d-i-n-s) water use efficiency, and (e-j-o-t) concentration ratio as a function or (a-e) irradiance, (f-j) temperature, (k-o) vapor pressure deficit and (p-t) external CO_2 concentration for basil exposed to different light treatments. The reference climatic variables are representative of growth chambers conditions, with irradiance, temperature, relative humidity and CO_2 concentration equal to 80 Wm^{-2}, 24°C, 70%, and 450 *ppm*.

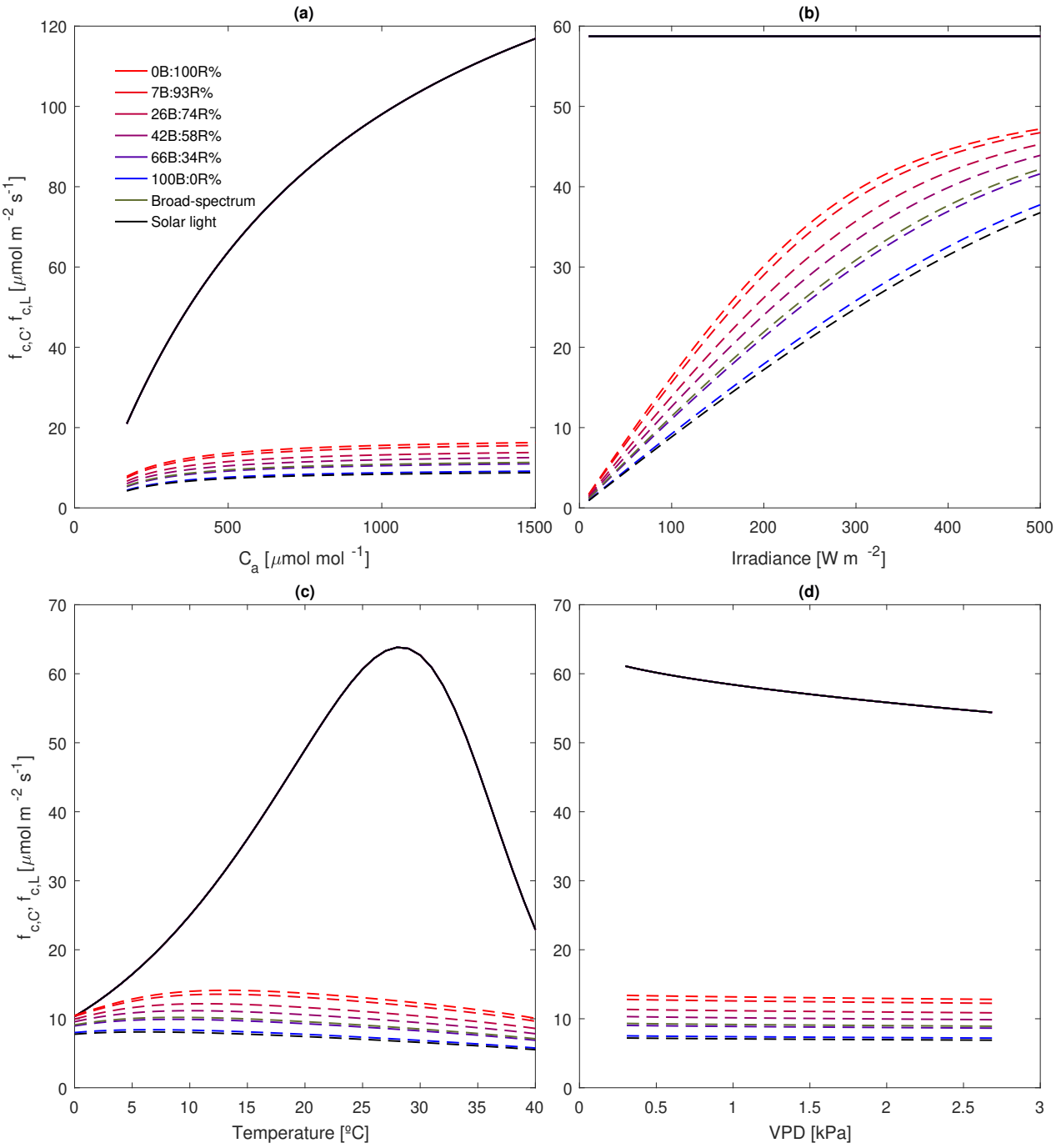

Figure A.4: Linear Katul model. Rubisco-limited ($f_{c,C}$, solid lines) and RuBP-regeneration limited ($f_{c,L}$, dashed lines) as a function of (a) air CO_2 concentration, (b) irradiance, (c) temperature, (d) vapor pressure deficit for basil subjected to different light treatments. The reference values for the climatic variables are as in Figure A.3.

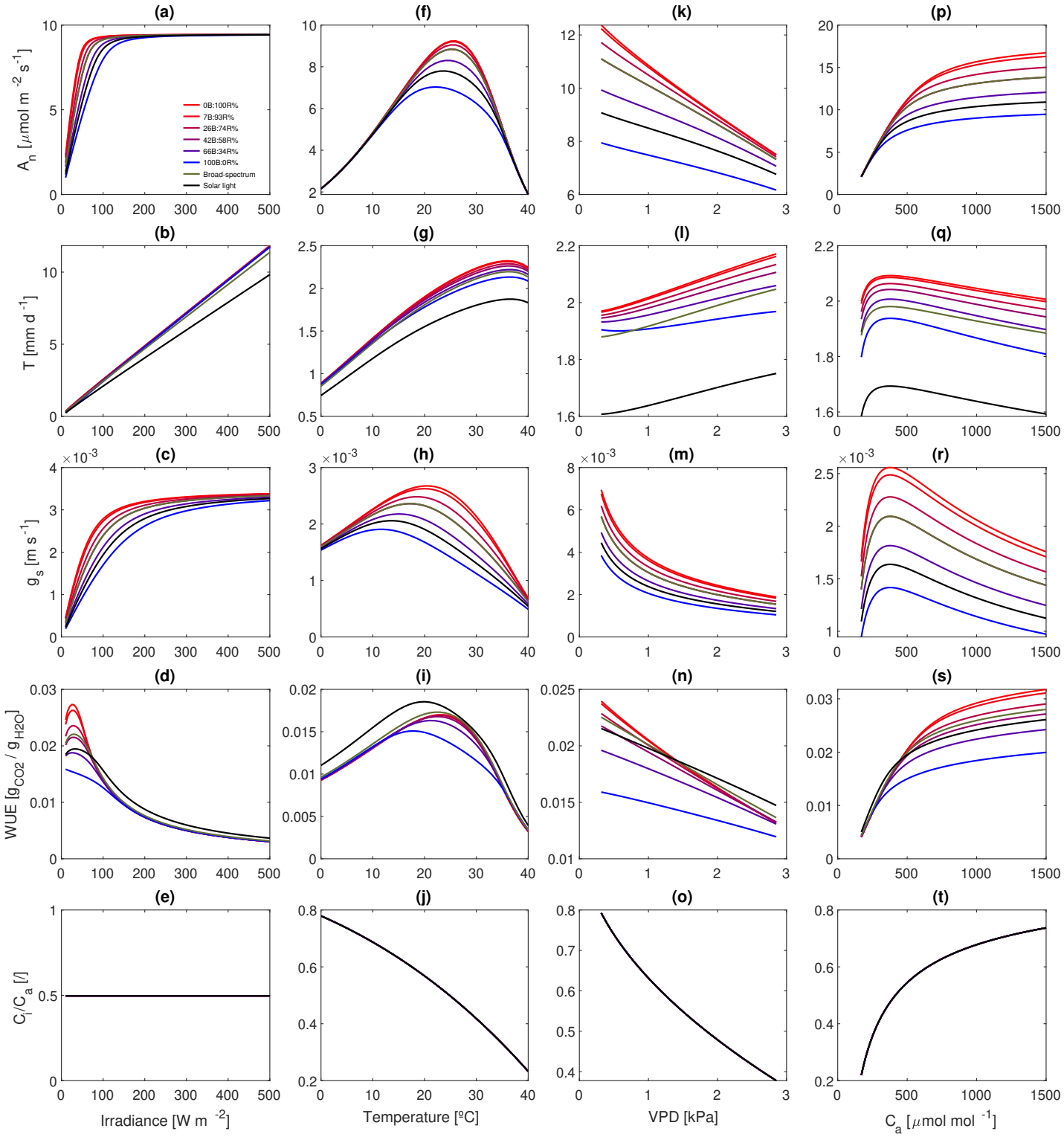

Figure A.5: Linear Medlyn model. (a-f-k-p) photosynthetic rate, (b-g-l-q) transpiration rate, (c-h-m-r) stomatal conductance, (d-i-n-s) water use efficiency, and (e-j-o-t) concentration ratio as a function or (a-e) irradiance, (f-j) temperature, (k-o) vapor pressure deficit and (p-t) external CO_2 concentration for strawberry exposed to different light treatments. The reference climatic variables are representative of growth chambers conditions, with irradiance, temperature, relative humidity and CO_2 concentration equal to 80 Wm^{-2}, 25°C, 41.2%, and 410 *ppm*.

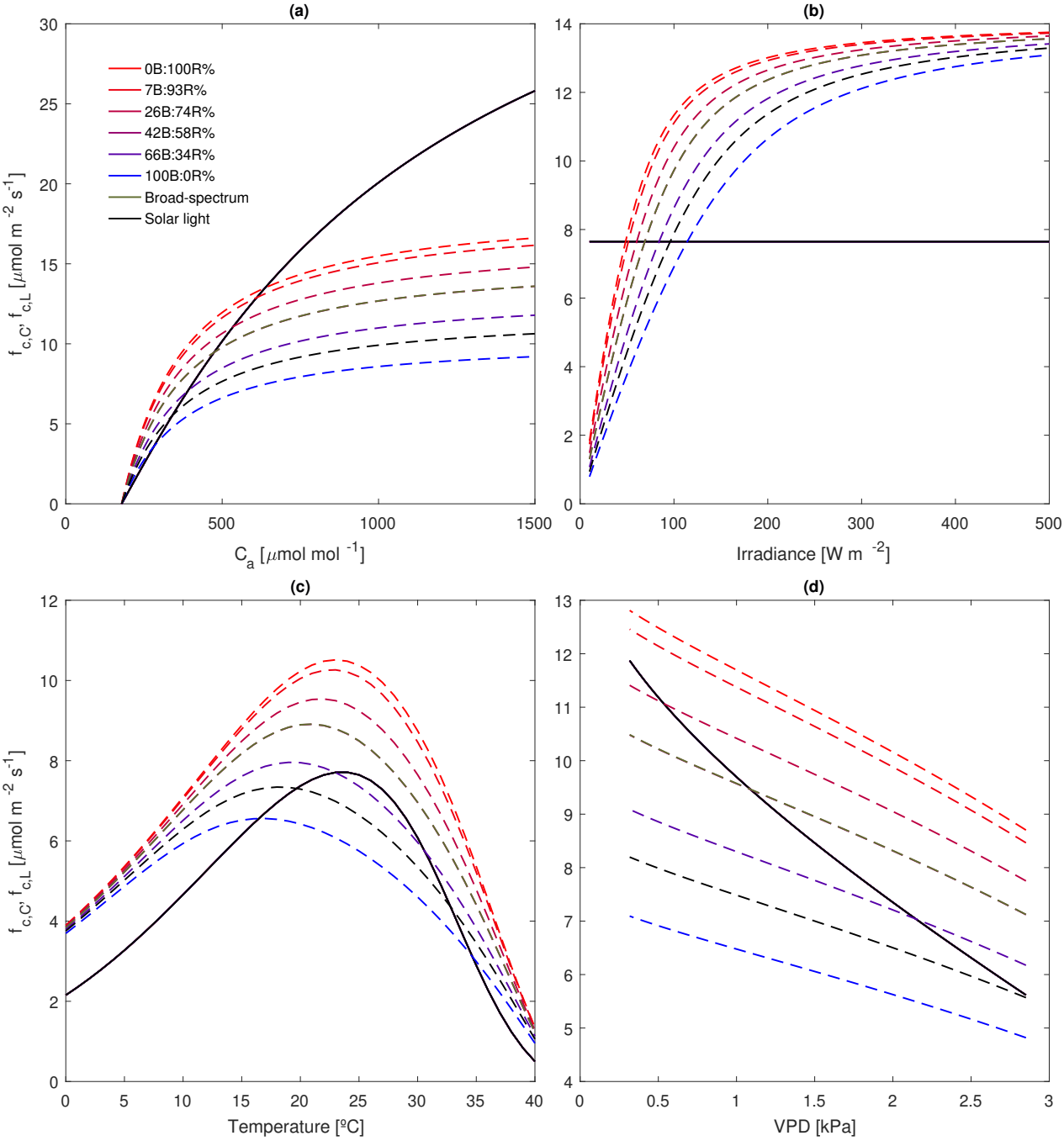

Figure A.6: Linear Medlyn model. Rubisco-limited ($f_{c,C}$, solid lines) and RuBP-regeneration limited ($f_{c,L}$, dashed lines) as a function of (a) air CO_2 concentration, (b) irradiance, (c) temperature, (d) vapor pressure deficit for strawberry subjected to different light treatments. The reference values for the climatic variables are as in Figure A.5.

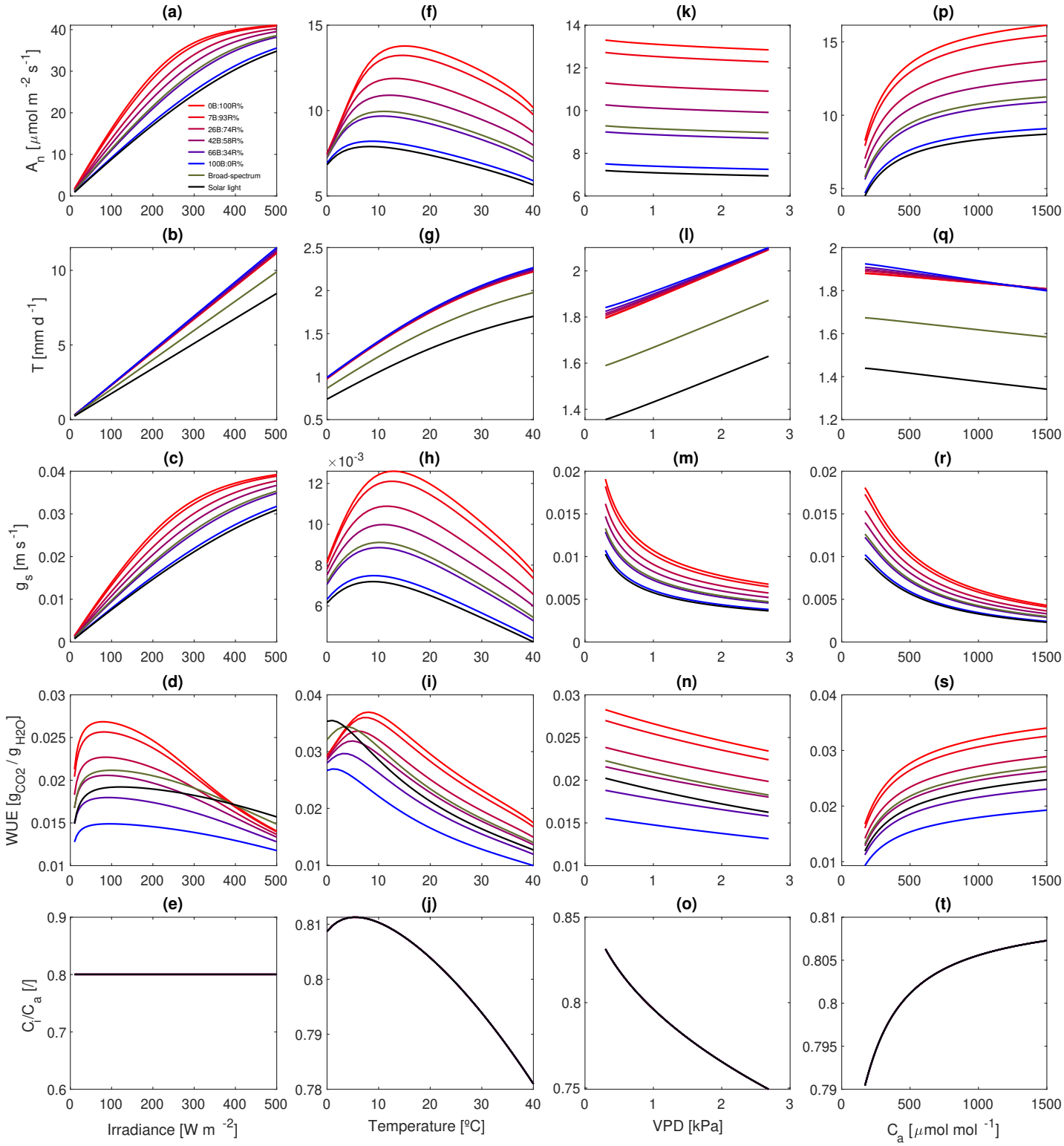

Figure A.7: Non-linear Katul model. (a-f-k-p) photosynthetic rate, (b-g-l-q) transpiration rate, (c-h-m-r) stomatal conductance, (d-i-n-s) water use efficiency, and (e-j-o-t) concentration ratio as a function or (a-e) irradiance, (f-j) temperature, (k-o) vapor pressure deficit and (p-t) external CO_2 concentration for basil exposed to different light treatments. The reference climatic variables are representative of growth chambers conditions, with irradiance, temperature, relative humidity and CO_2 concentration equal to 80 Wm^{-2}, 24°C, 70%, and 450 *ppm*.

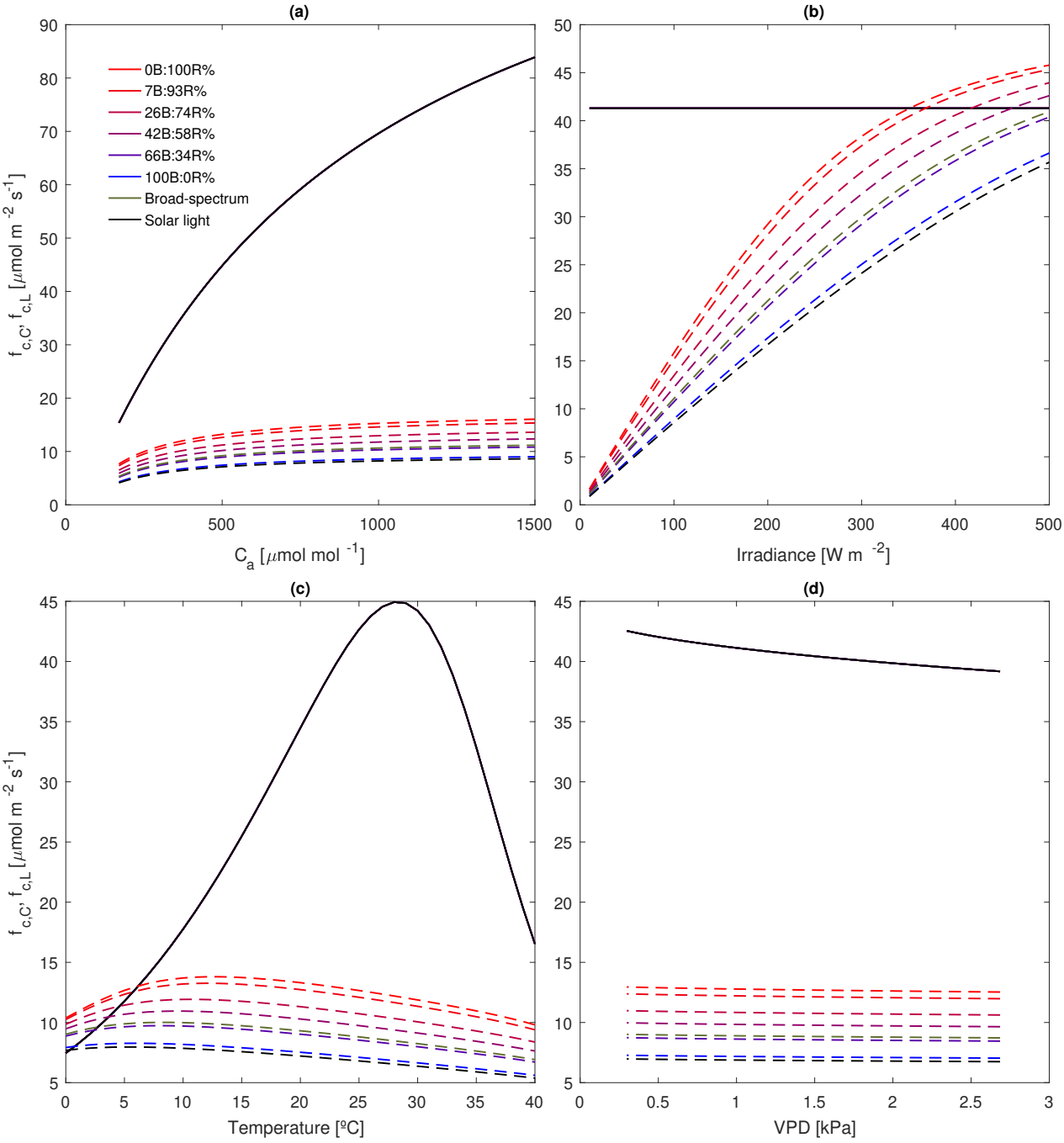

Figure A.8: Non-linear Katul model. Rubisco-limited ($f_{c,C}$, solid lines) and RuBP-regeneration limited ($f_{c,L}$, dashed lines) as a function of (a) air CO_2 concentration, (b) irradiance, (c) temperature, (d) vapor pressure deficit for basil subjected to different light treatments. The reference values for the climatic variables are as in Figure A.7.

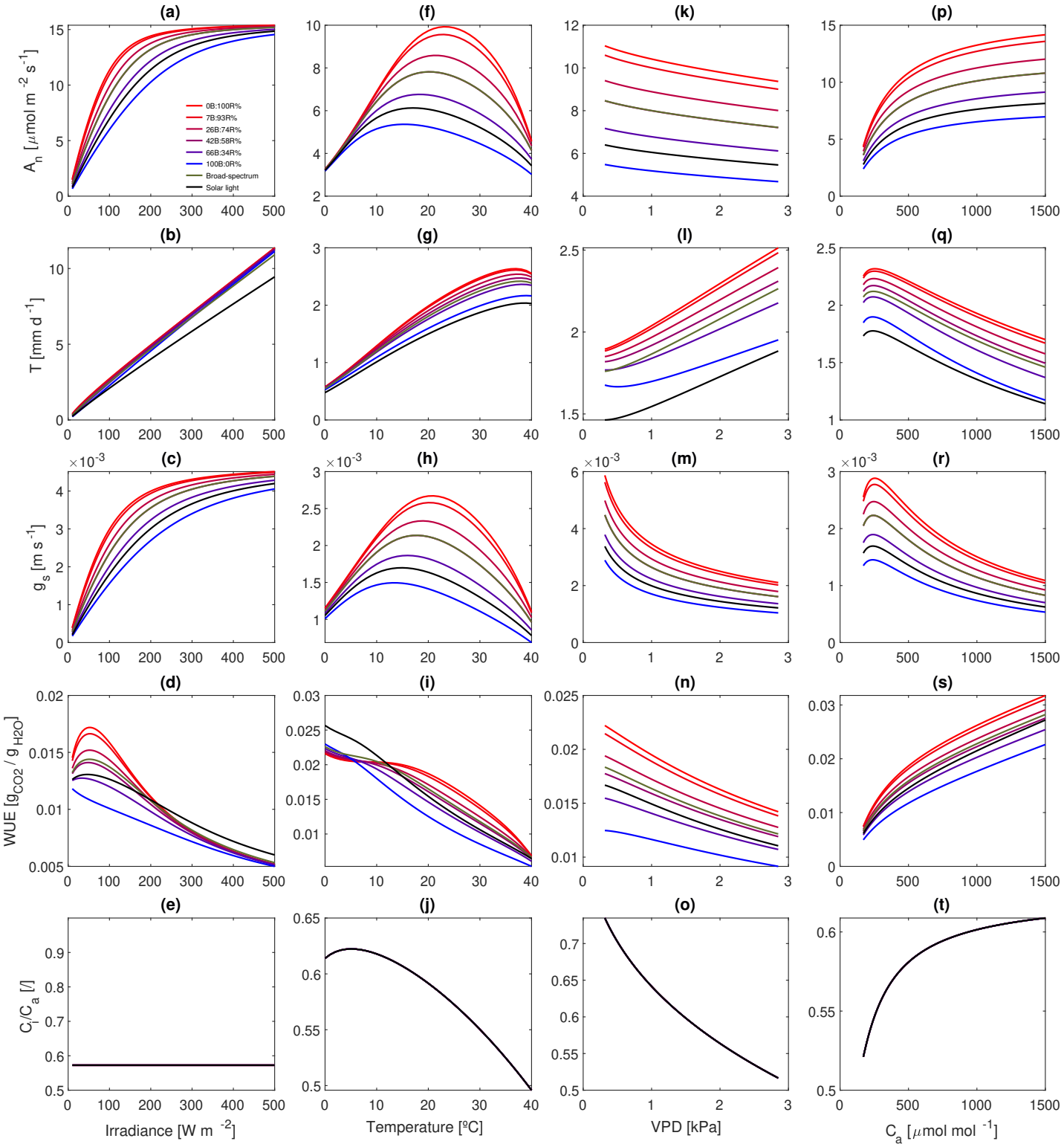

Figure A.9: Non-linear Katul model. (a-f-k-p) photosynthetic rate, (b-g-l-q) transpiration rate, (c-h-m-r) stomatal conductance, (d-i-n-s) water use efficiency, and (e-j-o-t) concentration ratio as a function or (a-e) irradiance, (f-j) temperature, (k-o) vapor pressure deficit and (p-t) external CO_2 concentration for strawberry exposed to different light treatments. The reference climatic variables are representative of growth chambers conditions, with irradiance, temperature, relative humidity and CO_2 concentration equal to 80 Wm^{-2}, 25°C, 41.2%, and 410 *ppm*.

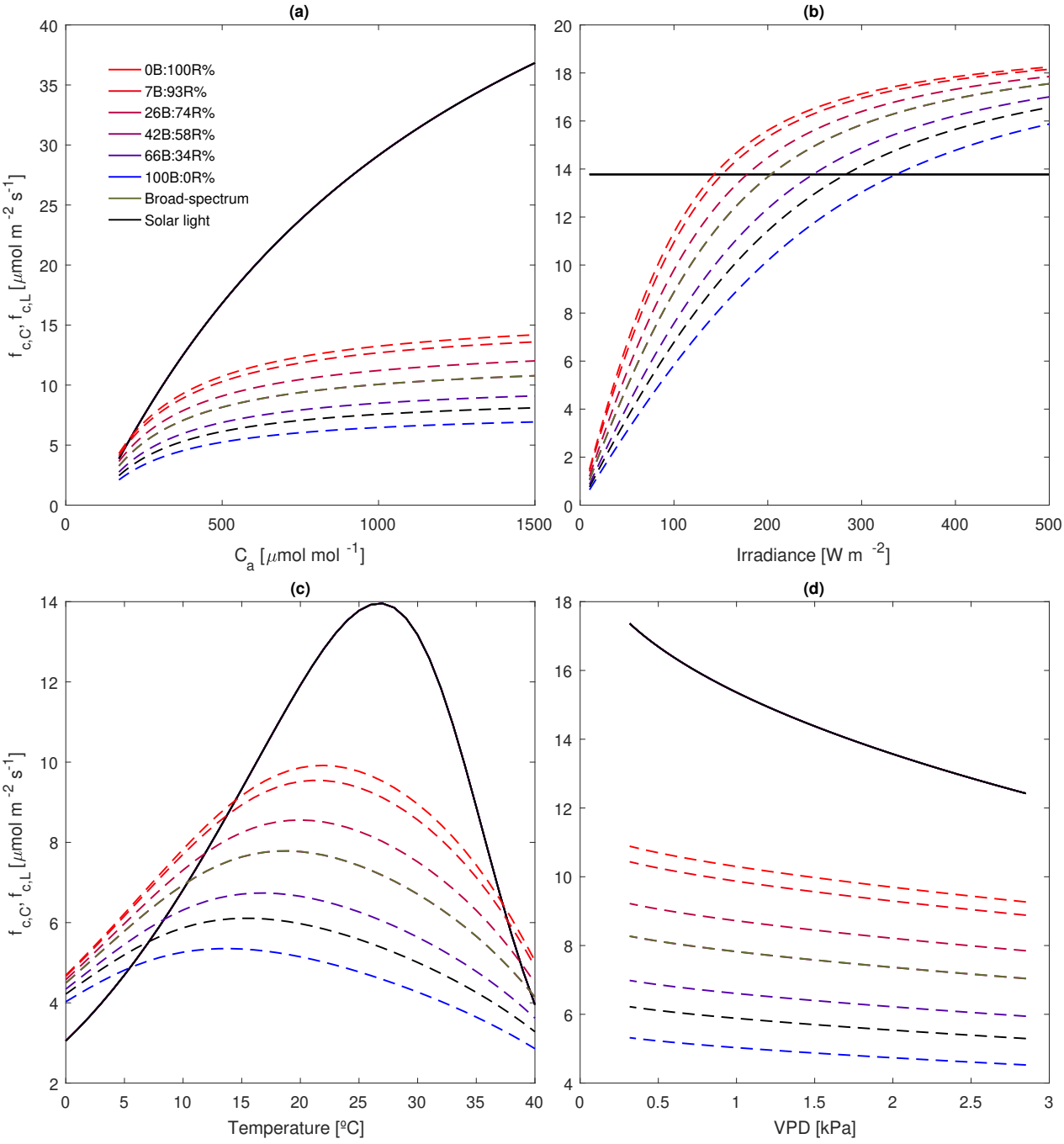

Figure A.10: Non-linear Katul model. Rubisco-limited ($f_{c,C}$, solid lines) and RuBP-regeneration limited ($f_{c,L}$, dashed lines) as a function of (a) air CO_2 concentration, (b) irradiance, (c) temperature, (d) vapor pressure deficit for strawberry subjected to different light treatments. The reference values for the climatic variables are as in Figure A.9

.

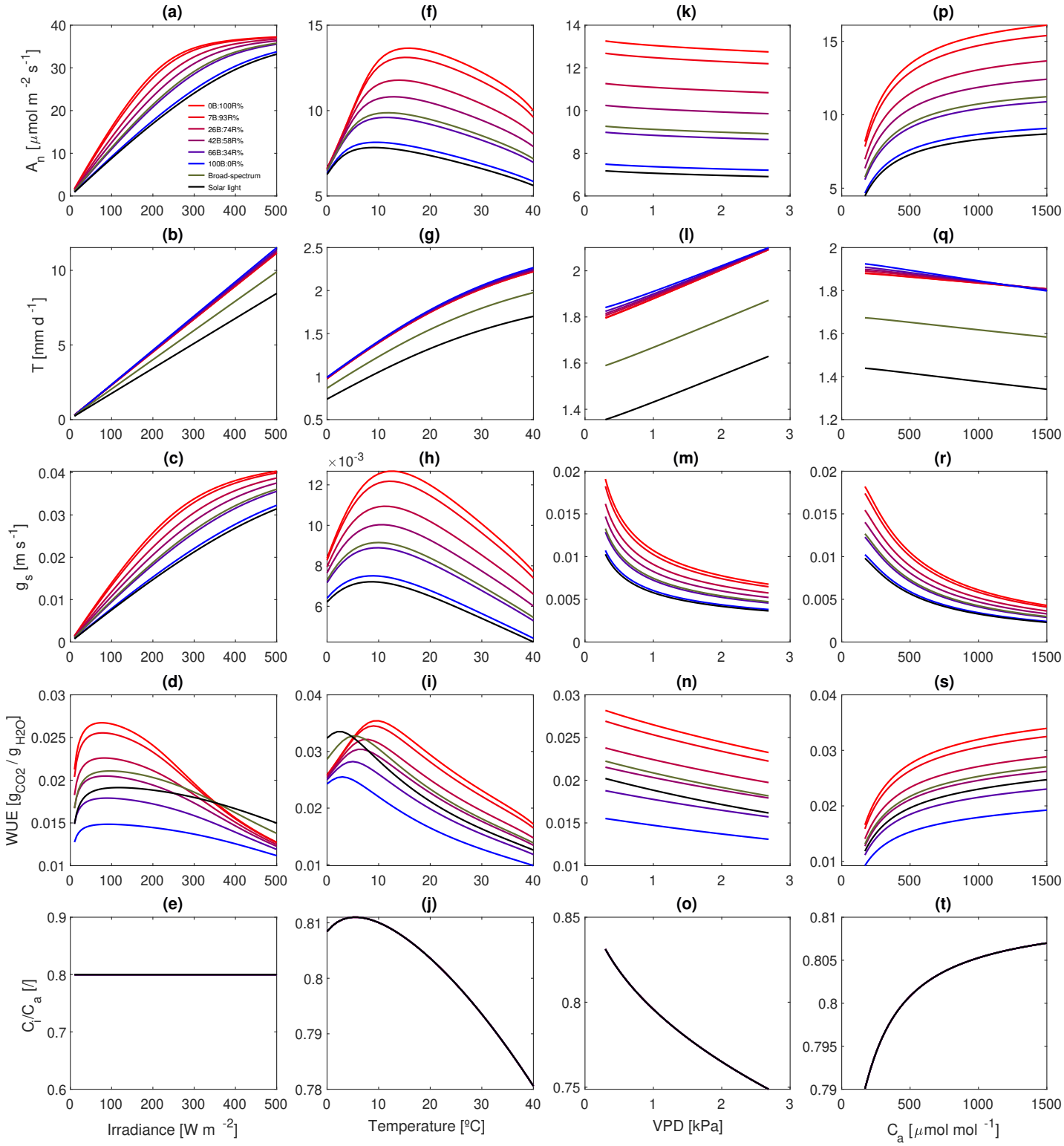

Figure A.11: Non-linear Medlyn model. (a-f-k-p) photosynthetic rate, (b-g-l-q) transpiration rate, (c-h-m-r) stomatal conductance, (d-i-n-s) water use efficiency, and (e-j-o-t) concentration ratio as a function or (a-e) irradiance, (f-j) temperature, (k-o) vapor pressure deficit and (p-t) external CO_2 concentration for basil exposed to different light treatments. The reference climatic variables are representative of growth chambers conditions, with irradiance, temperature, relative humidity and CO_2 concentration equal to 80 Wm^{-2}, 24°C, 70%, and 450 *ppm*.

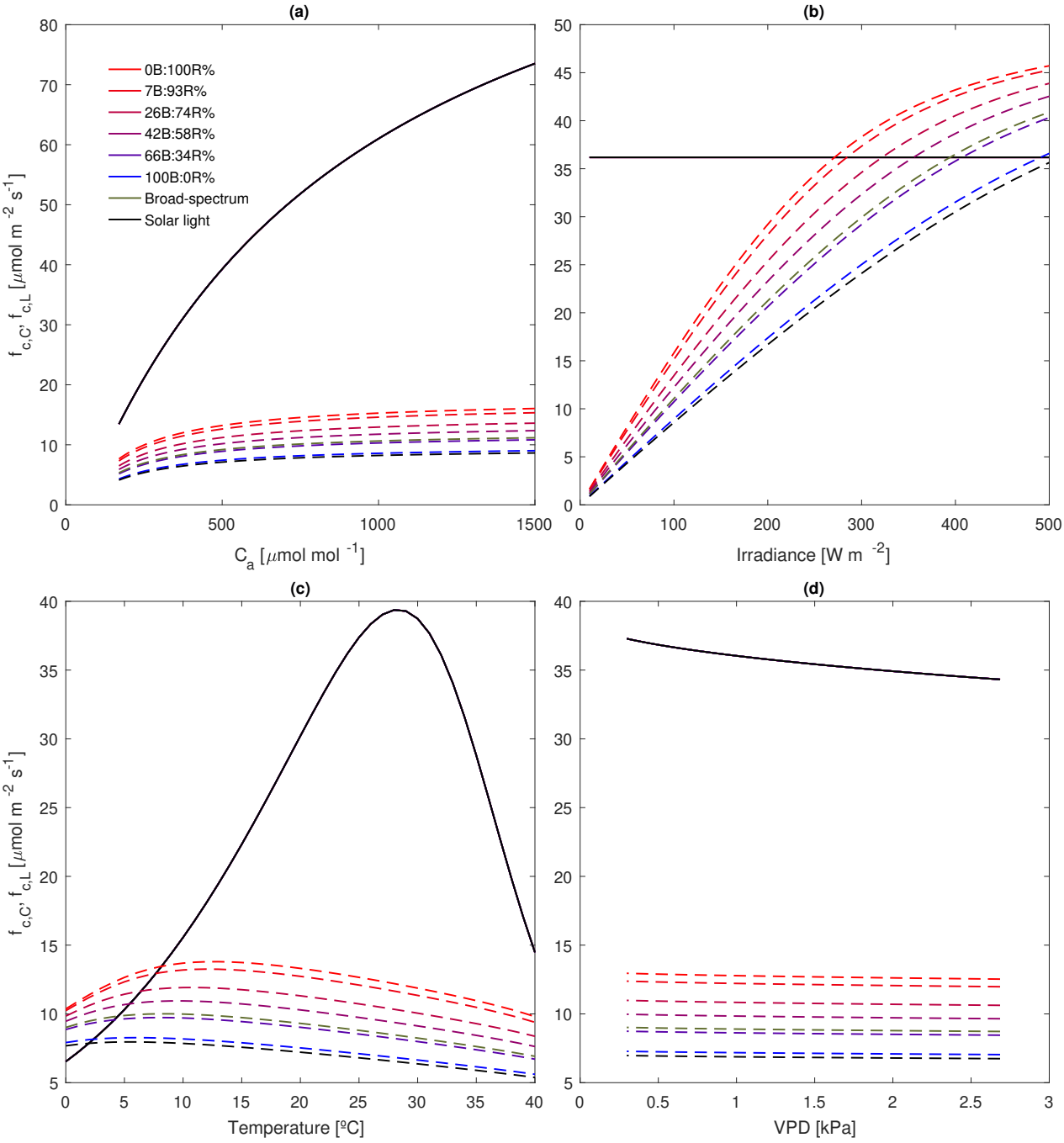

Figure A.12: Non-linear Medlyn model. Rubisco-limited ($f_{c,C}$, solid lines) and RuBP-regeneration limited ($f_{c,L}$, dashed lines) as a function of (a) air CO_2 concentration, (b) irradiance, (c) temperature, (d) vapor pressure deficit for basil subjected to different light treatments. The reference values for the climatic variables are as in Figure A.11.

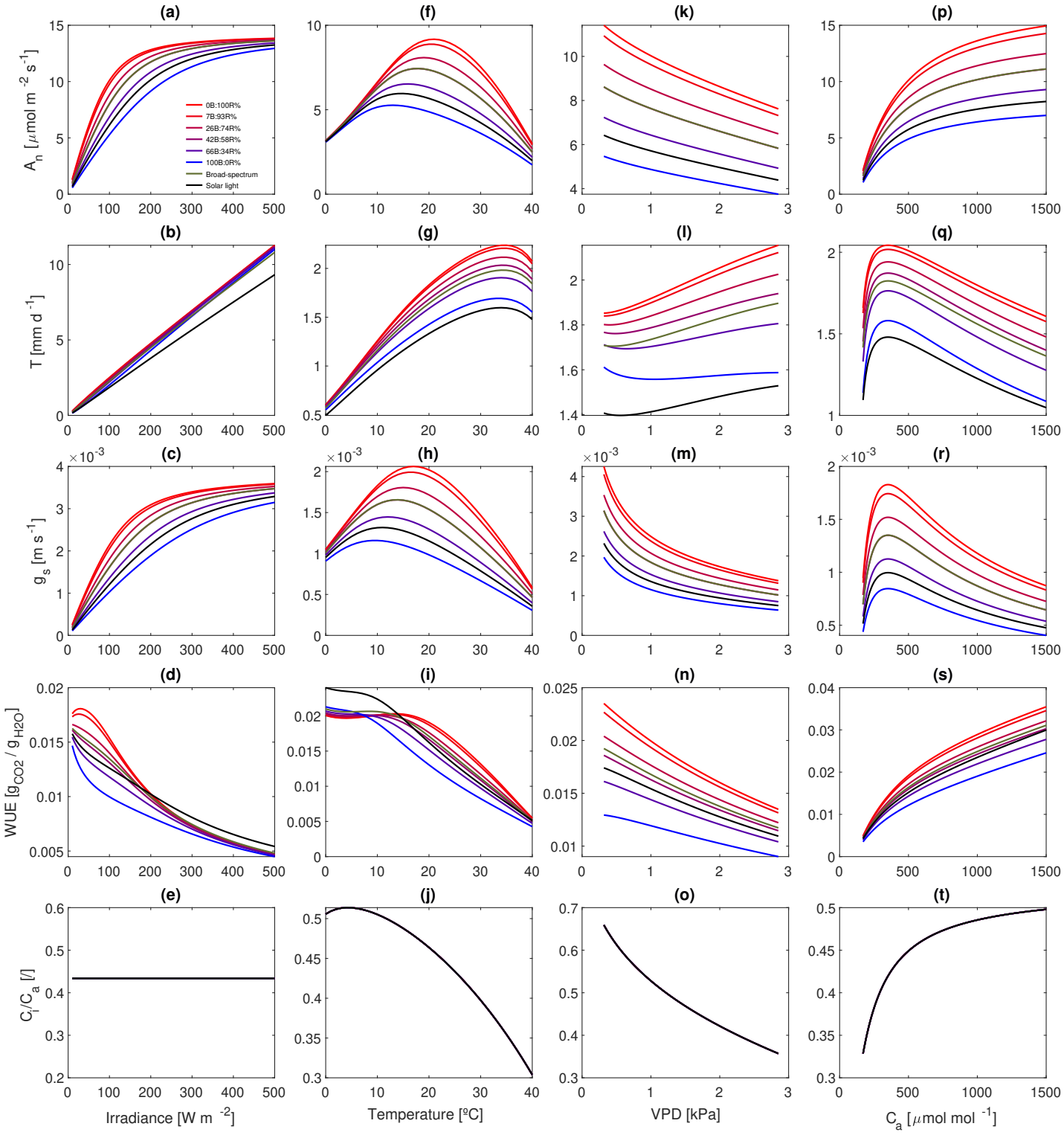

Figure A.13: Non-linear Medlyn model. (a-f-k-p) photosynthetic rate, (b-g-l-q) transpiration rate, (c-h-m-r) stomatal conductance, (d-i-n-s) water use efficiency, and (e-j-o-t) concentration ratio as a function or (a-e) irradiance, (f-j) temperature, (k-o) vapor pressure deficit and (p-t) external CO_2 concentration for strawberry exposed to different light treatments. The reference climatic variables are representative of growth chambers conditions, with irradiance, temperature, relative humidity and CO_2 concentration equal to 80 Wm^{-2}, 25°C, 41.2%, and 410 *ppm*.

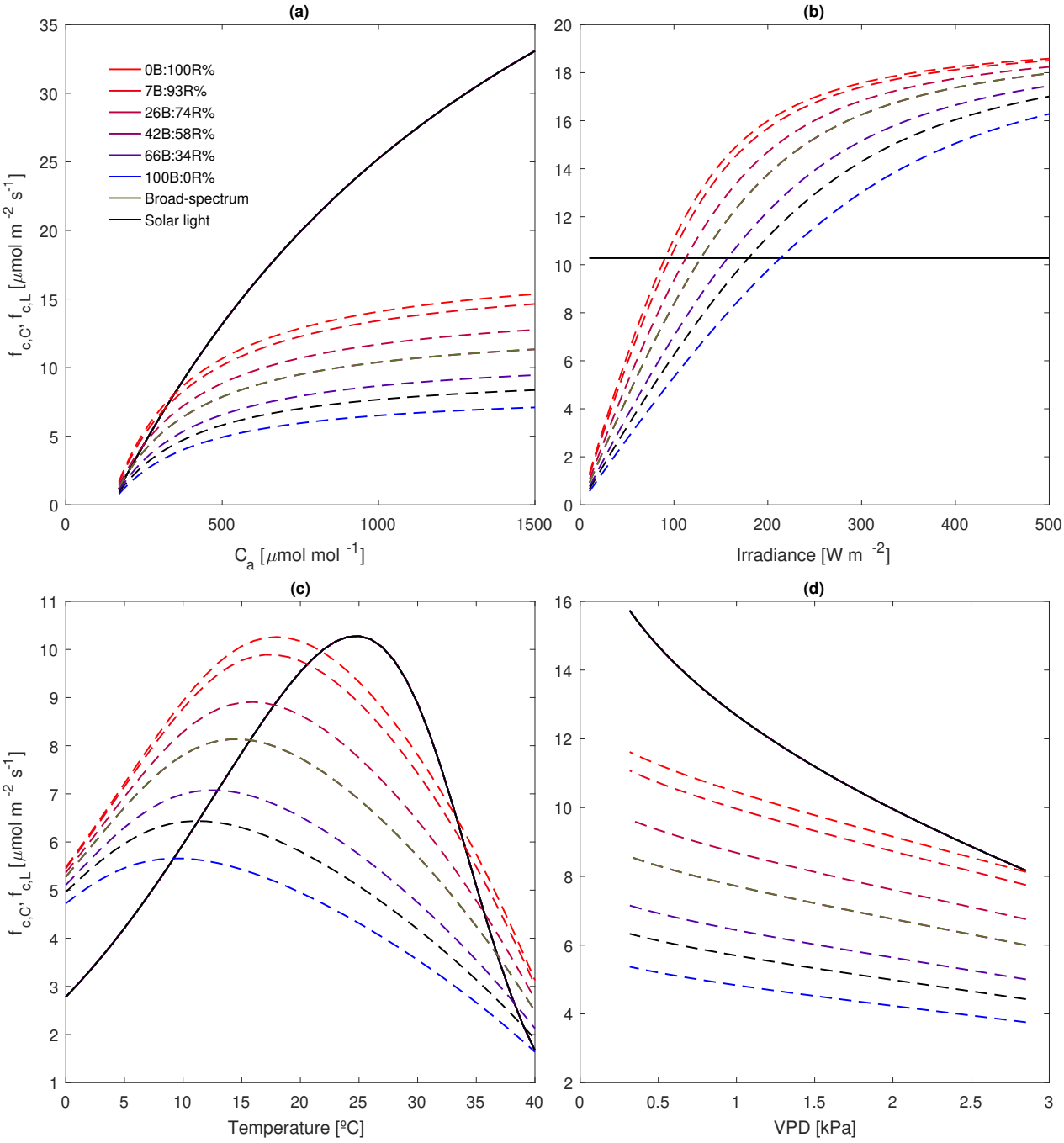

Figure A.14: Non-linear Medlyn model. Rubisco-limited ($f_{c,C}$, solid lines) and RuBP-regeneration limited ($f_{c,L}$, dashed lines) as a function of (a) air CO_2 concentration, (b) irradiance, (c) temperature, (d) vapor pressure deficit for strawberry subjected to different light treatments. The reference values for the climatic variables are as in Figure A.13.

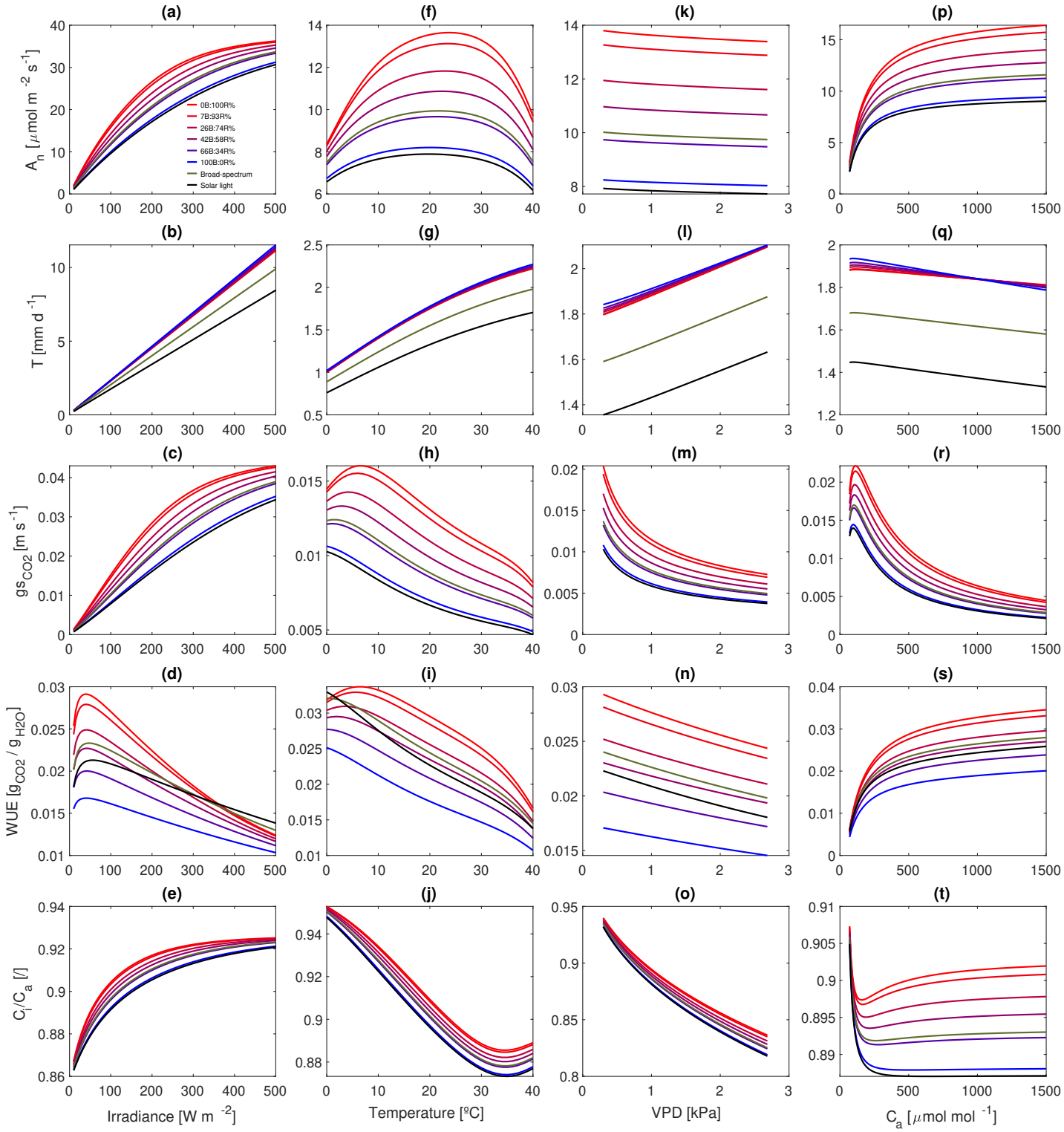

Figure A.15: Co-limitation model. (a-f-k-p) photosynthetic rate, (b-g-l-q) transpiration rate, (c-h-m-r) stomatal conductance, (d-i-n-s) water use efficiency, and (e-j-o-t) concentration ratio as a function or (a-e) irradiance, (f-j) temperature, (k-o) vapor pressure deficit and (p-t) external CO_2 concentration for basil exposed to different light treatments. The reference climatic variables are representative of growth chambers conditions, with irradiance, temperature, relative humidity and CO_2 concentration equal to 80 Wm^{-2}, 24°C, 70%, and 450 *ppm*.

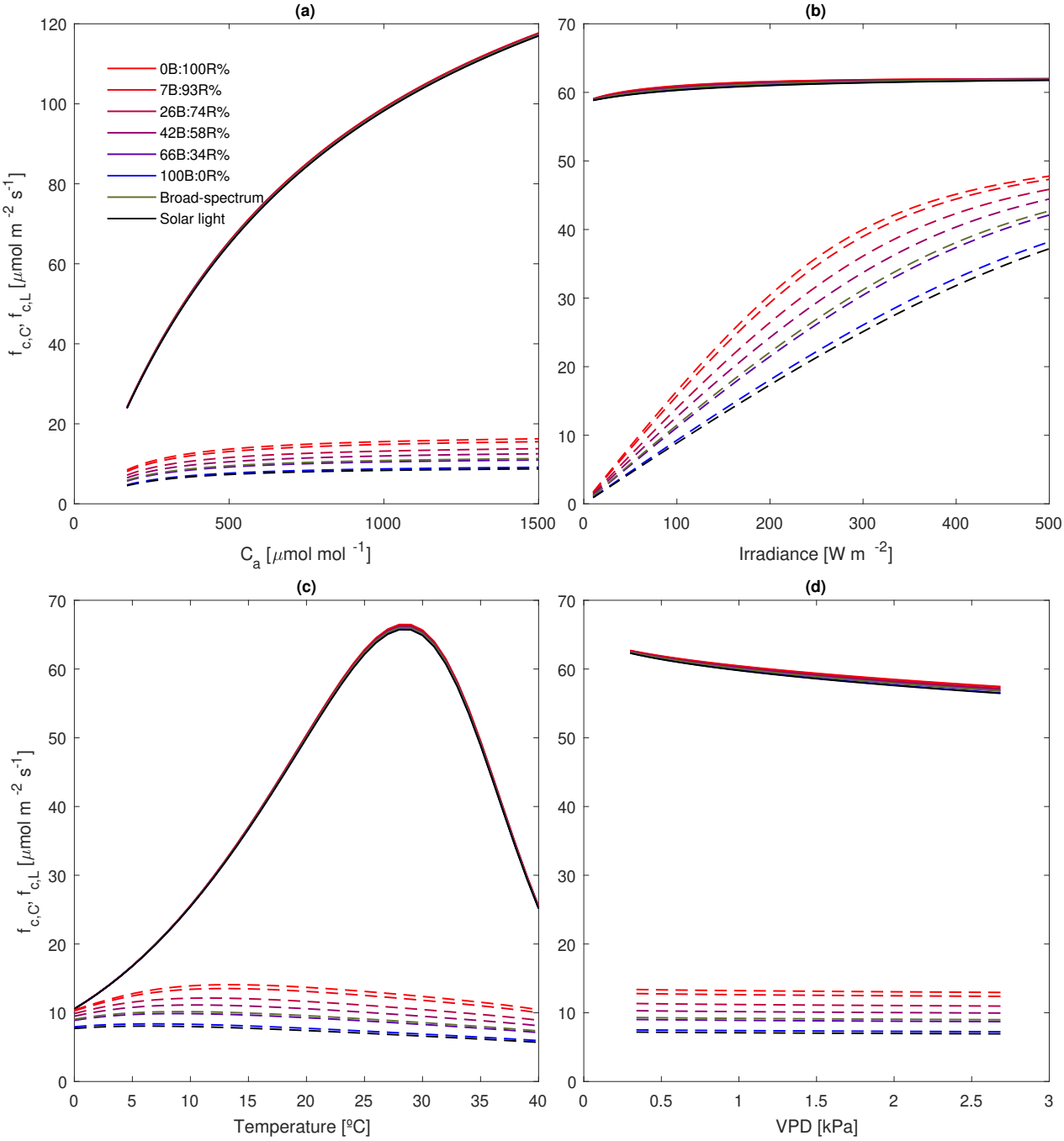

Figure A.16: Co-limitation model. Rubisco-limited ($f_{c,C}$, solid lines) and RuBP-regeneration limited ($f_{c,L}$, dashed lines) as a function of (a) air CO_2 concentration, (b) irradiance, (c) temperature, (d) vapor pressure deficit for basil subjected to different light treatments. The reference values for the climatic variables are as in Figure A.15.

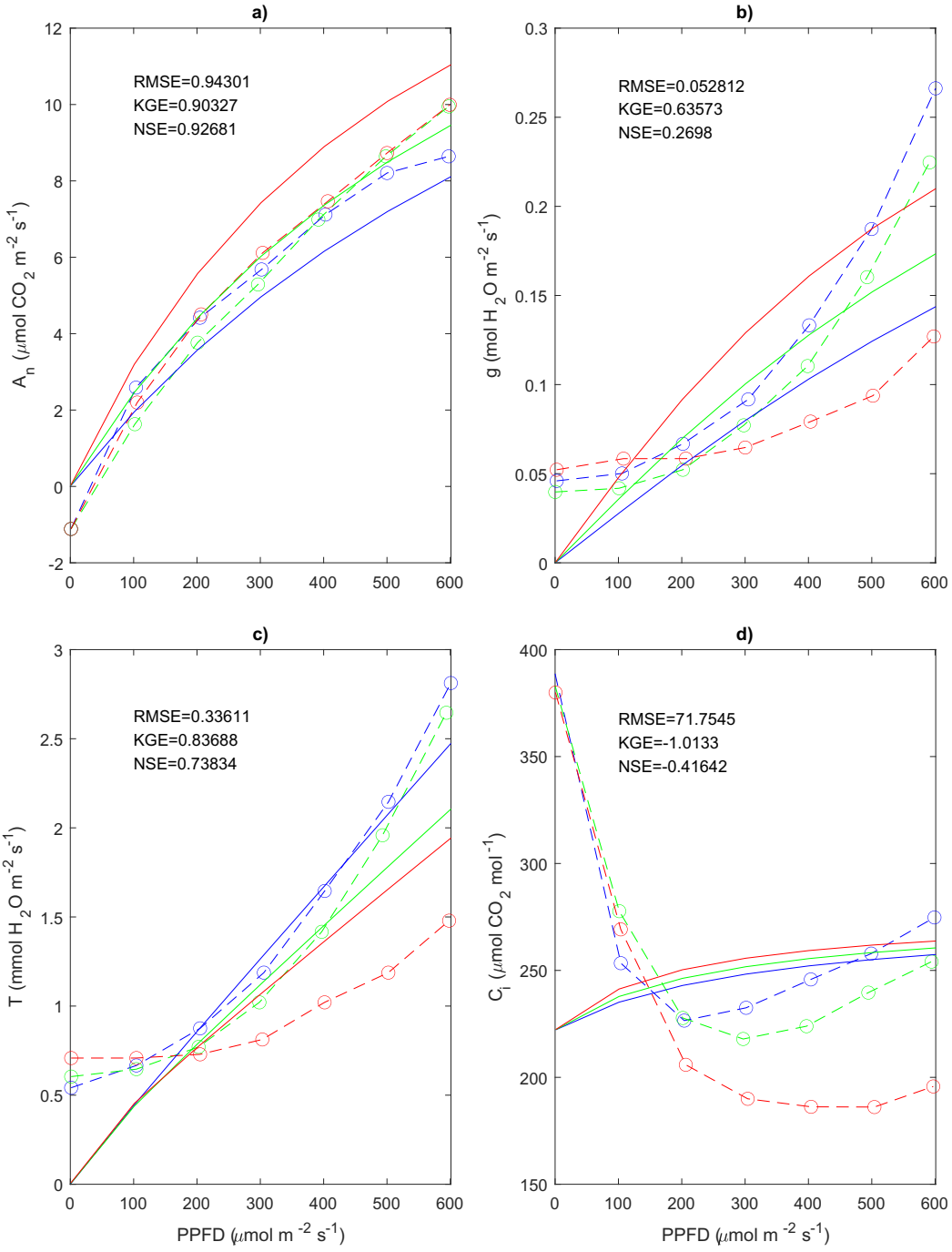

Figure A.17: Simulated (solid lines) photosynthetic rate (A_n), stomatal conductance (g), transpiration rate (T) and intercellular CO_2 concentration (c_i) for the co-limitation model with linear dependence of λ on c_a, compared with observations (symbols with dashed lines) in the experiments by Mochizuki et al. (2019) with strawberry subjected to different light treatments and photon flux densities. The blue, green and red colors indicate treatments with blue, green, and red LEDs, respectively.

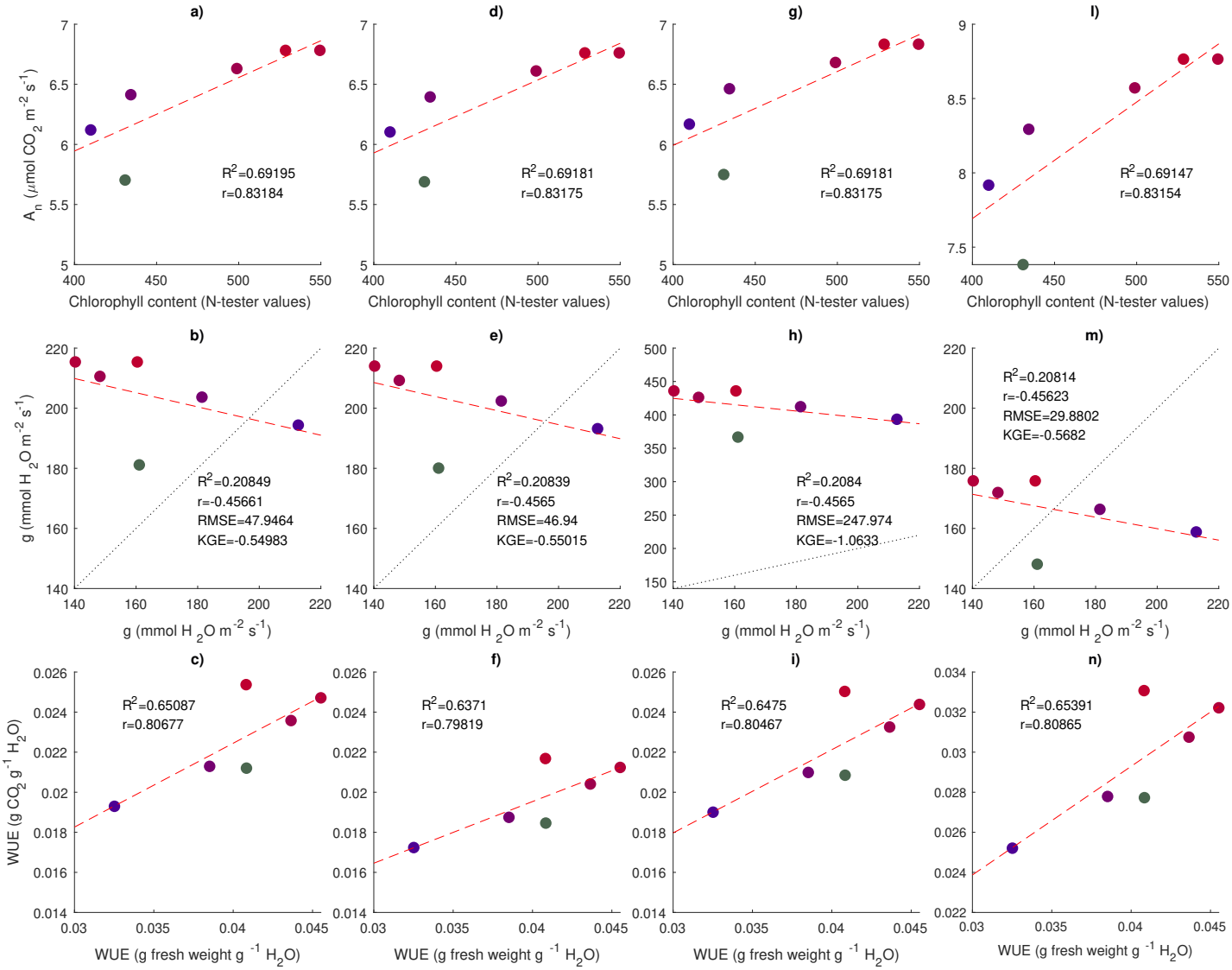

Figure A.18: Simulated (solid lines) photosynthetic rate (A_n), stomatal conductance (g) and water use efficiency (WUE) for the linear Katul model compared with observations (symbols with dashed lines) in the experiments by Mochizuki et al. (2019) with strawberry subjected to different light treatments and photon flux densities. The first column refers to the joint calibration with KGE, the second to the calibration of only g with KGE as objective function, the third to the pair $A_n - WUE$ with KGE and the fourth to the joint calibration with $RMSE$. The blue and red colors indicate treatments with blue, green, and red LEDs, respectively.

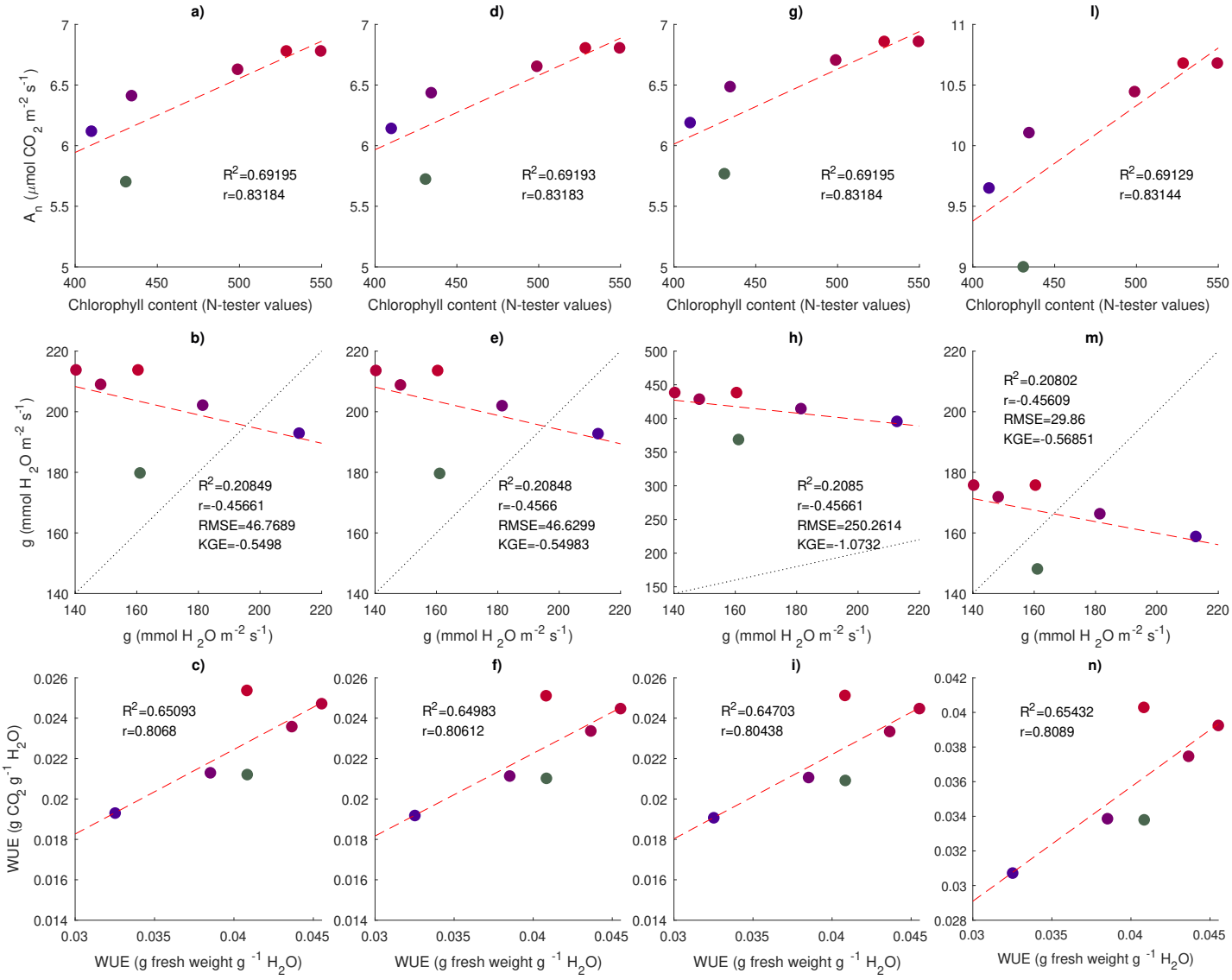

Figure A.19: Simulated (solid lines) photosynthetic rate (A_n), stomatal conductance (g) and water use efficiency (WUE) for the linear Katul model compared with observations (symbols with dashed lines) in the experiments by Mochizuki et al. (2019) with strawberry subjected to different light treatments and photon flux densities. The first column refers to the joint calibration with KGE, the second to the calibration of only g with KGE as objective function, the third to the pair $A_n - WUE$ with KGE and the fourth to the joint calibration with $RMSE$. The blue and red colors indicate treatments with blue, green, and red LEDs, respectively.

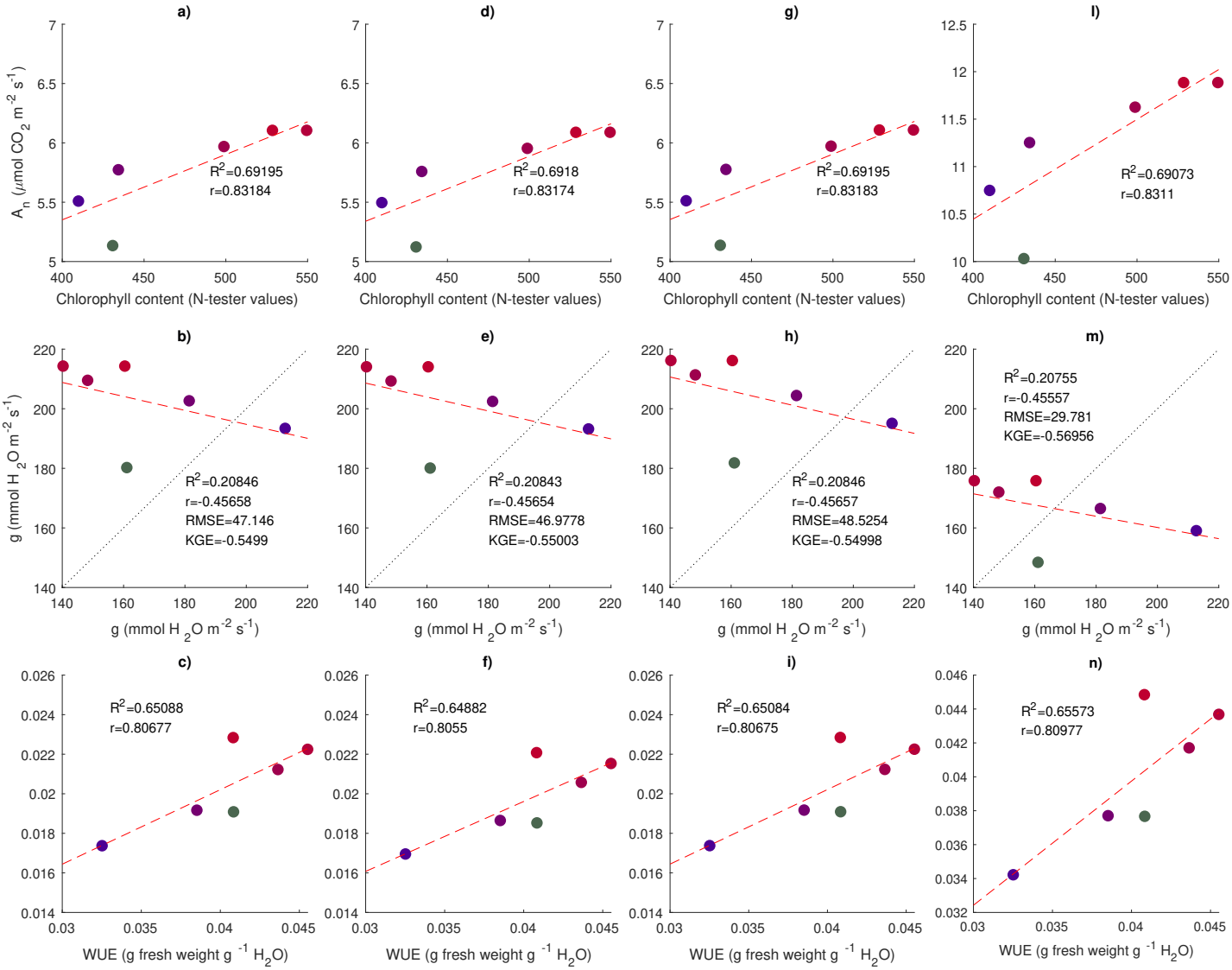

Figure A.20: Simulated (solid lines) photosynthetic rate (A_n), stomatal conductance (g) and water use efficiency (WUE) for the linear Katul model compared with observations (symbols with dashed lines) in the experiments by Mochizuki et al. (2019) with strawberry subjected to different light treatments and photon flux densities. The first column refers to the joint calibration with KGE, the second to the calibration of only g with KGE as objective function, the third to the pair $A_n - WUE$ with KGE and the fourth to the joint calibration with $RMSE$. The blue and red colors indicate treatments with blue, green, and red LEDs, respectively.

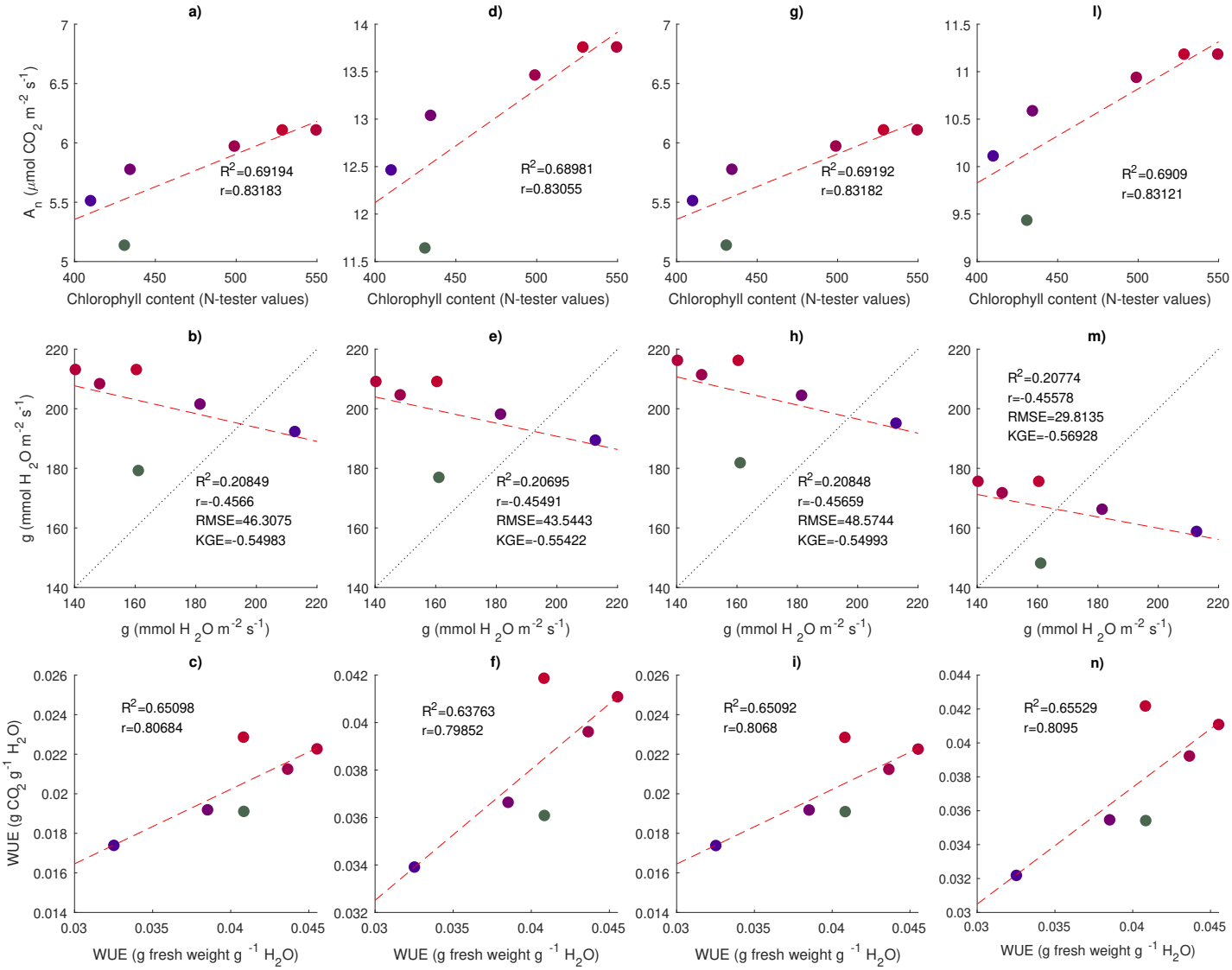

Figure A.21: Simulated (solid lines) photosynthetic rate (A_n), stomatal conductance (g) and water use efficiency (WUE) for the linear Katul model compared with observations (symbols with dashed lines) in the experiments by Mochizuki et al. (2019) with strawberry subjected to different light treatments and photon flux densities. The first column refers to the joint calibration with KGE, the second to the calibration of only g with KGE as objective function, the third to the pair $A_n - WUE$ with KGE and the fourth to the joint calibration with $RMSE$. The blue and red colors indicate treatments with blue, green, and red LEDs, respectively.

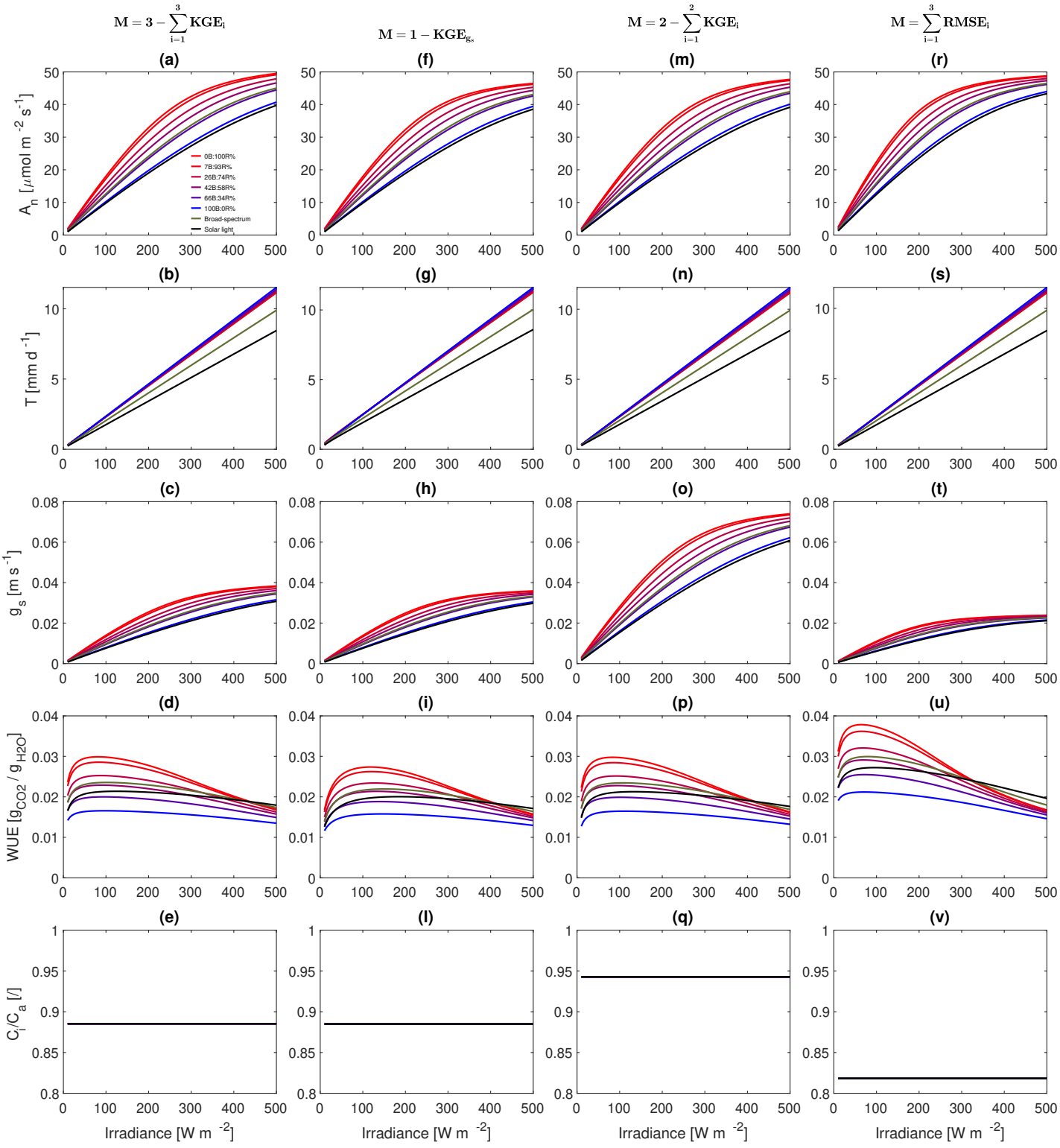

Figure A.22: The image represents the irradiance sensitivity of the linear Katul model. The first column (a-b-c-d-e) refers to the calibrated parameters using the KGE joint calibration, the second (f-g-h-i-l) to the KGE calibration with g, the third (m-n-o-p-q) to the pair $A_n - WUE$ with KGE as objective function and the fourth (r-s-t-u-v) to the joint $RMSE$ calibration. Each column shows the response of basil exposed to different light treatments. The reference climatic variables are representative of growth chambers conditions, with irradiance, temperature, relative humidity and CO_2 concentration equal to 80 Wm^{-2}, 24°C, 70%, and 450 *ppm*.

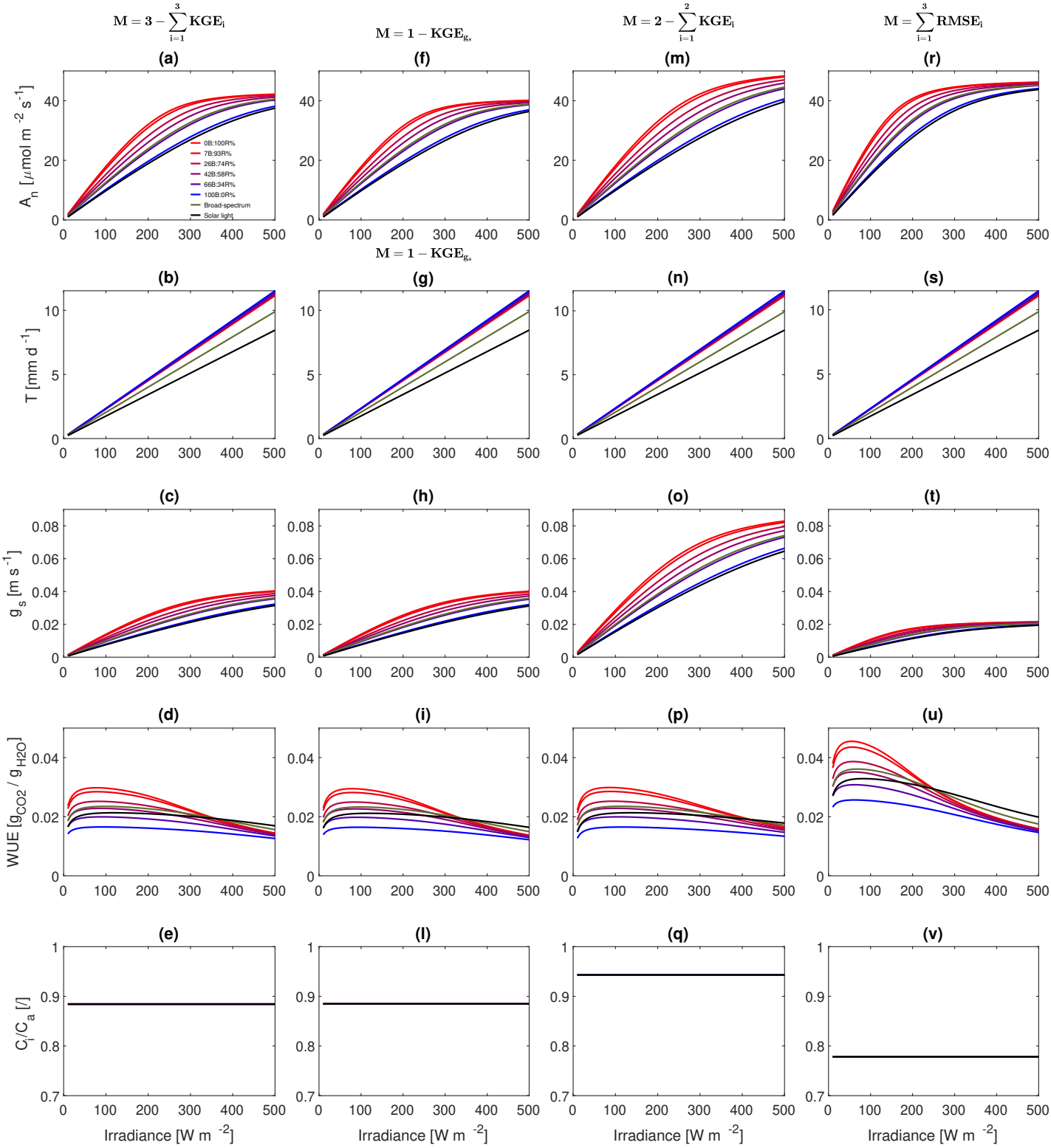

Figure A.23: The image represents the irradiance sensitivity of the linear Medlyn model. The first column (a-b-c-d-e) refers to the calibrated parameters using the KGE joint calibration, the second (f-g-h-i-l) to the KGE calibration with g, the third (m-n-o-p-q) to the pair $A_n - WUE$ with KGE as objective function and the fourth (r-s-t-u-v) to the joint $RMSE$ calibration. Each column shows the response of basil exposed to different light treatments. The reference climatic variables are representative of growth chambers conditions, with irradiance, temperature, relative humidity and CO_2 concentration equal to 80 Wm^{-2}, 24°C, 70%, and 450 ppm.

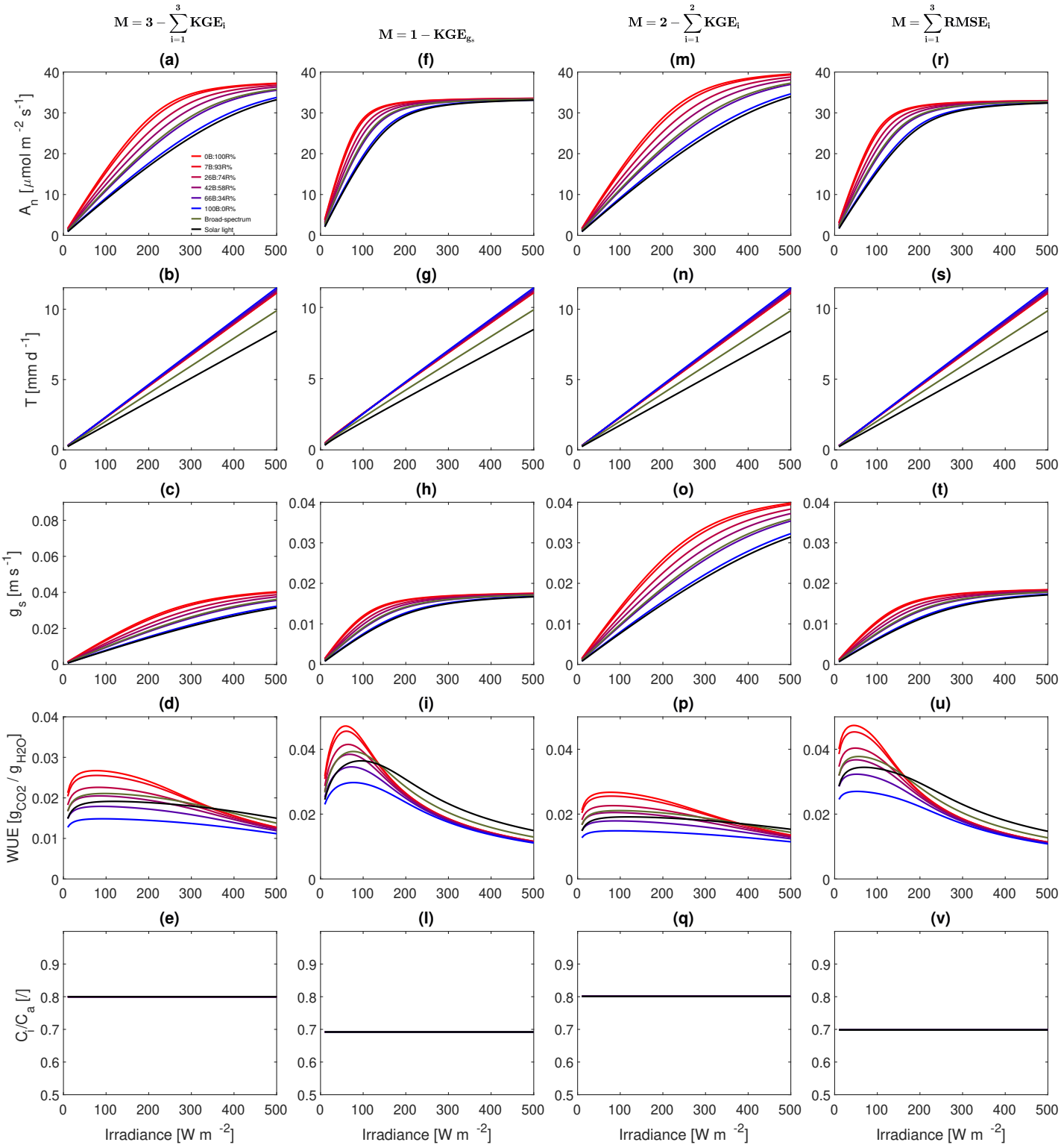

Figure A.24: The image represents the irradiance sensitivity of the non-linear Katul model. The first column (a-b-c-d-e) refers to the calibrated parameters using the KGE joint calibration, the second (f-g-h-i-l) to the KGE calibration with g, the third (m-n-o-p-q) to the pair $A_n - WUE$ with KGE as objective function and the fourth (r-s-t-u-v) to the joint $RMSE$ calibration. Each column shows the response of basil exposed to different light treatments. The reference climatic variables are representative of growth chambers conditions, with irradiance, temperature, relative humidity and CO_2 concentration equal to 80 Wm^{-2}, 24°C, 70%, and 450 *ppm*.

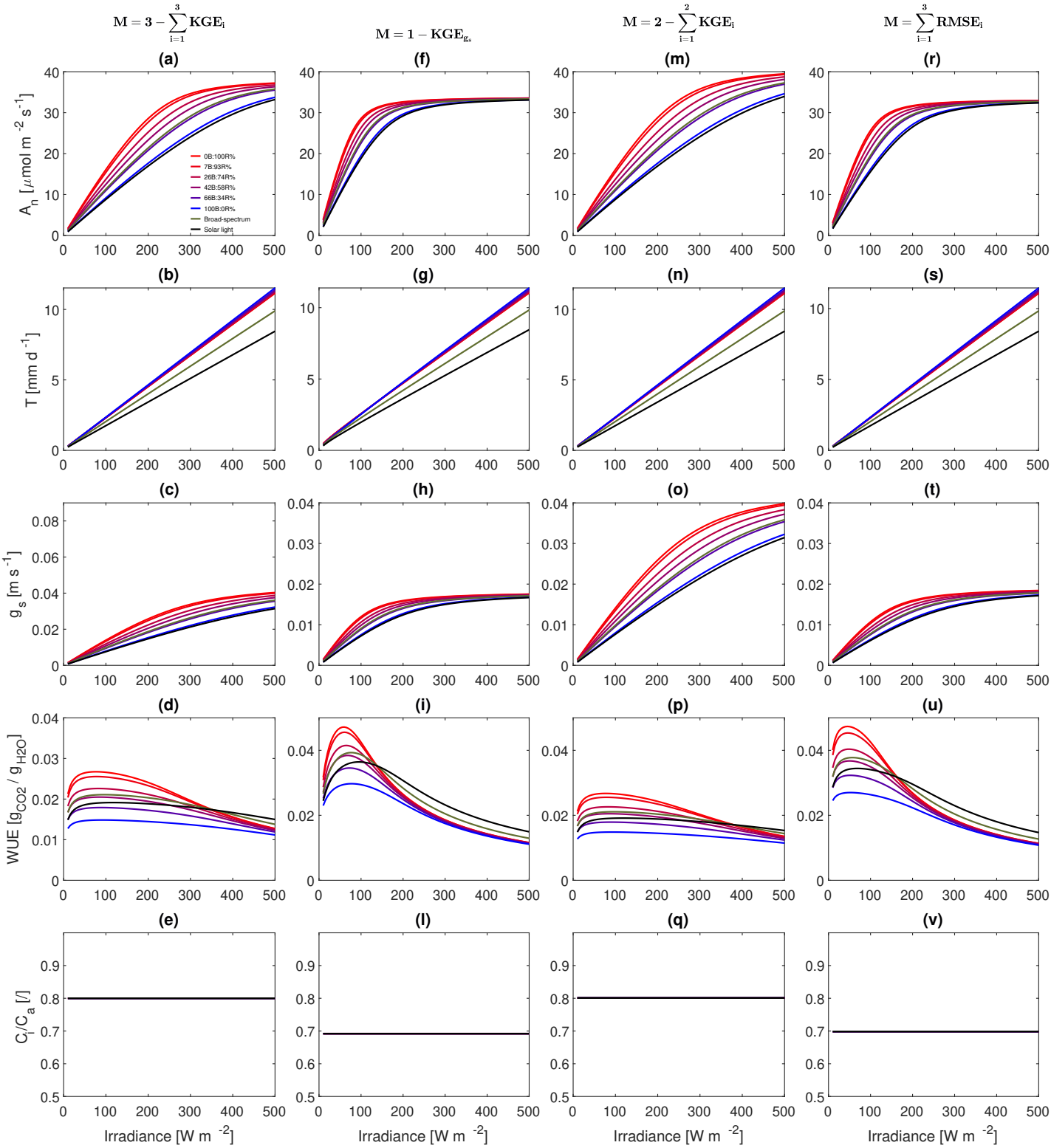

Figure A.25: The image represents the irradiance sensitivity of the non-linear Medlyn model. The first column (a-b-c-d-e) refers to the calibrated parameters using the KGE joint calibration, the second (f-g-h-i-l) to the KGE calibration with g, the third (m-n-o-p-q) to the pair $A_n - WUE$ with KGE as objective function and the fourth (r-s-t-u-v) to the joint $RMSE$ calibration. Each column shows the response of basil exposed to different light treatments. The reference climatic variables are representative of growth chambers conditions, with irradiance, temperature, relative humidity and CO_2 concentration equal to 80 Wm^{-2}, 24°C, 70%, and 450 ppm.

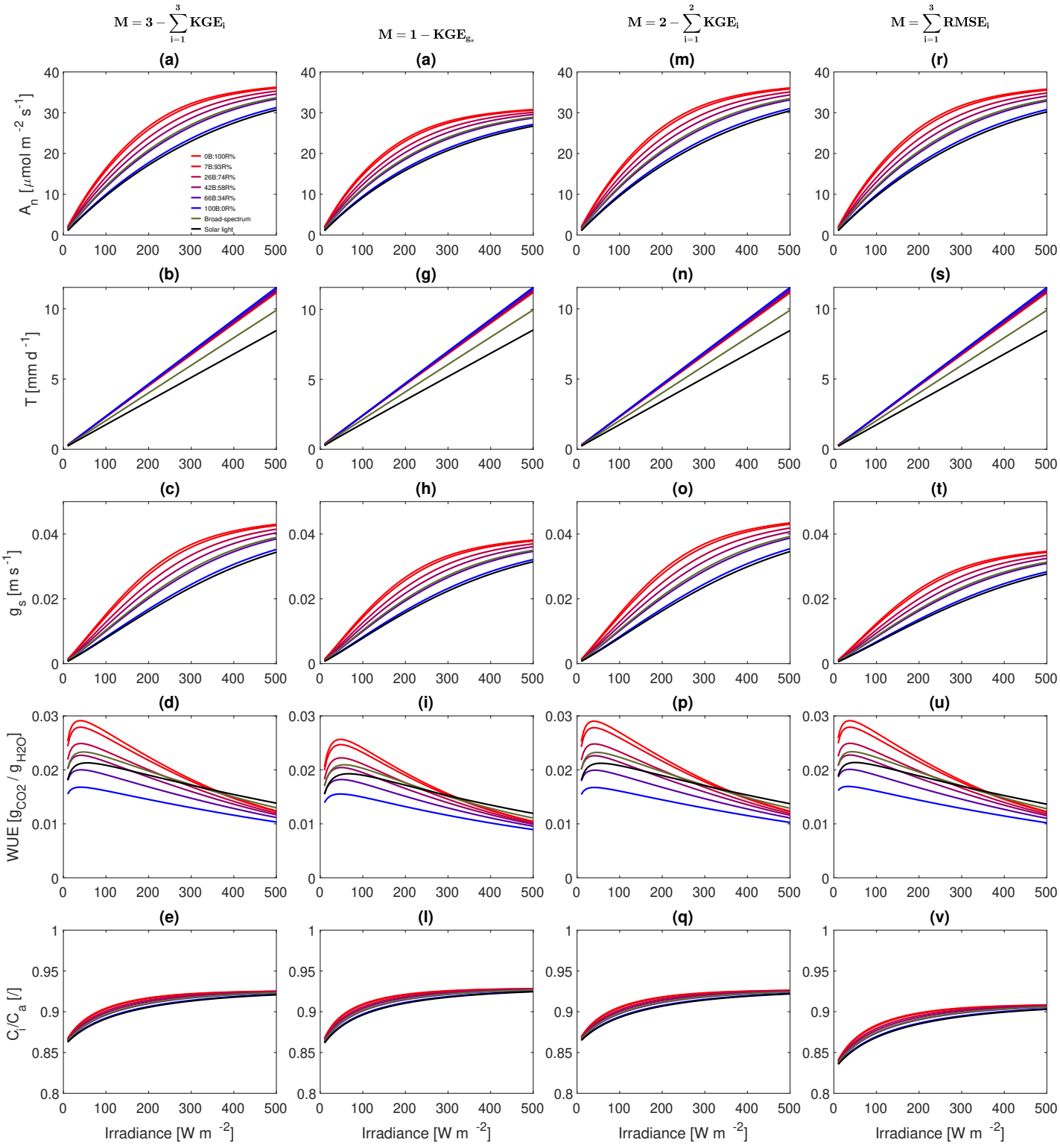

Figure A.26: The image represents the irradiance sensitivity of the co-limitation model. The first column (a-b-c-d-e) refers to the calibrated parameters using the KGE joint calibration, the second (f-g-h-i-l) to the KGE calibration with g, the third (m-n-o-p-q) to the pair $A_n - WUE$ with KGE as objective function and the fourth (r-s-t-u-v) to the joint $RMSE$ calibration. Each column shows the response of basil exposed to different light treatments. The reference climatic variables are representative of growth chambers conditions, with irradiance, temperature, relative humidity and CO_2 concentration equal to 80 Wm^{-2}, 24°C, 70%, and 450 *ppm*.

Joint calibration with KGE as objective function						
Parameter	$\mathbf{J_{max,0}}$	**rjv**	$\mathbf{r_a}$	$\boldsymbol{\theta}$	$\boldsymbol{\alpha}$	$\boldsymbol{\lambda}$
Unit	μmol $m^{-2}s^{-1}$	*dimensionless*	sm^{-1}	*dimensionless*	*dimensionless*	μmol $mol^{-1}kPa^{-1}$
Linear Katul	299.78	1.53	599.96	0.89	0.20	4.14
Linear Medlyn	298.41	2.20	599.90	0.89	0.20	4.20
Non-linear Katul	299.71	2.02	598.45	0.89	0.20	1.04
Non-linear Medlyn	299.33	2.30	599.21	0.89	0.20	1.04
Co-limitation	299.92	1.50	599.97	0.89	0.20	0.87
Calibration on g with KGE as objective function						
Linear Katul	298.99	1.85	185.03	0.89	0.20	4.16
Linear Medlyn	299.91	2.35	532.35	0.89	0.20	4.18
Non-linear Katul	297.51	1.62	54.45	0.89	0.20	1.04
Non-linear Medlyn	290.68	2.35	140.53	0.88	0.49	7.09
Co-limitation	290.00	2.08	281.91	0.89	0.20	0.92
Calibration on A_n – WUE with KGE as objective function						
Linear Katul	298.88	1.83	599.89	0.89	0.20	1.03
Linear Medlyn	299.91	1.81	599.84	0.90	0.20	1.02
Non-linear Katul	299.25	2.17	599.67	0.89	0.20	1.01
Non-linear Medlyn	289.73	2.00	599.95	0.90	0.20	1.01
Co-limitation	299.47	1.50	599.80	0.89	0.20	0.84
Joint calibration with RMSE as objective function						
Linear Katul	298.69	1.62	599.47	0.89	0.26	10.37
Linear Medlyn	296.10	1.76	599.05	0.89	0.32	15.41
Non-linear Katul	298.84	1.62	599.72	0.89	0.42	7.54
Non-linear Medlyn	297.73	2.49	590.54	0.89	0.39	6.54
Co-limitation	299.88	1.50	597.91	0.89	0.20	1.33

Table A.1: Calibrated model parameters using the SCE-UA algorithm and different objective functions relative to the basil case.

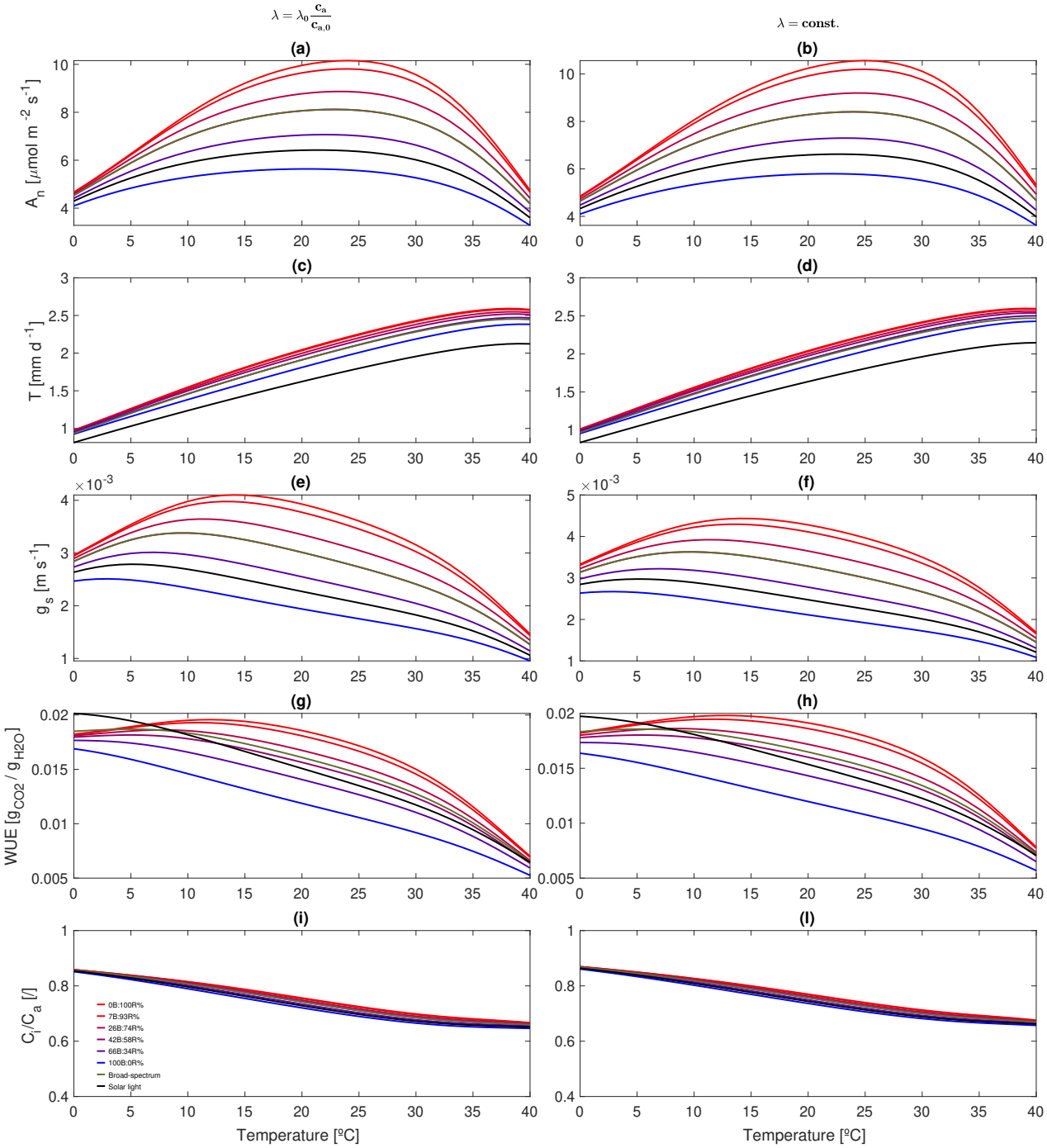

Figure A.27: Sensitivity to changing temperature for the co-limitation model with different hypothesis on the dependence of λ on c_a. The reference values for the climatic variables are as in Figure 4.3.

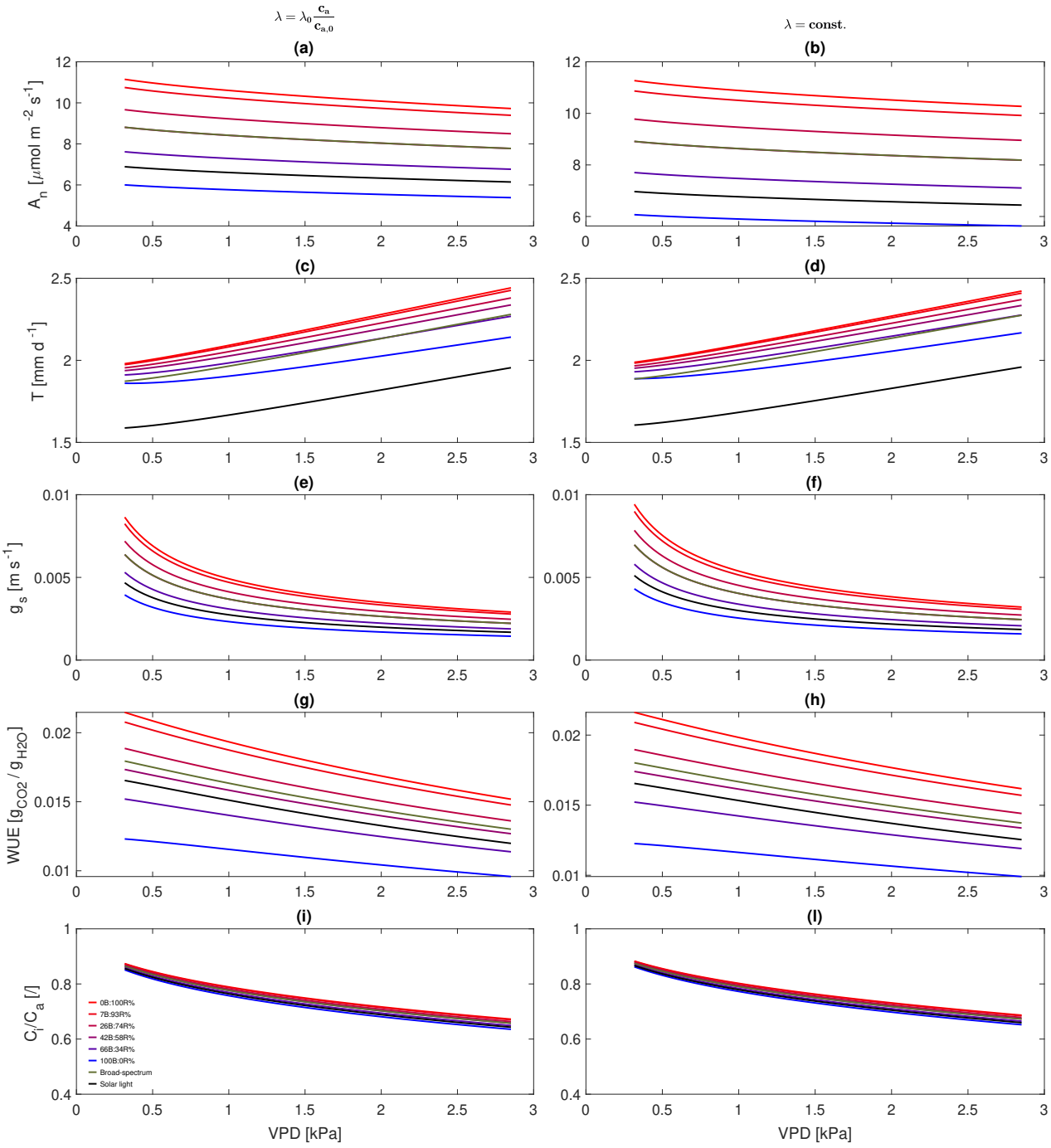

Figure A.28: Sensitivity to changing vapor pressure deficit for the co-limitation model with different hypothesis on the dependence of λ on c_a. The reference values for the climatic variables are as in Figure 4.3.

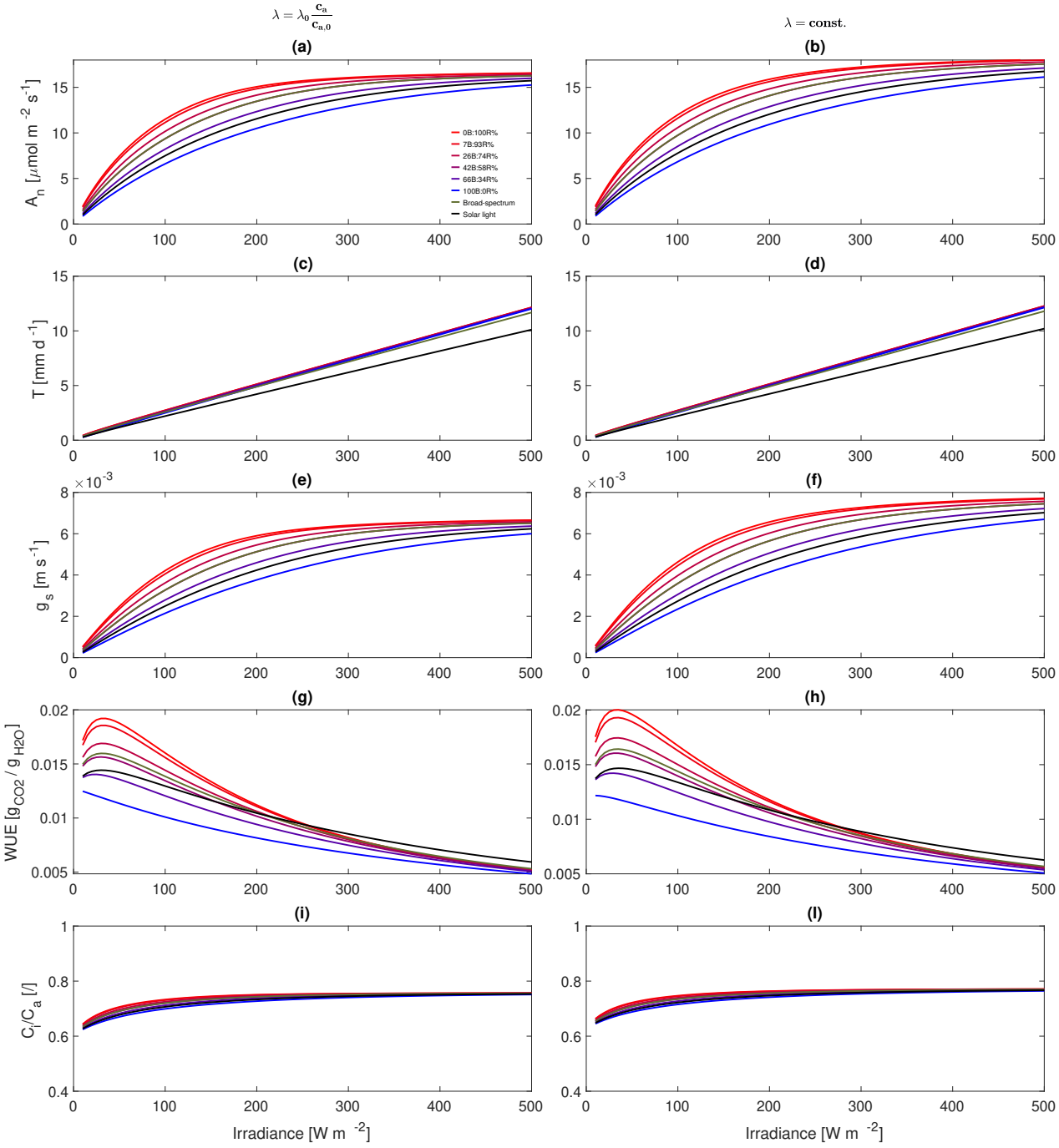

Figure A.29: Sensitivity to changing irradiance for the co-limitation model with different hypothesis on the dependence of λ on c_a. The reference values for the climatic variables are as in Figure 4.3.

Bibliography

Abidin, M. A. Z., Mahyuddin, M. N., and Zainuri, M. A. A. M. Solar Photovoltaic Architecture and Agronomic Management in Agrivoltaic System: A Review. *Sustainability*, 13(14):1–27, 2021. doi:https://doi.org/10.3390/su13147846. URL https://ideas.repec.org//a/gam/jsusta/v13y2021i14p7846-d593841.html.

Adeh, E. H., Selker, J. S., and Higgins, C. W. Remarkable agrivoltaic influence on soil moisture, micrometeorology and water-use efficiency. *PLOS ONE*, 13(11): e0203256, Nov. 2018. ISSN 1932-6203. doi:10.1371/journal.pone.0203256. URL https://journals.plos.org/plosone/article?id=10.1371/journal.pone.0203256.

Aktaş, A. and Kirçiçek, Y. Chapter 2 - Eliminate the Disadvantages of Renewable Energy Sources. In Aktaş, A. and Kirçiçek, Y., editors, *Solar Hybrid Systems*, pages 25–45. Academic Press, Jan. 2021. ISBN 978-0-323-88499-0. doi:10.1016/B978-0-323-88499-0.00002-1. URL https://www.sciencedirect.com/science/article/pii/B9780323884990000021.

Allen, R. G., Pereira, L. S., Raes, D., and Smith, M. Chapter 5 - Introduction to crop evapotranspiration (ETc), Jan. 1998. URL https://www.fao.org/3/X0490E/x0490e0a.htm#factors%20determining%20the%20crop%20coefficient.

Anderson, L. J., Maherali, H., Johnson, H. B., Polley, H. W., and Jackson, R. B. Gas exchange and photosynthetic acclimation over subambient to elevated CO $_2$ in a C $_3$ –C $_4$ grassland. *Global Change Biology*, 7(6):693–707, Aug. 2001. ISSN 1354-1013, 1365-2486. doi:10.1046/j.1354-1013.2001.00438.x. URL https://onlinelibrary.wiley.com/doi/10.1046/j.1354-1013.2001.00438.x.

Ball, J., Woodrow, I., and Berry, J. A Model Predicting Stomatal Conductance and Its Contribution to the Control of Photosynthesis Under Different Environmental Conditions. *Progress in Photosynthesis Research*, 4:221–224, Jan. 1987. ISSN 978-94-017-0521-9. doi:10.1007/978-94-017-0519-6_48.

Ben Mariem, S., Soba, D., Zhou, B., Loladze, I., Morales, F., and Aranjuelo, I. Climate Change, Crop Yields, and Grain Quality of C3 Cereals: A Meta-Analysis of [CO2], Temperature, and Drought Effects. *Plants*, 10(6):1052, June 2021. ISSN 2223-7747. doi:10.3390/plants10061052. URL https://www.mdpi.com/2223-7747/10/6/1052.

Bisbis, M. B., Gruda, N., and Blanke, M. Potential impacts of climate change on vegetable production and product quality – A review. *Journal of Cleaner Production*, 170:1602–1620, Jan. 2018. ISSN 0959-6526. doi:10.1016/j.jclepro.2017.09.224. URL https://www.sciencedirect.com/science/article/pii/S095965261732228X.

Camporese, M. and Abou Najm, M. Not All Light Spectra Were Created Equal: Can We Harvest Light for Optimum Food-Energy Co-Generation? *Earth's Future*, 10(12):

e2022EF002900, 2022. ISSN 2328-4277. doi:10.1029/2022EF002900. URL https://onlinelibrary.wiley.com/doi/abs/10.1029/2022EF002900.

Cox, P. Description of the TRIFFID dynamic global vegetation model. *Hadley Centre Technical Note*, 24, Jan. 2001. URL https://www.researchgate.net/publication/245877262_Description_of_the_TRIFFID_dynamic_global_vegetation_model.

Currie, M. J., Mapel, J. K., Heidel, T. D., Goffri, S., and Baldo, M. A. High-Efficiency Organic Solar Concentrators for Photovoltaics. *Science*, 321(5886):226–228, July 2008. doi:10.1126/science.1158342. URL https://www.science.org/doi/10.1126/science.1158342. Publisher: American Association for the Advancement of Science.

Daly, E., Porporato, A., and Rodriguez-Iturbe, I. Coupled Dynamics of Photosynthesis, Transpiration, and Soil Water Balance. Part I: Upscaling from Hourly to Daily Level. *Journal of Hydrometeorology*, 5(3):546–558, June 2004. ISSN 1525-7541, 1525-755X. doi:10.1175/1525-7541(2004)005<0546:CDOPTA>2.0.CO;2. URL https://journals.ametsoc.org/view/journals/hydr/5/3/1525-7541_2004_005_0546_cdopta_2_0_co_2.xml. Publisher: American Meteorological Society Section: Journal of Hydrometeorology.

Duan, Q. Y., Gupta, V. K., and Sorooshian, S. Shuffled complex evolution approach for effective and efficient global minimization. *Journal of Optimization Theory and Applications*, 76(3):501–521, Mar. 1993. ISSN 1573-2878. doi:10.1007/BF00939380. URL https://doi.org/10.1007/BF00939380.

Düring, H. Stomatal and mesophyll conductances control CO_2 transfer to chloroplasts in leaves of grapevine (*Vitis vinifera* L.). *VITIS - Journal of Grapevine Research*, 42(2):65–65, 2003. ISSN 2367-4156. doi:10.5073/vitis.2003.42.65-68. URL https://ojs.openagrar.de/index.php/VITIS/article/view/4393. Number: 2.

Ehleringer, J. R. and Cerling, T. E. Atmospheric CO2 and the ratio of intercellular to ambient CO2 concentrations in plants. *Tree Physiology*, 15(2):105–111, Feb. 1995. ISSN 0829-318X. doi:10.1093/treephys/15.2.105. URL https://doi.org/10.1093/treephys/15.2.105.

Elamri, Y., Cheviron, B., Lopez, J. M., Dejean, C., and Belaud, G. Water budget and crop modelling for agrivoltaic systems: Application to irrigated lettuces. *Agricultural Water Management*, 208:440–453, Sept. 2018. ISSN 0378-3774. doi:10.1016/j.agwat.2018.07.001. URL https://www.sciencedirect.com/science/article/pii/S0378377418309545.

Farquhar, G. D., von Caemmerer, S., and Berry, J. A. A biochemical model of photosynthetic CO2 assimilation in leaves of C3 species. *Planta*, 149(1):78–90, June 1980. ISSN 1432-2048. doi:10.1007/BF00386231. URL https://doi.org/10.1007/BF00386231.

Georgieva, K. and Yordanov, I. Temperature Dependence of Photochemical and Non-Photochemical Fluorescence Quenching in Intact *Pea Leaves*. *Journal of Plant Physiology*, 144(6):754–759, Nov. 1994. ISSN 0176-1617. doi:10.1016/S0176-1617(11)80673-5. URL https://www.sciencedirect.com/science/article/pii/S0176161711806735.

Giri, A., Heckathorn, S., Mishra, S., and Krause, C. Heat Stress Decreases Levels of Nutrient-Uptake and -Assimilation Proteins in Tomato Roots. *Plants*, 6(1):6, Mar. 2017. ISSN 2223-7747. doi:10.3390/plants6010006. URL https://www.mdpi.com/

2223-7747/6/1/6. Number: 1 Publisher: Multidisciplinary Digital Publishing Institute.

Gueymard, C. A., Myers, D., and Emery, K. Proposed reference irradiance spectra for solar energy systems testing. *Solar Energy*, 73(6):443–467, Dec. 2002. ISSN 0038-092X. doi:10.1016/S0038-092X(03)00005-7. URL https://www.sciencedirect.com/science/article/pii/S0038092X03000057.

Głowacka, K., Kromdijk, J., Kucera, K., Xie, J., Cavanagh, A. P., Leonelli, L., Leakey, A. D. B., Ort, D. R., Niyogi, K. K., and Long, S. P. Photosystem II Subunit S overexpression increases the efficiency of water use in a field-grown crop. *Nature Communications*, 9(1):868, Mar. 2018. ISSN 2041-1723. doi:10.1038/s41467-018-03231-x. URL https://www.nature.com/articles/s41467-018-03231-x. Number: 1 Publisher: Nature Publishing Group.

Hendrickson, L., Förster, B., Pogson, B. J., and Chow, W. S. A simple chlorophyll fluorescence parameter that correlates with the rate coefficient of photoinactivation of Photosystem II. *Photosynthesis Research*, 84(1):43–49, June 2005. ISSN 1573-5079. doi:10.1007/s11120-004-6430-4. URL https://doi.org/10.1007/s11120-004-6430-4.

Hernández, G. G., Winter, K., and Slot, M. Similar temperature dependence of photosynthetic parameters in sun and shade leaves of three tropical tree species. *Tree Physiology*, 40(5):637–651, May 2020. ISSN 1758-4469. doi:10.1093/treephys/tpaa015. URL https://doi.org/10.1093/treephys/tpaa015.

Hilker, J., Busse, M., Müller, K., and Zscheischler, J. Photovoltaics in agricultural landscapes: "Industrial land use" or a "real compromise" between renewable energy and biodiversity? Perspectives of German nature conservation associations, May 2023.

Inada, K. Action spectra for photosynthesis in higher plants. *Plant and Cell Physiology*, 17(2):355–365, Apr. 1976. ISSN 0032-0781. doi:10.1093/oxfordjournals.pcp.a075288. URL https://doi.org/10.1093/oxfordjournals.pcp.a075288.

Jørgensen, S. E. and Bendoricchio, G. Chapter 3 Ecological processes. In *Fundamentals of Ecological Modelling*, volume 21, pages 93–209. Elsevier, 2001. ISBN 978-0-08-044015-6. doi:10.1016/S0167-8892(01)80005-1. URL https://linkinghub.elsevier.com/retrieve/pii/S0167889201800051.

Kattge, J. and Knorr, W. Temperature acclimation in a biochemical model of photosynthesis: a reanalysis of data from 36 species. *Plant, Cell & Environment*, 30(9):1176–1190, 2007. ISSN 1365-3040. doi:10.1111/j.1365-3040.2007.01690.x. URL https://onlinelibrary.wiley.com/doi/abs/10.1111/j.1365-3040.2007.01690.x. _eprint: https://onlinelibrary.wiley.com/doi/pdf/10.1111/j.1365-3040.2007.01690.x.

Katul, G., Manzoni, S., Palmroth, S., and Oren, R. A stomatal optimization theory to describe the effects of atmospheric CO2 on leaf photosynthesis and transpiration. *Annals of Botany*, 105(3):431–442, Mar. 2010. ISSN 0305-7364. doi:10.1093/aob/mcp292. URL https://doi.org/10.1093/aob/mcp292.

Konrad, W., Roth-Nebelsick, A., and Grein, M. Modelling of stomatal density response to atmospheric CO2. *Journal of Theoretical Biology*, 253(4):638–658, Aug. 2008. ISSN 0022-5193. doi:10.1016/j.jtbi.2008.03.032. URL https://www.sciencedirect.com/science/article/pii/S0022519308001677.

Kromdijk, J., Głowacka, K., and Long, S. P. Predicting light-induced stomatal movements based on the redox state of plastoquinone: theory and validation. *Photosynthesis Research*, 141(1):83–97, July 2019. ISSN 1573-5079. doi:10.1007/s11120-019-00632-x. URL https://doi.org/10.1007/s11120-019-00632-x.

Kumar, B., Kaushik, B. K., and Negi, Y. Organic Thin Film Transistors: Structures, Models, Materials, Fabrication, and Applications: A Review. *Polymer Reviews*, 54, Feb. 2014. doi:10.1080/15583724.2013.848455.

Leuning, R. A critical appraisal of a combined stomatal-photosynthesis model for C3 plants. *Plant, Cell & Environment*, 18(4):339–355, 1995. ISSN 1365-3040. doi:10.1111/j.1365-3040.1995.tb00370.x. URL https://onlinelibrary.wiley.com/doi/abs/10.1111/j.1365-3040.1995.tb00370.x. _eprint: https://onlinelibrary.wiley.com/doi/pdf/10.1111/j.1365-3040.1995.tb00370.x.

Li, H., Lian, Y., Wang, X., Ma, W., and Zhao, L. Solar constant values for estimating solar radiation. *Energy*, 36(3):1785–1789, Mar. 2011. ISSN 0360-5442. doi:10.1016/j.energy.2010.12.050. URL https://www.sciencedirect.com/science/article/pii/S0360544210007565.

Li, P.-C. and Ma, H.-w. Evaluating the environmental impacts of the water-energy-food nexus with a life-cycle approach. *Resources, Conservation and Recycling*, 157: 104789, June 2020. ISSN 0921-3449. doi:10.1016/j.resconrec.2020.104789. URL https://www.sciencedirect.com/science/article/pii/S0921344920301105.

Liu, J. and van Iersel, M. W. Photosynthetic Physiology of Blue, Green, and Red Light: Light Intensity Effects and Underlying Mechanisms. *Frontiers in Plant Science*, 12: 619987, Mar. 2021. ISSN 1664-462X. doi:10.3389/fpls.2021.619987. URL https://www.ncbi.nlm.nih.gov/pmc/articles/PMC7977723/.

Loik, M. E., Carter, S. A., Alers, G., Wade, C. E., Shugar, D., Corrado, C., Jokerst, D., and Kitayama, C. Wavelength-Selective Solar Photovoltaic Systems: Powering Greenhouses for Plant Growth at the Food-Energy-Water Nexus. *Earth's Future*, 5 (10):1044–1053, 2017. ISSN 2328-4277. doi:10.1002/2016EF000531. URL https://onlinelibrary.wiley.com/doi/abs/10.1002/2016EF000531.

Lombardozzi, D. L., Smith, N. G., Cheng, S. J., Dukes, J. S., Sharkey, T. D., Rogers, A., Fisher, R., and Bonan, G. B. Triose phosphate limitation in photosynthesis models reduces leaf photosynthesis and global terrestrial carbon storage. *Environmental Research Letters*, 13(7):074025, July 2018. ISSN 1748-9326. doi:10.1088/1748-9326/aacf68. URL https://dx.doi.org/10.1088/1748-9326/aacf68. Publisher: IOP Publishing.

Lu, Y. Identification and Roles of Photosystem II Assembly, Stability, and Repair Factors in Arabidopsis. *Frontiers in Plant Science*, 7:168, Feb. 2016. ISSN 1664-462X. doi:10.3389/fpls.2016.00168. URL https://www.ncbi.nlm.nih.gov/pmc/articles/PMC4754418/.

Macmillan Learning, The Electromagnetic Spectrum. Chempendix - EM Spectrum, Apr. 2023. URL https://sites.google.com/site/chempendix/em-spectrum.

Malu, P. R., Sharma, U. S., and Pearce, J. M. Agrivoltaic potential on grape farms in India. *Sustainable Energy Technologies and Assessments*, 23:104–110, Oct. 2017. ISSN 22131388. doi:10.1016/j.seta.2017.08.004. URL https://linkinghub.elsevier.com/retrieve/pii/S2213138817302096.

Marrou, H., Dufour, L., and Wery, J. How does a shelter of solar panels influence water flows in a soil–crop system? *European Journal of Agronomy*, 50:38–51, Oct. 2013a. ISSN 1161-0301. doi:10.1016/j.eja.2013.05.004. URL https://www.sciencedirect.com/science/article/pii/S1161030113000683.

Marrou, H., Wery, J., Dufour, L., and Dupraz, C. Productivity and radiation use efficiency of lettuces grown in the partial shade of photovoltaic panels. *European Journal of Agronomy*, 44:54–66, Jan. 2013b. ISSN 1161-0301. doi:10.1016/j.eja.2012.08.003. URL https://www.sciencedirect.com/science/article/pii/S1161030112001177.

Marucci, A., Zambon, I., Colantoni, A., and Monarca, D. A combination of agricultural and energy purposes: Evaluation of a prototype of photovoltaic greenhouse tunnel. *Renewable and Sustainable Energy Reviews*, 82:1178–1186, Feb. 2018. ISSN 1364-0321. doi:10.1016/j.rser.2017.09.029. URL https://www.sciencedirect.com/science/article/pii/S136403211731273X.

McCree, K. J. The action spectrum, absorptance and quantum yield of photosynthesis in crop plants. *Agricultural Meteorology*, 9:191–216, Jan. 1971. ISSN 0002-1571. doi:10.1016/0002-1571(71)90022-7. URL https://www.sciencedirect.com/science/article/pii/0002157171900227.

Medlyn, B. E., Duursma, R. A., Eamus, D., Ellsworth, D. S., Prentice, I. C., Barton, C. V. M., Crous, K. Y., De Angelis, P., Freeman, M., and Wingate, L. Reconciling the optimal and empirical approaches to modelling stomatal conductance. *Global Change Biology*, 17(6):2134–2144, 2011. ISSN 1365-2486. doi:10.1111/j.1365-2486.2010.02375.x. URL https://onlinelibrary.wiley.com/doi/abs/10.1111/j.1365-2486.2010.02375.x.

Miskin, C. K., Li, Y., Perna, A., Ellis, R. G., Grubbs, E. K., Bermel, P., and Agrawal, R. Sustainable co-production of food and solar power to relax land-use constraints. *Nature Sustainability*, 2(10):972–980, Oct. 2019. ISSN 2398-9629. doi:10.1038/s41893-019-0388-x. URL https://www.nature.com/articles/s41893-019-0388-x. Number: 10 Publisher: Nature Publishing Group.

Mochizuki, Y., Sekiguchi, S., Horiuchi, N., Aung, T., and Ogiwara, I. Photosynthetic Characteristics of Individual Strawberry (Fragaria ×ananassa Duch.) Leaves under Short-distance Lightning with Blue, Green, and Red LED Lights. *HortScience*, 54 (3):452–458, Mar. 2019. ISSN 0018-5345, 2327-9834. doi:10.21273/HORTSCI13560-18. URL https://journals.ashs.org/hortsci/view/journals/hortsci/54/3/article-p452.xml. Publisher: American Society for Horticultural Science Section: HortScience.

Morison, J. Stomatal response to increased CO2 concentration. *Journal of Experimental Botany - J EXP BOT*, 49:443–452, Mar. 1998. doi:10.1093/jexbot/49.suppl_1.443.

Munns, R., Schmidt, S., Beveridge, C., and Mathesius, U. Chapter 12 - Sunlight and plant production | Plants in Action, Mar. 2018. URL https://www.rseco.org/content/chapter-12-sunlight-and-plant-production.html.

Orsini, F., Pennisi, G., Mancarella, S., Al Nayef, M., Sanoubar, R., Nicola, S., and Gianquinto, G. Hydroponic lettuce yields are improved under salt stress by utilizing white plastic film and exogenous applications of proline. *Scientia Horticulturae*, 233: 283–293, Mar. 2018. ISSN 0304-4238. doi:10.1016/j.scienta.2018.01.019. URL https://www.sciencedirect.com/science/article/pii/S0304423818300256.

Oxborough, K. and Baker, N. R. Resolving chlorophyll a fluorescence images of photosynthetic efficiency into photochemical and non-photochemical components – calculation of qP and Fv-/Fm-; without measuring Fo-;. *Photosynthesis Research*, 54(2):135–142, Nov. 1997. ISSN 1573-5079. doi:10.1023/A:1005936823310. URL https://doi.org/10.1023/A:1005936823310.

Palmeri, L., Barausse, A., and Jørgensen, S. E. Chapter 2 Physical Processes. In *Ecological Processes Handbook*, pages 73–124. CRC Press, Boca Raton, Aug. 2013. ISBN 978-0-429-09799-7. doi:10.1201/b15380. URL https://www.taylorfrancis.com/books/mono/10.1201/b15380/ecological-processes-handbook-luca-palmeri-sven-erik-jorgensen-alberto-barausse.

Pang, K., Van Sambeek, J. W., Navarrete-Tindall, N. E., Lin, C.-H., Jose, S., and Garrett, H. E. Responses of legumes and grasses to non-, moderate, and dense shade in Missouri, USA. I. Forage yield and its species-level plasticity. *Agroforestry Systems*, 93(1):11–24, Feb. 2019. ISSN 1572-9680. doi:10.1007/s10457-017-0067-8. URL https://doi.org/10.1007/s10457-017-0067-8.

Park, K. S., Bekhzod, K., Kwon, J. K., and Son, J. E. Development of a coupled photosynthetic model of sweet basil hydroponically grown in plant factories. *Horticulture, Environment, and Biotechnology*, 57(1):20–26, Feb. 2016. ISSN 2211-3460. doi:10.1007/s13580-016-0019-7. URL https://doi.org/10.1007/s13580-016-0019-7.

Pascaris, A. S., Schelly, C., and Pearce, J. M. A First Investigation of Agriculture Sector Perspectives on the Opportunities and Barriers for Agrivoltaics. *Agronomy*, 10 (12):1885, Dec. 2020. ISSN 2073-4395. doi:10.3390/agronomy10121885. URL https://www.mdpi.com/2073-4395/10/12/1885. Number: 12 Publisher: Multidisciplinary Digital Publishing Institute.

Patel, B., Gami, B., Baria, V., Patel, A., and Patel, P. Co-Generation of Solar Electricity and Agriculture Produce by Photovoltaic and Photosynthesis—Dual Model by Abellon, India. *Journal of Solar Energy Engineering*, 141(031014), Nov. 2018. ISSN 0199-6231. doi:10.1115/1.4041899. URL https://doi.org/10.1115/1.4041899.

Pathakoti, K., Manubolu, M., and Hwang, H.-M. Chapter 48 - Nanotechnology Applications for Environmental Industry. In Mustansar Hussain, C., editor, *Handbook of Nanomaterials for Industrial Applications*, Micro and Nano Technologies, pages 894–907. Elsevier, Jan. 2018. ISBN 978-0-12-813351-4. doi:10.1016/B978-0-12-813351-4.00050-X. URL https://www.sciencedirect.com/science/article/pii/B978012813351400050X.

Pennisi, G., Blasioli, S., Cellini, A., Maia, L., Crepaldi, A., Braschi, I., Spinelli, F., Nicola, S., Fernandez, J. A., Stanghellini, C., Marcelis, L. F. M., Orsini, F., and Gianquinto, G. Unraveling the Role of Red:Blue LED Lights on Resource Use Efficiency and Nutritional Properties of Indoor Grown Sweet Basil. *Frontiers in Plant Science*, 10, 2019. ISSN 1664-462X. URL https://www.frontiersin.org/articles/10.3389/fpls.2019.00305.

Pereira, L. S., Allen, R. G., Smith, M., and Raes, D. Crop evapotranspiration estimation with FAO56: Past and future. *Agricultural Water Management*, 147:4–20, Jan. 2015. ISSN 0378-3774. doi:10.1016/j.agwat.2014.07.031. URL https://www.sciencedirect.com/science/article/pii/S0378377414002315.

Proctor, K. W., Murthy, G. S., and Higgins, C. W. Agrivoltaics Align with Green New Deal Goals While Supporting Investment in the US' Rural Economy. *Sustainability*, 13(1):137, Jan. 2021. ISSN 2071-1050. doi:10.3390/su13010137. URL https://www.mdpi.com/2071-1050/13/1/137. Number: 1 Publisher: Multidisciplinary Digital Publishing Institute.

Rastogi, R. P., Richa, Kumar, A., Tyagi, M. B., and Sinha, R. P. Molecular Mechanisms of Ultraviolet Radiation-Induced DNA Damage and Repair. *Journal of Nucleic Acids*, 2010:592980, Dec. 2010. ISSN 2090-0201. doi:10.4061/2010/592980. URL https://www.ncbi.nlm.nih.gov/pmc/articles/PMC3010660/.

Ravi, S., Macknick, J., Lobell, D., Field, C., Ganesan, K., Jain, R., Elchinger, M., and Stoltenberg, B. Colocation opportunities for large solar infrastructures and agriculture in drylands. *Applied Energy*, 165:383–392, Mar. 2016. ISSN 0306-2619. doi:10.1016/j.apenergy.2015.12.078. URL https://www.sciencedirect.com/science/article/pii/S0306261915016517.

Rho, H., Yu, D. J., Kim, S. J., Chun, C., and Lee, H. J. Estimation of carboxylation efficiency from net CO2 assimilation rate as a function of chloroplastic CO2 concentration in strawberry (Fragaria × ananassa cv. Maehyang) leaves. *Horticulture, Environment, and Biotechnology*, 52(6):547–552, Dec. 2011. ISSN 2211-3460. doi:10.1007/s13580-011-0035-6. URL https://doi.org/10.1007/s13580-011-0035-6.

Ruban, A. V. Nonphotochemical Chlorophyll Fluorescence Quenching: Mechanism and Effectiveness in Protecting Plants from Photodamage. *Plant Physiology*, 170(4):1903, Apr. 2016. doi:10.1104/pp.15.01935. URL https://www.ncbi.nlm.nih.gov/pmc/articles/PMC4825125/. Publisher: Oxford University Press.

Schindele, S., Trommsdorff, M., Schlaak, A., Obergfell, T., Bopp, G., Reise, C., Braun, C., Weselek, A., Bauerle, A., Högy, P., Goetzberger, A., and Weber, E. Implementation of agrophotovoltaics: Techno-economic analysis of the price-performance ratio and its policy implications. *Applied Energy*, 265(C), 2020. doi:10.1016/j.apenergy.2020.114737. URL https://ideas.repec.org//a/eee/appene/v265y2020ics030626192030249x.html. Publisher: Elsevier.

Shybut, M. Watch: The Role of Agrivoltaics in California's Water-Energy-Food Nexus, Aug. 2023. URL https://ccst.us/register-the-role-of-agrivoltaics-in-californias-water-energy-food-nexus/.

Slot, M., Krause, G., Krause, B., Hernández, G., and Winter, K. Photosynthetic heat tolerance of shade and sun leaves of three tropical tree species. *Photosynthesis Research*, 141, July 2019. doi:10.1007/s11120-018-0563-3.

Streck, N. A. STOMATAL RESPONSE TO WATER VAPOR PRESSURE DEFICIT: AN UNSOLVED ISSUE. *Current Agricultural Science and Technology*, 9(4), 2003. ISSN 2317-2436. URL https://periodicos.ufpel.edu.br/index.php/CAST/article/view/649. Number: 4.

Thompson, E. P., Bombelli, E. L., Shubham, S., Watson, H., Everard, A., D'Ardes, V., Schievano, A., Bocchi, S., Zand, N., Howe, C. J., and Bombelli, P. Tinted Semi-Transparent Solar Panels Allow Concurrent Production of Crops and Electricity on the Same Cropland. *Advanced Energy Materials*, 10(35):2001189, 2020. ISSN 1614-6840. doi:10.1002/aenm.202001189. URL https://onlinelibrary.wiley.com/doi/abs/10.1002/aenm.202001189.

Trommsdorff, M., Dhal, I. S., Özdemir, E., Ketzer, D., Weinberger, N., and Rösch, C. Chapter 5 - Agrivoltaics: solar power generation and food production. In Gorjian, S. and Campana, P. E., editors, *Solar Energy Advancements in Agriculture and Food Production Systems*, pages 159–210. Academic Press, Jan. 2022. ISBN 978-0-323-89866-9. doi:10.1016/B978-0-323-89866-9.00012-2. URL https://www.sciencedirect.com/science/article/pii/B9780323898669000122.

Urban, J., Ingwers, M., McGuire, M. A., and Teskey, R. O. Stomatal conductance increases with rising temperature. *Plant Signaling & Behavior*, 12(8): e1356534, Aug. 2017. ISSN null. doi:10.1080/15592324.2017.1356534. URL https://doi.org/10.1080/15592324.2017.1356534. Publisher: Taylor & Francis _eprint: https://doi.org/10.1080/15592324.2017.1356534.

Valle, B., Simonneau, T., Sourd, F., Pechier, P., Hamard, P., Frisson, T., Ryckewaert, M., and Christophe, A. Increasing the total productivity of a land by combining mobile photovoltaic panels and food crops. *Applied Energy*, 206:1495–1507, Nov. 2017. ISSN 0306-2619. doi:10.1016/j.apenergy.2017.09.113. URL https://www.sciencedirect.com/science/article/pii/S0306261917313971.

Vico, G., Manzoni, S., Palmroth, S., Weih, M., and Katul, G. A perspective on optimal leaf stomatal conductance under CO2 and light co-limitations. *Agricultural and Forest Meteorology*, 182-183:191–199, Dec. 2013. ISSN 0168-1923. doi:10.1016/j.agrformet.2013.07.005. URL https://www.sciencedirect.com/science/article/pii/S0168192313001858.

Wang, S., Wang, X., Shi, X., Wang, B., Zheng, X., Wang, H., and Liu, F. Red and Blue Lights Significantly Affect Photosynthetic Properties and Ultrastructure of Mesophyll Cells in Senescing Grape Leaves. *Horticultural Plant Journal*, 2(2):82–90, Mar. 2016. ISSN 2468-0141. doi:10.1016/j.hpj.2016.03.001. URL https://www.sciencedirect.com/science/article/pii/S2468014116300358.

Weselek, A., Ehmann, A., Zikeli, S., Lewandowski, I., Schindele, S., and Högy, P. Agrophotovoltaic systems: applications, challenges, and opportunities. A review. *Agronomy for Sustainable Development*, 39(4):35, June 2019. ISSN 1773-0155. doi:10.1007/s13593-019-0581-3. URL https://doi.org/10.1007/s13593-019-0581-3.

Whiteman, P. C. and Koller, D. Interactions of Carbon Dioxide Concentration, Light Intensity and Temperature on Plant Resistances to Water Vapour and Carbon Dioxide Diffusion. *New Phytologist*, 66(3):463–473, 1967. ISSN 1469-8137. doi:10.1111/j.1469-8137.1967.tb06025.x. URL https://onlinelibrary.wiley.com/doi/abs/10.1111/j.1469-8137.1967.tb06025.x. _eprint: https://onlinelibrary.wiley.com/doi/pdf/10.1111/j.1469-8137.1967.tb06025.x.

Williams, H. J., Hashad, K., Wang, H., and Max Zhang, K. The potential for agrivoltaics to enhance solar farm cooling. *Applied Energy*, 332:120478, Feb. 2023. ISSN 0306-2619. doi:10.1016/j.apenergy.2022.120478. URL https://www.sciencedirect.com/science/article/pii/S0306261922017354.

Zhang, F., Li, M., Zhang, W., Liu, W., Ali Abaker Omer, A., Zhang, Z., Zheng, J., Liu, W., and Zhang, X. Large-scale and cost-efficient agrivoltaics system by spectral separation. *iScience*, 26(11):108129, Nov. 2023. ISSN 2589-0042. doi:10.1016/j.isci.2023.108129. URL https://www.sciencedirect.com/science/article/pii/S258900422302206X.

Ögren, E. and Evans, J. R. Photosynthetic light-response curves. *Planta*, 189(2):182–190, Feb. 1993. ISSN 1432-2048. doi:10.1007/BF00195075. URL https://doi.org/10.1007/BF00195075.